LOCALIZATION AND TRAFFICKING OF THE *CAENORHABDITIS ELEGANS* DOPAMINE TRANSPORTER (DAT-1).

By

Paul W. McDonald

Dissertation

Submitted to the Faculty of the

Graduate School of Vanderbilt University

in partial fulfillment of the requirements

of the degree of

DOCTOR OF PHILOSOPHY

in

Neuroscience

May, 2006

Nashville, Tennessee

Approved by:

Professor Lou DeFelice

Professor Randy D. Blakely

Professor Al George Jr.

Professor Andy Link

Professor David Miller

For my parents, who saw me through dark times and believed in me when I didn't believe in myself. And of course, to the love of my life, Sarah, thank you for everything.

ACKNOWLEDGEMENTS

This dissertation would not have been completed or written without the help of numerous people who helped me along the way. I was originally introduced to graduate level science as a technician in the laboratory of Dr. Michael McLean, who encouraged me to join the graduate school. I owe many thanks to Drs. McLean and Robert Holcomb who believed in my talents and paid my way when I first came to Nashville.

As I began graduate work two professors were instrumental in forging my path to neuroscience research. Dr. Lou DeFelice kindled a fire for electrophysiology and a search for basic truth. Dr. Janette Nordon best illustrated the compassion and integrity that I feel is paramount to success in research dealing with debilitating disease. Without either of their influence, I certainly would not have finished the work presented here.

I would also like to acknowledge my mentor Dr. Randy Blakely, who entrusted me with a novel and ambitious research topic. His constant optimism and advice helped propel my work forward. To all the members of the lab, and especially to Tammy Jessen, thank you, for camaraderie and an undying dedication. Your enthusiasm and drive motivated me daily. And thank you to the National Institute on Drug Addiction (NIDA) and the National Institutes of Health (NIH) for funding this research.

TABLE OF CONTENTS

Page

LIST OF TABLES

LIST OF FIGURES

LIST OF ABREVIATIONS

5HT	Serotonin
6-OHDA	6-Hydroxydopamine
AADC	Aromatic Amino Acid Decarboxylase
AC	Adenylate Cyclase
ACHE	Acetylcholinesterase
ADE	Anterior Deirid Neurons
ADHD	Attention Deficit Hyperactivity Disorder
AMPH	Amphetamine
ARS	Area Restricted Search
bDAT	Bovine Dopamine Transporter
cAMP	Cyclic Adenosine Mono Phosphate
CAT	Catecholamine Deficient Mutants
CEP	Cephalic Neuron
CNS	Central Nervous System
COMT	Catechol-o-methyl Transferase
DA	Dopamine
DAT	Dopamine Transporter
DAT-1	*C. elegans* Dopamine Transporter
DOPA	3,4-Dihydroxyphenylalanine
EM	Electron Microscopy
EMC	Enteric Muscle Contraction

EMS	Ethyl-methane Sulfonate
FIF	Formaldehyde Induced Fluorescence
GABA	γ-amino butyric Acid
GIRK	G-protein couple Inwardly Rectifying Potasium Channel
GTPCH	GTPcyclohydrolase
hDAT	Human Dopamine Transporter
HSN	Hermaphrodite Specific Neuron
KO	Knock Out
MAOB	Monoamine Oxidase B
mRNA	Messenger Ribonucleic Acid
MAPK	Mitogen-activated Protein Kinase
NAc	Nucleus Accumbens
NE	Norepinephrine
NET	Norepinephrine Transporter
NR	Nerve Ring
PDE	Posterior Deirid Neuron
PKA	Protein Kinase A
PKC	Protein Kinase C
PMA	Phorbol 12-myristlate 13-acetate
PP2A	Protein Phosphatase 2A
rDAT	Rat Dopamine Transporter
SERT	Serotonin Transporter
SN	Substantia Nigra

SZ	Schizophrenia
TH	Tyrosine Hydroxylase
THB	Tetrahydrobiopterin
UNC	Uncoordinated phenotype
VMAT	Vesicular Monoamine Transporter
VTA	Ventral Tegmental Area

CHAPTER I

DOPAMINERGIC NEUROTRANSMISSION IN THE CENTRAL NERVOUS SYSTEM.

INTRODUCTION

The catecholamine dopamine (DA) is one of several neurotransmitters that are produced and released in a specific subset of neurons in the central nervous system. DA is synthesized via a series of enzymatic reactions that initiate with the cytosolic amino acid tyrosine (Fig 1). DA is then packaged into synaptic vesicles by a vesicular monoamine transporter (VMAT) and released at nerve terminals into the synapse upon depolarization by an afferent stimulus (Fig 2). Synaptic DA then binds both pre- and postsynaptic receptors leading to a number of intracellular responses that modulated excitability. DA signaling is terminated by the reuptake of DA into the presynaptic neuron by the DA transporter (DAT). DA is also metabolized by monoamine oxidase B (MAOB) and catechol-o-methyl transferase (COMT), although these are thought to control intraneuronal levels of DA versus inactivating DA in the synapse. DA that is reabsorbed by DAT is then repackaged into vesicles by VMAT and is ready for another subsequent round of release.

THE IDENTIFICATION OF DOPAMINE AS A NEUROTRANSMITTER

DA was originally assumed to be a mere intermediate in the biosynthesis of norepinephrine until Carlsson and coworkers performed experiments on reserpinized animals and revealed a previously unrecognized role for DA in the central nervous

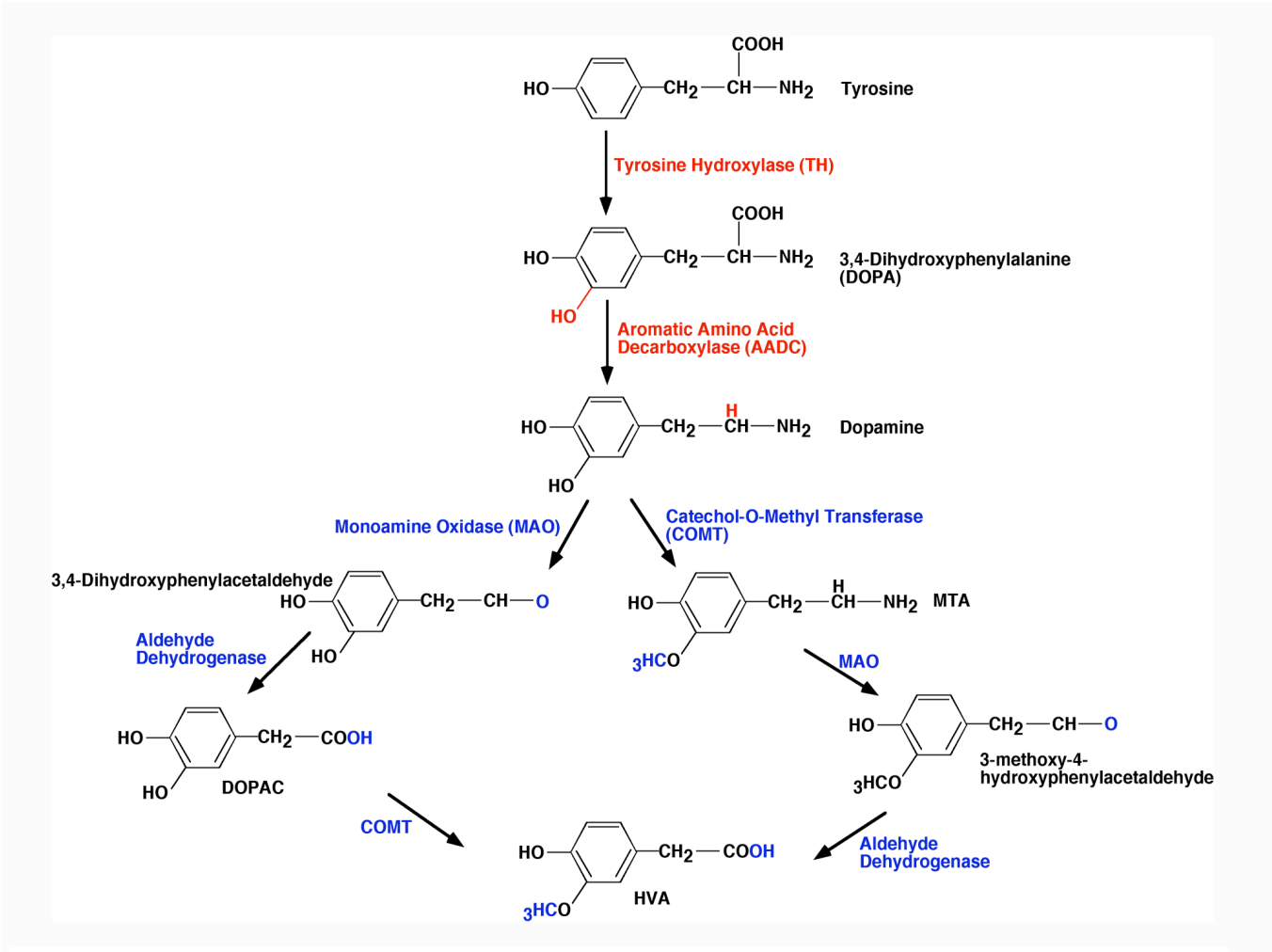

Figure 1. Biosynthesis and Degradation of Dopamine.

Synthetic enzymes are labeled in red and enzymes involved in dopamine metabolism are labeled in blue. (Image compliments of M. Mazei-Robison)

system (Carlsson et al., 1957). The neurotoxin reserpine alters the pH gradient required for monoamine uptake into the synaptic vesicle via VMAT. Initial studies revealed that the administration of reserpine depleted serotonin (5HT) brain levels in a dose dependent manner (Pletscher et al., 1955). At the time, the mechanism of action was unclear at a molecular level, however, animals treated with reserpine became immobile, contributing to what is known as reserpine syndrome. Loss of norepinephrine (NE) was assumed to be the cause of this syndrome and as expected, treatment of reserpinized animals with the NE precursor 3,4-Dihydroxyphenylalanine (DOPA), reversed reserpine syndrome. The development of the Aminco-Bowman Spectrophotofluorimeter made measurements of norepinephrine levels in tissue samples possible. Analysis of tissue from reserpinized and DOPA treated rabbits revealed that while animals regained mobility, there was only modest recovery of norepinephrine levels in the brain, (Carlsson et al., 1957).

Intrigued by these findings, Carlsson and colleagues examined norepinephrine intermediates that might be responsible for the reversal of reserpine syndrome. After development of a method for determining DA levels in the brain, they found that not only was DA maintained at an elevated level in the brain under basal conditions (compared to NE), but it was also completely depleted by reserpine. The return of DA but not NE by administration of DOPA was then found to be correlated with recovery from reserpine syndrome (Carlsson and Waldeck, 1958). (For a personal account, read Arvid Carlsson's Nobel lecture (Carlsson, 2001)).

Several years after the discovery of DA as a potential neuromodulator of movement defects, it was discovered that DA was synthesized and stored in a specific subset of neurons in the brain. The largest collection of DA containing neurons was

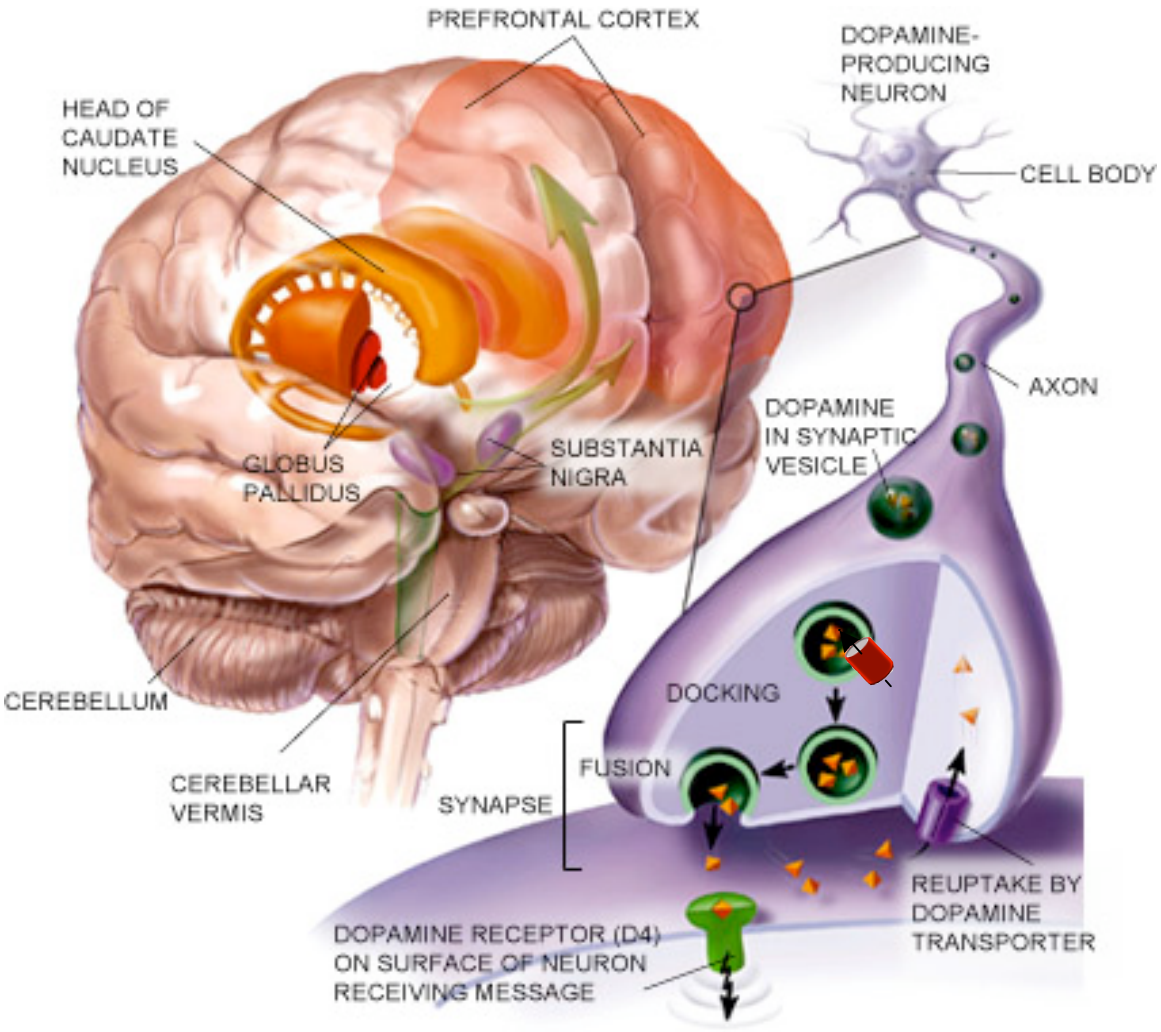

Figure 2. Illustration of the Dopaminergic Synapse.

Substantia Nigra projections to both the striatum (Caudate, Putamen, and Globus Palidus) and prefrontal cortex are illustrated. A dopaminergic neuron elaborating a synaptic terminal is highlighted with emphasis on the presynaptic DAT (purple) and VMAT (red) loading synaptic vesicles containing dopamine. A post synaptic dopamine receptor (D4) is also illustrated. Original Image adapted from www.liebermanparkinsonclinic.com

found in the basal ganglia (Bertler and Rosengren, 1959), and the discovery of the fluorescent properties of catecholamines when reacted with formaldehyde (creating formaldehyde-induced fluorescence (FIF)) resulted in the ability of researchers to trace specific connections of DA neurons in the brain (originally (Falck et al., 1962) and reprinted (Falck et al., 1982)) This allowed for the visualization of the major DA pathways in the central nervous system (Dahlstrom and Fuxe, 1964; Fuxe, 1965; Hillarp et al., 1966).

DOPAMINE PATHWAYS IN THE MAMMALIAN BRAIN

The neurons that synthesize and release DA represent only a small fraction of all neurons in the central nervous system and form the central DA nervous system. There are three basic tracts of DA neurons: the nigrostriatal pathway, the mesocorticolimbic pathway, and the tuberoinfundibular pathway (Fig 3), although DA neurons are also found in other brain areas including the retina and olfactory bulbs (Fallon, 1988; Compton and Miller, 2002). Of these, most is known about the effects of DA in the nigrostriatal pathway (from the substantia nigra to the striatum) and the mesocorticolimbal pathways (from the ventral tegmental area (VTA) to both the cortex (including the prefrontal, cingulate, and entorhinalcortices) and the limbic system (including projections to the nucleus accumbens septi, amygdala, olfactory tubercle and piriform cortex).

The nigrostriatal pathway has its cell bodies in the substantia nigra (SN) of the midbrain and sends axonal projections to the caudate and putamen nuclei in the striatum (Fig 2 & 3). These projections have been shown to be crucial for motor function with

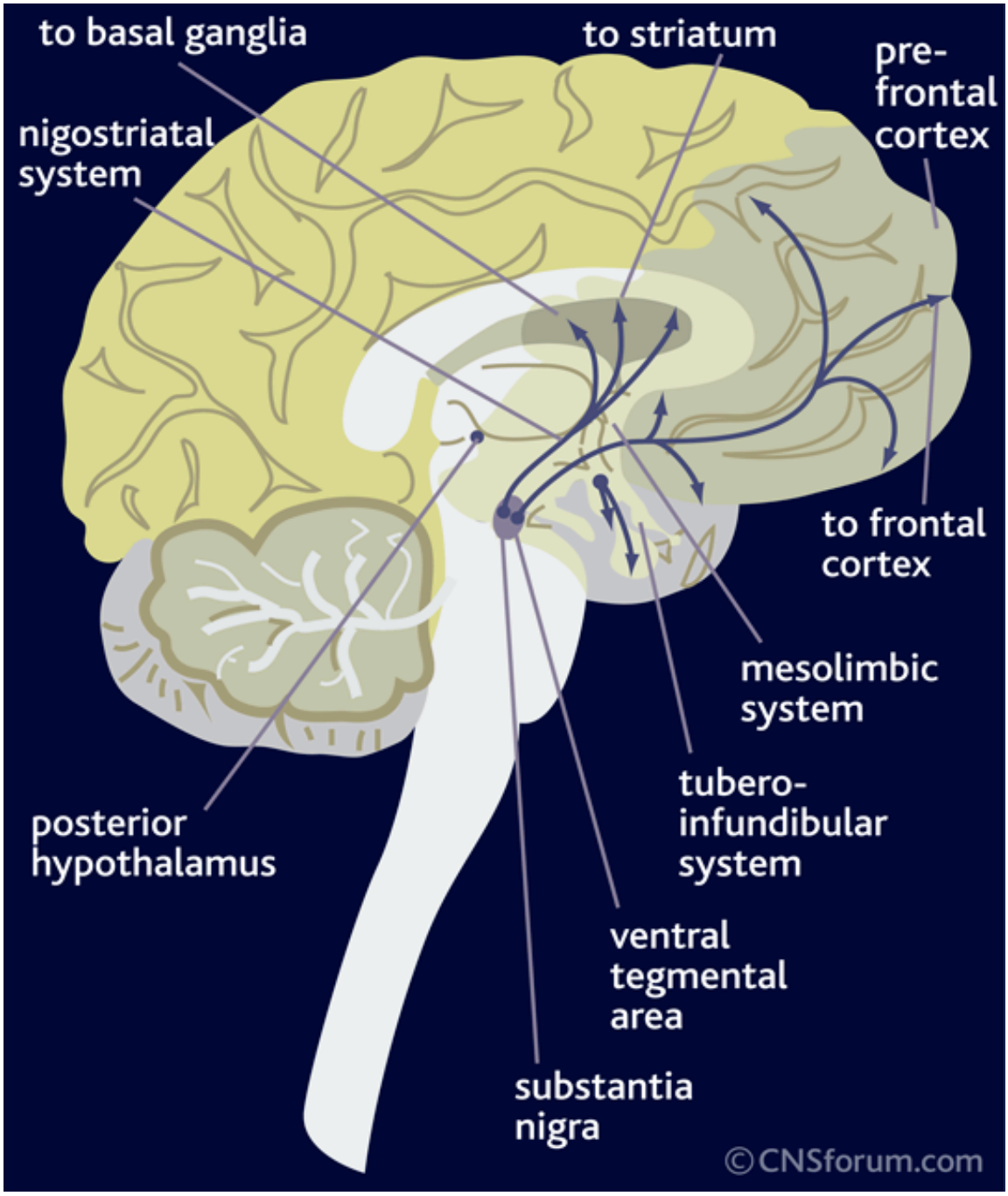

Figure 3. Dopaminergic Projections in the Mammalian Brain

Illustration of major DA projections in the central nervous system. The nigrostriatal pathway originates in the substantia nigra and projects to the striatum. The mesolimbic projections originate in the VTA and project both to the nucleus accumbens (not shown) and areas in the prefrontal cortex. The final system is the tuberoinfundibular system which projects from the hypotlamamus to the pituitary. Figure originally posted at www.cnsforum.com

loss of this pathway leading to Parkinson's Disease (Ehringer and Hornykiewicz, 1960). Original studies using reserpinised animals that recovered from reserpine syndrome after DOPA treatment lead to work which demonstrated that motor dysfunction in Parkinson's patients could be overcome with L-DOPA treatments (Birkmayer and Hornykiewicz, 1961). It was later shown that selective loss of DA neurons in this pathway was the hallmark of idiopathic Parkinson's disease (Graybiel et al., 1990). Selective lesioning of this projection with injections of DA neuron specific neurotoxins, including 6-hydroxydopamine (6-OHDA), recapitulate Parkinsonian akinesia, demonstrating that this DA pathway is responsible for motor impairments typically noted in Parkinson's patients (Burns et al., 1985; Rodriguez Diaz et al., 2001; Sherer et al., 2003).

The mesocorticolimbal pathway begins in the ventral tegmental area of the midbrain and sends long axonal projections to structures including the nucleus accumbens (NAc) and to diffuse cortical areas in the forebrain. Mesocortical projections to the NAc have been associated with addiction and reward while diffuse projections to higher cortical areas are associated with more cognitive functions. A loss of cortical DA signaling results in a spectrum of disease states ranging from attention-deficit hyperactivity disorder (ADHD) to schizophrenia (SZ).

A role for DA in the mesocoritical pathway was first discussed by Olds and Milner in 1954, when it was revealed that rats would self stimulate to receive electrical input into the septal area (which included the NAc) (Olds and Milner, 1954). After mapping of DA circuits by Fuxe revealed monoamine neurons projecting into this area (Fuxe, 1965), Crow examined the role of catecholamine containing neurons in the induction of this self stimulation paradigm (Crow, 1971). This work set the stage for

investigation of DA's role in rewarding behavior. Subsequently, DA antagonists were demonstrated to block the maintenance of electrical self stimulation in this area, solidifying a role for DA in reward (Mogenson et al., 1979).

A link between drugs of abuse and DA release in the NAc was later revealed by DiChiara and Imperato in 1988, when they reported that rats administered with drugs typically abused by humans resulted in an increase in DA concentrations in both the NAc and the striatum (specifically the caudate) (Di Chiara and Imperato, 1988). Despite increased density of DA inputs into the striatum, DA concentrations were more significantly increased in the NAc. Amphetamine and cocaine preferentially displayed the highest level of DA increase over baseline, but other substances of abuse including ethanol, nicotine, and several opiates (morphine and methadone) also elicited significant NAc DA increases. Taken together, these studies differentiated the effects of the different DA pathways, revealing that DA was a principle neurotransmitter that modulated not only movement (with it's effects in the striatum) but also played a crucial role in addictive behaviors (in the NAc).

The final major DA pathway, the tuberoinfundibular tract projects from the hypothalamus to the infundibulum of the posterior pituitary (Gudelsky, 1981). Here, DA release inhibits the release of the hormone prolactin, which is important in reproduction and the reproductive cycle.

TERMINATION OF DOPAMINE SIGNALING: THE DISCOVERY OF THE DOPMAINE TRANSPORTER

Breakdown of acetylcholine at the neuromuscular junction via the enzyme acetylcholine esterase (ACHE) was recognized as the predominant mechanism by which

neurotransmitter-based signaling was terminated. Insight into biogenic amine signaling termination was first discussed by Hertting and Axelrod who reported that circulating NE could be accumulated by sympathetic nerve endings and subsequently released by stimulation of the terminals (Hertting and Axelrod, 1961). Work identifying catecholamine uptake regions in the brain revealed that both NE and DA could be specifically accumulated by distinct regions of the brain, and that this accumulation could be inhibited by co-application of either tricyclic antidepressants or drugs of abuse including cocaine and amphetamine (AMPH) (Glowinski and Axelrod, 1964; Ross and Renyi, 1967). While cocaine and AMPH inhibited both DA and NE uptake in both the cortex and striatum, the tricyclic antidepressant desipramine selectively affected NE uptake in the cortex, with little effect on DA uptake in the striatum (Ross and Renyi, 1967). The two brain regions also displayed differential accumulation kinetics for either compound suggesting the existence of different molecular mechanisms that might underlie this specificity (Coyle and Snyder, 1969).

The first discussion of cocaine binding and DA uptake inhibition comes from work by Kennedy and Hanbauer, who first correlated sodium-dependent binding of cocaine with an inhibition of DA uptake, and postulated that the cocaine binding was inhibiting DA uptake at terminals in striatum (Kennedy and Hanbauer, 1983). At the same time that DiChiara and Imperato were reporting that both cocaine and AMPH potently increased DA levels in the NAc, Ritz and co-workers showed that there was a direct correlation between displacement of the tritiated tricyclic antidepressant mazindol, and self administration of cocaine and cocaine like drugs in rats (Ritz et al., 1987). For the first time it appeared that inhibition of uptake by cocaine and cocaine analogues

might be the molecular trigger for the establishment of self-administration of these compounds in animal models. This indicated that there must be a cocaine "receptor" that was somehow coupled to DA uptake.

The cloning of the DA transporter came in 1991 when several groups using information from other recently cloned biogenic amine transporters, produced cDNA capable of mediating DA uptake into non-DA cells. Cloning of the γ-amino butyric acid (GABA) transporter sequence from rat brain tissue provided a template for investigation of other transporters which were postulated to mediate uptake of biogenic amines (Guastella et al., 1990). Soon after, the NE transporter (NET) (Pacholczyk et al., 1991), 5HT transporter (SERT) (Blakely et al., 1991; Hoffman et al., 1991), and both the rat and bovine DA transporter (rDAT, bDAT) (Giros et al., 1991; Kilty et al., 1991; Shimada et al., 1991; Usdin et al., 1991) cDNA sequences had been established and functional transporters had been expressed in non-neuronal cell lines. Hydropathy plots generated from translated amino acid sequence, which was inferred from cDNA, revealed a putative 12 transmembrane domain protein, with intracellular amino and carboxy terminal regions (Fig 4A). A large extracellular loop region containing putative glycosylation sites was also noted for this sequence (Giros et al., 1991).

Antisense RNA probes targeted against rDAT mRNA sequence confirmed expression of rDAT in the SN and VTA, and pharmacological profiling of rDAT in COS-7 cells transfected with rDAT cDNA confirmed that this sequence coded for a *bone fide* DA transporter with sodium dependent DA transport which was inhibited by AMPH, cocaine, mazindol and several GBR compounds (Giros et al., 1991). Soon after rDAT and bDAT were cloned, the human DAT (hDAT) was cloned from human SN cDNA

libraries, and revealed similar predicted topology and pharmacology as the previously cloned DATs (Giros et al., 1992; Vandenbergh et al., 1992). The cloning of the various DATs opened the door for focused studies on transporter localization and function both *in vitro* and *in vivo*.

DAT LOCALIZATION AND FUNCTION IN MAMMALIAN SYSTEMS

Initial studies of DAT localization were performed using antibodies directed against hDAT at both the amino terminus and second extracellular loop (Ciliax et al., 1995) as predicted for the hDAT structure (Giros et al., 1992; Vandenbergh et al., 1992). Initial studies using hDAT antibodies displayed specificity for both hDAT and rDAT. When tested on rat brain sections, specific rDAT staining was noted in the striatum, NAc, olfactory tubercle, and cingulate cortex (Ciliax et al., 1995). This low-resolution immunocytochemistry also revealed that DAT reactivity was limited to neuronal perikarya, as well as in dendrites and axons (Fig 4C). The highest signal emanated from terminals in the striatum (Fig 4B), and was dependent upon DA neuron elaboration into this area (as defined by 6-OHDA lesioning studies). This distribution was evocative of the earlier FIF studies examining DA in fixed brain slices, placing DAT in regions consistent with DA synthesis and storage (Fuxe, 1965).

High-resolution electron microscopy studies visualizing gold labeled antibodies directed against the rat DA transporter (rDAT) demonstrated that, that rDAT is located at the plasma membrane in various compartments of DA neurons. In the cell body, DAT was found at the plasma membrane in tubulovesicular structures. DAT was also found associated with the plasma membranes in intermediate and distal dendrites in the VTA

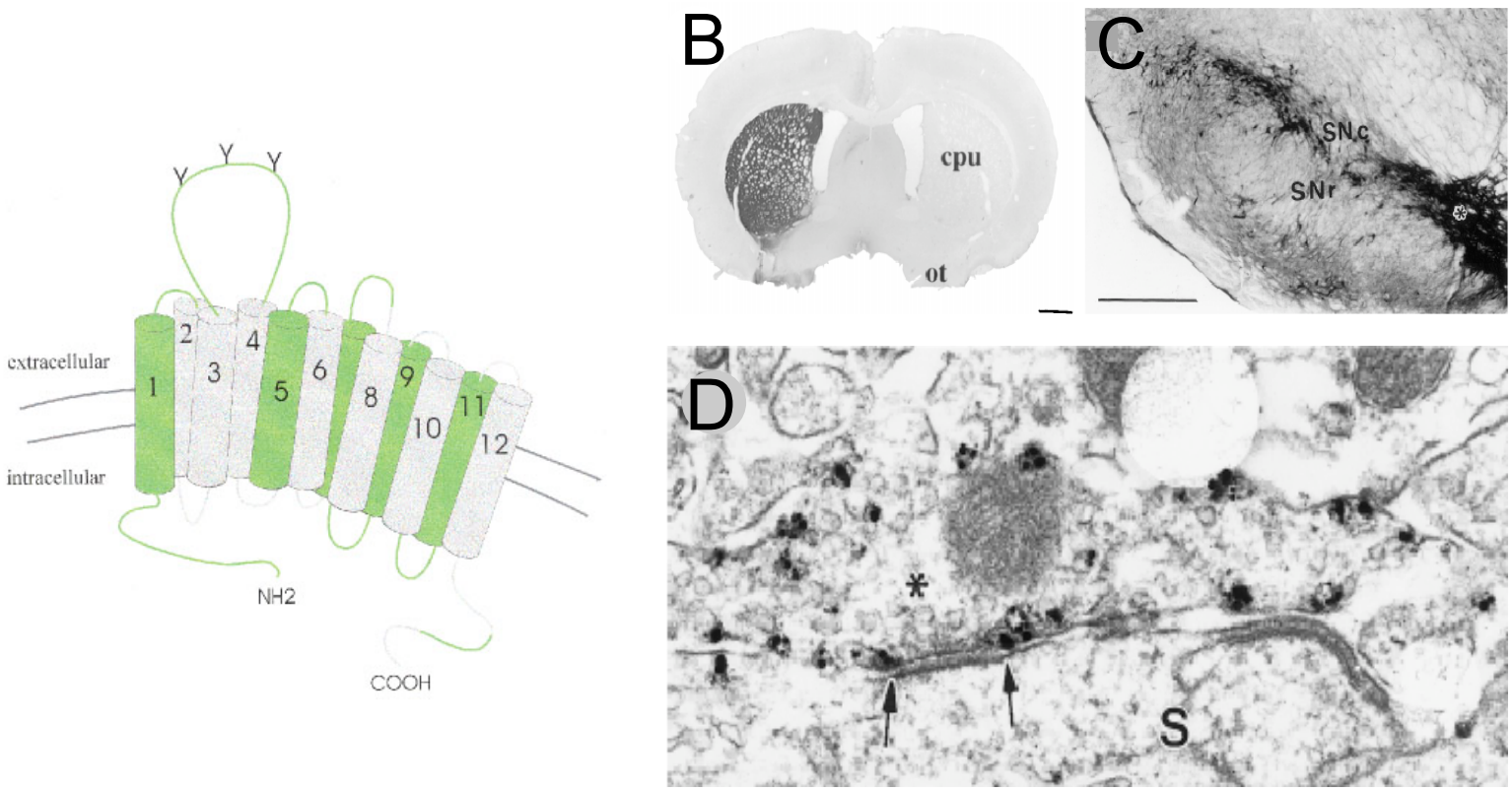

Figure 4. Dopamine Transporter Membrane Topology and Localization Within the DA Neuron.

A. Illustration of DAT inserted into the plasma membrane with putative 12 transmembrane domain topology including long intracellular NH2- and COOH-termini. A large 2nd extracellular loop that is the site of DAT glycosylation is shown. **B.** Specific staining from rat brain tissue revealing extensive rDAT localization in the striatim that is reduced with 6-OHDA lesioning. **C.** Cells in the substantia nigra also display robust labeling for rDAT in dendritic and cell body regions. **D.** High resolution imaging of a DA synapse displaying the "peri-synaptic" localization of rDAT (arrows). Images B-D originally published by Hersch et al., 1997

and SN (Hersch et al., 1997; Nirenberg et al., 1997). More specifically, DAT signal was present in the cell body in intracellular membranes, but was not detected along the cell body plasma membrane (Nirenberg et al., 1997). DAT immunoreactivity was also noted in dendritic compartments in the VTA, with the majority of immunogold signal emanating from plasma membrane inserted DAT (Nirenberg et al., 1997). Examination of DA terminals in the NAc revealed that DAT immunogold labeling was present on the plasma membranes of axons associated with varicosities as well as in the more narrow intervaricose portions of the axon (Nirenberg et al., 1997).

High resolution immuogold EM was also performed by Hersch et al. examining both the topology of rDAT and specifically the synaptic localization of DAT (Hersch et al., 1997). These studies suggested the dendritic and plasma membrane localization noted by Nirenberg, but also revealed a "peri-synaptic" localization for DAT at the synapse (Fig 4D). These studies revealed for the first time that DATs were not part of the active zone *per se*, but rather occupied sites just outside the active zone, where it may function to limit synaptic spill over of DA.

Using both and NH_2-terminal and second extracellular loop antibodies, Hirsh also confirmed the topology of the transporter, verifying that the NH_2-terminus and second extracellular loop were found on opposing faces of the plasma membrane. Also noted in these studies was a co-localization of DAT with the DA autoreceptor (D2 receptor) on the presynaptic terminal. For the first time, the flow of DA from synthesis, to excretion, reuptake, and packaging back into synapses could be modeled (Fig 2). This localization was soon confirmed in humans with hDAT residing in similar somatodendritic, and axonal compartments of DA cells in the VTA. hDAT was also localized to terminals in

the striatum and in various cortical regions consistent with DA neuron elaboration into those areas. Interestingly, DAT levels varied in these different cortical area, confirming for the first time that native DAT levels differed across brain regions (Ciliax et al., 1999).

These studies give a static image of DAT localization in fixed and sectioned tissue and do not provide an evaluation of DAT distribution in different compartments within the same cell. Several *in vivo* imaging studies including imaging in rhesus monkeys using radiolabeled ligands specific for DAT show a high density of DAT in the striatum (Fischman et al., 1997) and is consistent with an accumulation of plasma membrane elaborated DAT at nerve terminals seen in the high resolution immuno EM antibody studies (Hersch et al., 1997; Nirenberg et al., 1997). With a static picture of DAT localization in several different mammalian systems, questions concerning the mechanisms of DAT regulation and localization moved to the forefront of DAT science.

DOPAMINE TRANSPORTER REGULATION

Publication of the various DAT sequences and the generation of antibodies specific for DAT paved the way for examination of DAT protein regulation. Examination of DAT sequence revealed a conserved protein kinase C (PKC) consensus sequence in the intracellular NH_2-terminus. It had been previously shown that phorbol esters including phorbol 12-myristlate 13-acetate (PMA) were capable of activating PKC (Isakov et al., 1985). PMA exposure to COS-7 cells transiently transfected with rDAT sequence displayed a reduced transport capacity (V_{max}) by reducing the number of transporters on the plasma membrane (Kitayama et al., 1994). Further investigation of DAT regulation in native synaptosome preparations recapitulated these findings,

suggesting that this was not an epiphenomenon associated with culture conditions (Copeland et al., 1996). Activation by phorbol esters was also shown to directly phosphorylate rDAT in a PKC dependent manner, which was coupled to a reduction in V_{max} (Huff et al., 1997). This reduction in transport capacity has been linked to alterations in PKC activation, as inactivation of PKC (or PKC inhibition using bisindolylmaleimide or staurosporine) suppresses the phorbol ester induced decrease in DA transport V_{max} (Zhang et al., 1997; Zhu et al., 1997). Consistent with the activity of a kinase, activation of PKC by inhibition of protein phosphatases using okadaic acid or calyculin, proved sufficient to increase the phosporylation state of rDAT in synaptosomes (Vaughan et al., 1997). The phosporylation state of DAT may also be altered via binding to protein phosphatase 2A (PP2A), bringing together both a potential kinase (PKC) and counter phosphatase (PP2A) for the first time (Bauman et al., 2000). Current models of PKC-induced DAT decrease in V_{max} involve DAT internalization after PKC induced phosphorylation of the transporter (Pristupa et al., 1998; Melikian and Buckley, 1999; Chang et al., 2001; Loder and Melikian, 2003)

While phosphorylation of DAT by PKC results in a decrease in V_{max} and internalization of the transporter, recent studies suggest that phosphorylation may not be required for PKC dependent internalization (Granas et al., 2003; Holton et al., 2005), which suggests determinants for PKC dependent internalization via other mechanisms. Moreover, these studies suggest that PKC modulation may affect a different aspect of DAT function, namely reverse transport capacity. Whereas DAT internalization undoubtedly occurs, altered efflux would explain some initial findings that reported a change in V_{max} without a change in binding capacity of the transporter (B_{max}) indicating

that while the number of transporters had not changed, their transport capacity had shifted (Kitayama et al., 1994; Copeland et al., 1996).

Initial studies examining reverse transport for DAT revealed that PKC activation increased DA release from striatal slices that could be blocked using DAT inhibitors (Cowell et al., 2000). Efflux of DA through DAT has been shown primarily using AMPH stimulation (Khoshbouei et al., 2003). A link to PKC and potential AMPH induced efflux came from studies using alanine substitution of five N-terminal serine residues in hDAT which had been postulated to be sites of PKC phosphorylation. While alanine substitution of these residues did not effect DA uptake or surface expression, AMPH mediated efflux was completely abolished. Substitution of these alanine residues with aspartic acid residues, which mimics phosrphorylation at these sights, restored AMPH mediated efflux (Khoshbouei et al., 2004). This work suggests that NH2-terminal phosphorylation directly by PKC or via another kinase, not only affects transporter surface expression, but also enables the transporter to efflux DA as was initially noted in the Cowell studies on striatal slices.

In addition to PKC regulation of DATs, there is evidence that other second messenger systems effect DAT plasma membrane localization and function. An initial report that insulin might have an effect on DAT function appeared in 2002, when Carvelli *et al*. demonstrated that insulin stimulated the activity of hDAT in HEK293 cells. This activation depended upon PI 3-kinase activity and inhibition of this pathway resulted in a decrease in DA uptake in both the HEK cell lines and striatal synaptosomes (Carvelli et al., 2002). This effect has since been replicated COS-7 cell lines (Lin et al., 2003). More evidence for the PI-3 kinase effect on DAT regulation was revealed when dominant

negative forms of AKT were used to block insulin effects on DAT regulation (Garcia et al., 2005).

In vivo studies on streptozotocin-induced diabetic rats revealed that animals lacking insulin signaling self-administered lower levels of AMPH after becoming diabetic. This streptozotocin treatment increased DA uptake (V_{max}) without changing binding of a tritiated cocaine analogue ([^{3}H]WIN35428) (Galici et al., 2003). This apparent paradoxical effect of insulin (insulin activation increases DA uptake capacity (Carvelli et al., 2002) v. lack of insulin in diabetic animals also increases DA uptake capacity (Galici et al., 2003)) was elucidated when Owens and colleges showed that acute hypoinsulinemia in fasting animals reduced DA uptake in synaptosomal preparations. However, animals pre-exposed to AMPH and then made diabetic displayed the opposite, or enhanced DA clearance. This was the first demonstration that insulin levels might effect AMPH modulation of DAT (Owens et al., 2005).

Recently, novel signaling pathways that participate in transporter regulation have been identified. Proteins involved in the activation of the mitogen-activated protein kinase (MAPK) family have been reported to both decrease DAT activity and internalize the transporter (Moron et al., 2003). Recent work in the Blakely lab on SERT and NET using p38 MAPK activation revealed an increased transport velocity (shift in K_m) for the endogenous solute of both transporters Chinese hamster ovary (CHO) cells (Zhu et al., 2005). This mechanism was not conserved for DAT however, indicting that p38 MAPK pathways may be SERT and NET specific.

Specific modulation of DAT surface expression and activity by endogenous signaling pathways reveals orchestrated movements of DAT under differential

physiological conditions. The initial discovery of PP2A/DAT protein-protein interactions began a search for yet unknown DAT interacting proteins that might mediate these selective movements of DAT between intracellular compartments and the plasma membrane.

DAT INTERACTING PROTEINS

Since the initial discover of a DAT/PP2A complex, several interacting proteins have been reported to associate with DAT including some linked to PKC activation pathways. Studies by Torres *et al.* first demonstrated that a protein that interacts with C kinase (PICK1), directly interacts with the COOH-terminus of hDAT via a type II PDZ binding motif. Truncation of this binding motif resulted in loss of PICK1-DAT interaction and intracellular accumulation of hDAT protein in transfected midbrain cultures (Torres et al., 2001). Co-expression of PICK1 with hDAT resulted in an increased V_{max} with increased surface clustering of DAT, indicating that PICK1 might stabilize DAT on the plasma membrane. This PDZ binding domain is important for DAT maturation in the Golgi, plasma membrane retention, and function (Torres et al., 2001; Bjerggaard et al., 2004). Evidence from Torres *et al.* suggested that this binding domain might also mediate synaptic targeting of DAT in midbrain cultures. However, Bjerggaard *et al*. went on to show that in cell culture, the PDZ binding domain is not critical for plasma membrane expression but that ablation may correlate with a decreased expression and result in intracellular accumulation. To date, the cellular and subcellular distribution of DATs *in vivo* remains unknown and the effects of PDZ ablation on DAT localization in an intact nervous system have not been studied.

Another PKC interacting protein, the receptor for activated C-kinase (RACK1) has also been reported to interact with the N-terminus of hDAT (Lee et al., 2004), which puts RACK1 close to NH_2-terminal PKC consensus sequences important for DAT modulation.

Non-PKC interacting proteins have also been found to physically associate with DATs *in vitro*. The SNARE protein syntaxin 1A has been reported to interact with the NH_2-terminus of several monoamine transporters and has recently been demonstrated to interact with DAT (Sung et al., 2000; Lee et al., 2004). The synaptic protein α-synuclein, which is implicated in the DA neurodegenerative disease, Parkinson's disease, has also been found to associate with DAT and results in a decrease in V_{max} with no change in DA affinity or K_m *in vitro* (Wersinger and Sidhu, 2003). *In vivo* expression of both mutant and normal human α-synuclein in *C. elegans* DA neurons resulted in an increased susceptibility to the neurotoxin 6-OHDA, a process that is known to be DAT-1 dependent (Lakso et al., 2003; Kuwahara et al., 2006).

Another presynaptic adaptor protein was recently demonstrated to interact with the COOH-terminus of DATs, providing a link to intracellular signaling pathways known to signal via tyrosine kinases. Yeast two hybrid experiments using the COOH-terminus of DAT revealed an interaction with the LIM domain containing protein Hic-5 (Carneiro et al., 2002). DAT interaction with Hic-5 resulted in reduced DA uptake in co-transfected cells due to a reduction in plasma membrane associated transporters. This interaction was dependent upon the Hic-5 LIM domain *in vitro*, and an *in vivo* interaction was reported using co-immunoprecipitation from striatal brain extracts.

Investigation into the human movement disorder, early onset torsin dystonia, which results from mutant torsinA protein accumulation in DA neurons, revealed an *in vivo* interaction of torsin with DAT. Expression of wild type torsinA in *C. elegans* DA neurons revealed that torsin expression reduced 6-OHDA induced DA toxicity and leads to sequestered GFP:DAT-1 fusion proteins in cell bodies within the DA neurons (Cao et al., 2005). Mutant torsins lack this protective effect in *C. elegans* DA neurons. Although direct interaction was not tested, GFP:DAT-1 sequestration in cell bodies indicates that torsin may form a complex with DAT-1 *in vivo*, an hypothesis that should be investigated further.

THE *C. elegans* DOPAMINE TRANSPORTER

Jayanthi *et al.* first described the cloning of a *C. elegans* DAT-1 protein and reported similar structure and pharmacology to other known DATs, with a 46% amino acid identity to the human DAT, including conservation of a type two PDZ binding domain at the distal COOH-terminus (IML) (Jayanthi et al., 1998). *In vivo*, DAT-1 acts as a gateway for the neurotoxin 6-OHDA, with either pharmacologic or genetic ablation of the transporter leading to a sparing of DA neurons in a *C. elegans* toxicity model (Nass et al., 2002). A 700 bp fragment 5' of the DAT-1 translational start is sufficient to drive expression of GFP in all DA neurons in *C. elegans*, providing an opportunity for targeted expression of fusion proteins in an intact nervous system *in vivo* (Nass et al., 2001).

The DA nervous system in *C. elegans* is well studied (for review see Chapter II) and the recent discovery of a DAT homologue (DAT-1) provides unique opportunities for

the examination of both native localization of DAT-1, but also study the dynamics of fluorescently labeled DAT-1 molecules *in vivo*, using intact *C. elegans* DA neurons.

SPECIFIC AIMS OF THIS THESIS

The C. elegans model presents important opportunities to gain insight into machinery supporting the cellular localization of DAT proteins. Germaine to our proposed study of DAT-1, the VMAT *C. elegans* homolog CAT-1 was examined by indirect immunofluorescence in both wild type (N2) and mutant *C. elegans* strains (Duerr et al., 1999). In terms of GFP translational fusions, the synaptic vesicle motor protein UNC-104 has been directly visualized in *C. elegans* neurons, and mobility rates for this protein have been determined (Zhou et al., 2001), providing a precedent for the study of GFP based trafficking studies *in vivo*. Cloning of the DAT-1 promoter region and transcriptional expression of GFP also offers DA specific expression of exogenously introduced proteins in living nematodes (Nass et al., 2002). DA specific toxicity using 6-OHDA, which has been demonstrated to be DAT-1 dependent, provides a basis for examination of DAT-1 function *in vivo*. Thus, the specific aims of my project were to:

I. Develop antibodies specific for DAT-1 and use these antibodies to determine the native localization of DAT-1 in wild-type (N2) animals and compare this localization to GFP:DAT-1 fusion proteins and establish whether DAT-1 is enriched in synaptic compartments as found in mammalian DA neurons.

II. Verify the function of GFP:-DAT-1 fusions using 6-OHDA toxicity assays and examine the impact of different mutant lines on GFP:DAT-1

localization, including examination of a truncated GFP:DAT-1 fusion lacking the PDZ binding domain *in vivo*.

III. Develop methods for examination of GFP:DAT-1 movements and localization in an intact DA nervous system *in vivo*.

CHAPTER II

THE *C. ELEGANS* DOPAMINERGIC NERVOUS SYSTEM

INTRODUCTION

The use of catecholamines as neurotransmitters in *C. elegans* was first suggested by Sulston and colleagues who, using formaldehyde induced fluorescence (FIF) techniques, identified both 5HT and DA in the *C. elegans* nervous system (Sulston et al., 1975). A combination of FIF and serial EM reconstruction resulted in an anatomical wiring of a DA nervous system in *C. elegans*, with a screen examining mutants that had lost FIF identifying several genes important for DA synthesis and accumulation. The first example of direct DA effects on *C.elegans* mediated behavior came in 1982 when Huang *et al.* identified several DA induced phenotypes including egg laying, movement, and male mating behavior (Huang et al., 1982). The publishing of the *C. elegans* genome (consortium, 1998) resulted in cloning of several DA receptors and the identification of the *C. elegans* DAT (DAT-1). Genetic manipulations further elucidated pathways of DA signaling, implicating cellular signaling networks responsible for DA mediated behavior. In this chapter, I will review what is known about the *C. elegans* DA nervous system, moving from DA anatomy, to DA-mediated behaviors, and finally to biological molecules that support DA synthesis, storage, reuptake and DA signaling.

C. elegans DA NEUROANATOMY

The *C. elegans* hermaphrodite, the principally propagated form of the organism, is comprised of 959 somatic cells including 302 neurons. Remarkably, all neuronal connections have been determined by serial EM reconstruction (Ward et al., 1975; White et al., 1986; Hall and Russell, 1991). At these synapses, nematodes rely on many of the same neurotransmitters used in mammalsincluding DA, 5HT, acetylcholine, glutamate and GABA (Rand et al., 1998; Koushika and Nonet, 2000). DA was originally detected in *C. elegans* by its characteristic formaldehyde-induced fluorescence (FIF), revealing 8 DA neurons in the hermaphrodite with an additional set of 6 DA neurons specific to male worms (Sulston et al., 1975). Sulston originally described the DA neurons in both the hermaphrodite and male, describing "bilateral symmetrical pairs and processes". The most anterior of these cell pairings is the left and right ventral cephalic neurons (CEPvL and R) (Fig 5A, B, & C). These neurons reside in the isthmus between the anterior pharangeal bulb and the posterior bulb or the "grinder", just anterior to the largest collection of ganglia in the worm known as the nerve ring (NR). These neurons send long "dendritic-like" projections up to the nose of the animal, and have been identified as important in dictating basal slowing in response to bacterial lawn (Sawin et al., 2000). The ventral CEP group also sends "axonal-like" projections into the NR where they make synaptic connections with multiple partners including reciprocal connections between CEPvL to CEPvR (Table 1). The next DA pairing lies just posterior to the NR on the dorsal aspect of the animal and is part of the cephalic neuron grouping (CEPdL and CEPdR). These neurons are just anterior to the posterior

The *C. elegans* Dopaminergic Nervous System

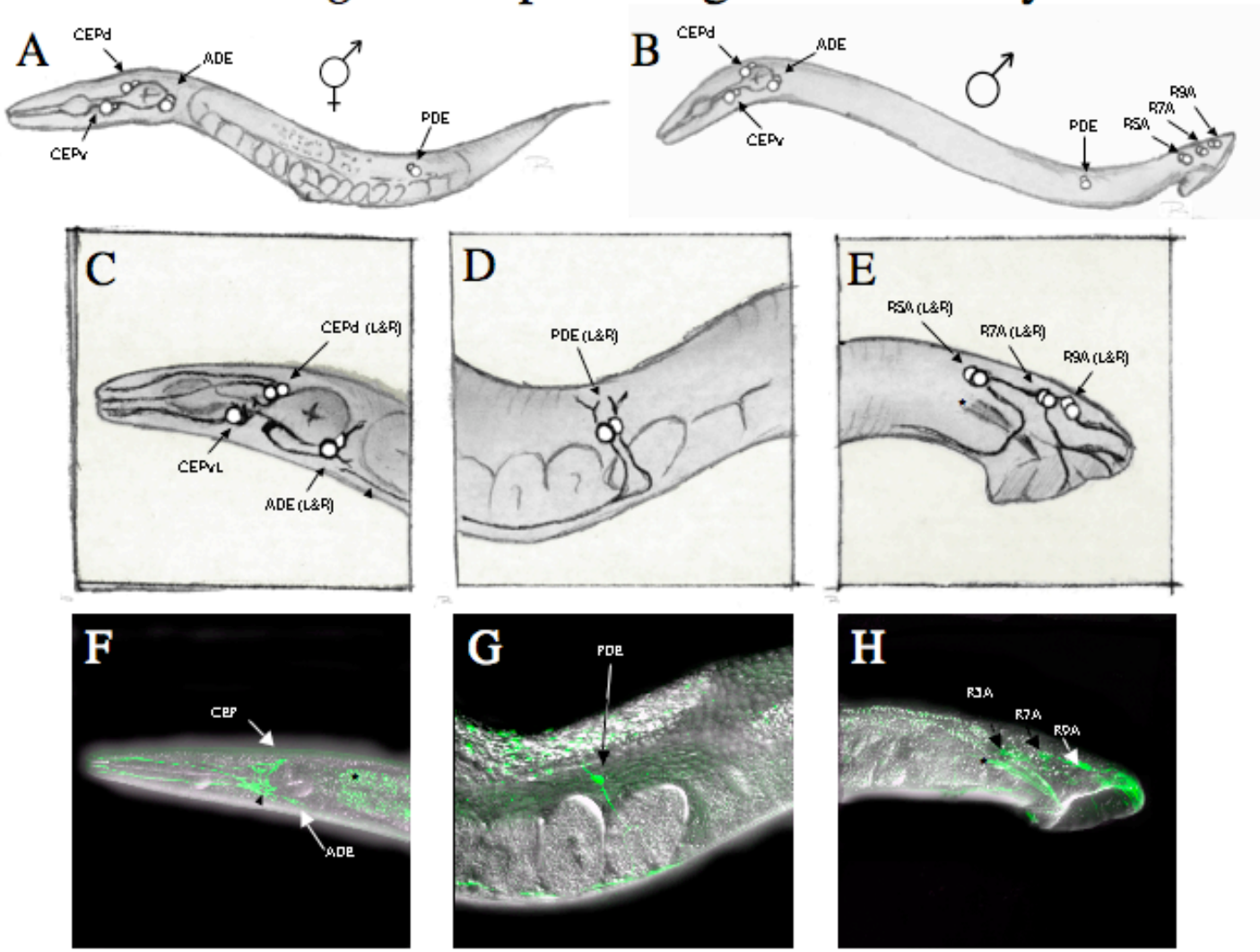

Figure 5. Anatomy of Dopaminergic Neurons in *C. elegans*.

A-E. Illistration of DA cell bodies and dendritic/axonal projections in both the hermaphrodite and male.

A. DA neuronal cell bodies in the hermaphrodite are illustrated as white spheres in their respective locations throughout the nematode body. The CEP cell bodies both dorsal (CEPd) and ventral (CEPv) reside in the isthmus between the pharangeal and terminal muscle bulbs used for feeding. The ADE neurons lie both posterior and ventral to the terminal bulb as depicted. The final DA neuronal pair in the hermaphrodite are the PDE cell bodies which lie halfway between the vulva and tail in the ventral aspect of the nematode body.

B. Male neuroanatomy of DA neurons includes the CEP, ADE, and PDE cell groups with an additional 6 cell bodies in the male tail used for mating. These neurons line the dorsal ridge of the tail and are divided into 3 sets called R5A, 57A, and R9A respectively.

C. Magnified illustrations of the DA neuron anatomy in the head. CEP (both dorsal and ventral) send small "axonal-like" projections into the nerve ring with long "dendritic-like" projections up to the nose which terminate in sensilar endings. The ADE neurons send "dendritic-like" projections to the lateral walls (both left and right) which terminate in sensilar endings. The ADE "axonal" projections move along the ventral aspect of the body anteriorly where they form a large ventral ganglion. PDE projection termination is noted (arrowhead) along the ventral aspect of the body, just posterior to the ADE cell bodies.

D. Magnified illustration of the DA neuron anatomy of the mid-body. PDE neurons send small "dendritic" projections to the lateral aspect of the muscle walls (both left and right) where they terminate in sensilar endings. The PDE sends a long "axonal" projection which begins ventrally, and then moves both anteriorly, and posteriorly (not shown) along the ventral nerve cord.

E. Magnified illustration of the male DA neuron anatomy in the tail. R5A, R7A, and R9A cell bodies send long projections along the dorsal ridge of the tail and into sensory rays of the tail. Autofluorescence from the mail spicule is seen in H and is noted in the illustration (asterisk).

F-H. Fluorescently labeled DA neurons in an intact living nematode. 3D reconstruction of confocal images used to visualize DA neurons *in vivo*. Image stacks were taken at 0.5μM using two-channel imaging for both green fluorescent protein (GFP) and differential interference contrast (DIC) conditions. 3D reconstruction was performed using Zeiss LSM 510 software.

F. DA neurons and projections in the head of the nematode using cytosolic GFP expressed using the DAT-1 promoter *in vivo*. Note long CEP projections into the nose of the animal and extensive elaboration of signal in the nerve ring (NR, arrowhead). A small amount of autofluorescence can be seen in the gut (asterisk).

G. PDE projections in the mid-body of the nematode *in vivo*. Only one of the two PDEs is visible in this image but both the apical "dendrite" and ventral "axonal" projections can be seen. Note that the predominance of the GFP signal is elaborated along the ventral nerve cord, projecting up to the head.

H. Male DA neuroanatomy *in vivo*. R5A, R7A, and R9A cell bodies can be visualized along the dorsal ridge of the male tail, sending projections down into the tail sensory rays. Spicule autofluorescence can be seen just below R5A cell body (asterisk).

bulb and send long "dendritic" projections up to the nose and short "axonal" projections into the nerve ring. All four of the CEP "dendritic" projections terminate in the nose where they are surrounded by both sheath and socket cells (CEPsh and CEPso), which envelope the sensilum ending (Ward et al., 1975). The CEP neurons as a group synapse on several neurons in the NR including the RIP neurons which are part of the pharangeal nervous system (Riddle, 1997) and neurons that are important for navigation in *C. elegans* (Gray et al., 2005) including the interneurons RIA and RIB and the head and neck motor neurons RIV, SIA, SIB, and SMB.

The third pair of neurons in the head of the worm is known as the anterior deirid neurons (ADEL and ADER) and are located both ventrally and posterior to the posterior bulb (Fig 5). ADE "dendrites" terminate in the anterior deirid located bilaterally on both sides of the worm head. These dendritic projections terminate in a sensory organ known as a sensillum, which is embedded in the cuticle and made up of the ADE dendritic projection and a sheath and socket cell. The ADEs send their "axonal" projections along the ventral aspect of the terminal bulb where they come together into what Sulston originally described as a "ventral ganglion" which lies just posterior to the NR. Synaptic connections from the ADEs can be traced to several neurons in the NR including ALM, AVA, and AVD neurons (Chalfie et al., 1985) involved in touch response.

The final pair of DA neurons in the hermaphrodite reside in the dorsal aspect of the worm, halfway between the vulva and the tail. This pair known as the posterior deirid neurons (PDEs) send "dendritic" projections that terminate in the posterior deirid and make up a sensilla similar to the sensillar ending noted for the ADE neurons. Again, the PDE ending is supported by both a sheath and a socket cell and embedded in the cuticle.

Table 1. Synaptic wiring of DA Neurons in *C. elegans*.

Connectivity of the DA head neurons was documented by White *et al*. and is annotated in wormbase (www.wormbase.org). DA neurons make extensive connections that are noted below. Each neuron listed receives input from one of the 6 DA head neurons. The specific neuron is noted using superscripted numbering system, with a key below the list.

DA wiring:

DA neurons synapse on: ADEL[2]R[1], ADAL[1]R[2], ADLL[5], ALA[2], ALMR[1,2], ASGR[6], AVAL[1,2]R[1,2], AVDL[1]R[2], AVEL[1,4,6]R[2,3,5,6], AVJR[1,2], AVKL[1,2]R[2], AVL[1], BDUL[1]R[4], CEPdL[1]R[2], CEPvR[6], FLPL[1,2]R[2], IL1L[1,3]R[4], IL2L[1], IL1dL[3]R[4], IL1vL[5]R[6], IL2vR[6], OLLL[5], OLL[1,3]R[2,4,6], OLQdL[3]R[4], OLQvL[5]R[6], PVR[2,6], RIAL[1], RIBL[3,5]R[4,6], RICL[3,4,5,6]R[3,4,5,6], RIFL[1]R[2], RIGL[1,2]R[1,2], RIH[1,2], RIPL[3,5]R[4,6], RIS[3,4], RIVL[1,6]R[1,2], RMDL[1]R[2], RMDdL[2,4,5]R[6], RMDvL[3]R[4], RMGL[1,3], RMFL[4,6], RMHL[1,2,4,5,6]R[3,4,5], RMGR[4,6], SAAvR[2], SDQR[2], SIAdL[4] R[1,3], SIAvL[5]R[2,6], SIBdR[1], SMBdR[1,3,4], URAdL[3]R[4], URAvL[5]R[6], URBL[1,3,5]R[4], URXL[3], URYdL[3]R[4], URYvL[5]. Mu_bod[4]

[1]ADEL, [2]ADER, [3]CEPDL, [4]CEPDR, [5]CEPVR, [6]CEPVL.

The PDE "axonal" projections project ventrally from the PDE cell body, and run both anteriorally and posteriorally along the ventral nerve cord. Little is known about the synaptic connections made by the PDE neurons.

The male tail contains 3 extra sets of DA containing neurons required for mating (Loer and Kenyon, 1993; Liu and Sternberg, 1995). With serial EM reconstruction done only in hermaphrodites, no specific synaptic connections are mapped for these neurons.

C. ELEGANS DOPAMINE SUPPORTED BEHAVIOR

The effects of DA in the nematode have primarily been elucidated through analysis of animals where DA has either been reduced to inhibit DA signaling, or augmented to enhance DA signaling. Reduction of DA can be achieved via laser ablation of DA specific neurons, whereas DA enhancement can be achieved via the exogenous application of DA. These studies have indicated a role for DA in a wide array of nematode behaviors including egg-laying, defecation, basal motor activity, sensation/response to food sources, and habituation to touch. Below, we review these behaviors as a context for understanding the physiological impact of DA signaling proteins and as a discussion of paradigms that show promise for further dissection of DA-linked genes.

Egg-laying:

Following the elucidation of egg-laying deficits arising from deficits in response to exogenous and endogenous 5-HT (Trent et al., 1983; Desai and Horvitz, 1989), Schafer and Kenyon described the effects of exogenous DA on both egg laying and

movement (Schafer and Kenyon, 1995). These effects display adaptation where, initially, animals exposed to high concentrations of DA (3mM) decrease egg-laying frequency and are rapidly paralyzed. Both egg-laying and movement return to normal over the course of several hours despite continued DA exposure. Increasing DA concentrations, once normal activity had returns, has no effect, indicating that both of these behaviors adapt in the presence of DA (Schafer and Kenyon, 1995). Adaptation to DA requires prolonged exposure (at least 3 hours) and is reversed in a similar time course. A forward genetic screen for mutants that failed to adapt to DA identified an animal that was UNC or uncoordinated and contained an allele of *unc-2*. This gene proved to be important for modulating this DA mediated plasticity. The UNC-2 protein is a voltage gated calcium channel required for proper movement in *C. elegans* (Brenner, 1974; Schafer and Kenyon, 1995). A novel allele of *unc-2* was identified in this screen, suggesting that DA-induced activation of unc-2 is required for this DA adaptation. Cloning of the unc-2 gene revealed homology to mammalian voltage gated Ca^{++} channels. Mosaic expression of UNC-2 coupled with *in situ* hybridization studies indicated that adaptation to DA is only rescued when UNC-2 is expressed in the VC and HSN neurons (Schafer and Kenyon, 1995). Recently, expression of the human migraine-associated Ca^{++} channel CACNA1A was found to be sufficient to rescue 5HT defects seen in *unc-2* animals but no DA behaviors were tested (Estevez et al., 2004). Interestingly, Olson and coworkers have established that D2 DA receptors regulate voltage-gated calcium channels in mammalian striatal medium spiny neurons via a macromolecular signaling network involving the proteins Shank and Homer (Olson et al., 2005). Further manipulation of adaptation supported by *C. elegans* calcium channels may allow for a richer examination of these

interactions *in vivo* as well as provide for the elucidation of additional effectors that lie downstream of DA-regulated calcium signaling and which likely have mammalian homologues.

Soon after Schafer and Kenyon reported their findings on DA and 5HT dependent adaptation, Weinshenker *et al.* re-examined 5HT effects on egg laying behavior and uncovered a 5HT independent pathway involving DA. In their proposed model for 5HT-induced egg laying, the hermaphrodite specific neuron (HSN) releases 5HT, which acts directly on egg laying muscles to induce their contraction. However, the egg laying defective (egl) mutant *egl-2(n693)* lays eggs in response to the 5HT transporter inhibitor imipramine but not 5HT itself (Trent et al., 1983). In an attempt to elucidate 5HT's role in egg laying in light of this result, Weinshenker *et al.* used an *egl* mutant that lacked the HSN neuron (*(egl-1 (n478)* and *(n986)*) and tested various compounds including imipramine and the D2 antagonists chlorpromazine on egg-laying. In their study, both imipramine and chlorpromazine induced egg-laying in the egl-1 background, implying that the effects of these compounds were not dependent on HSN release of 5HT. Further studies revealed that egl-2 encoded an imipramine-sensitive potassium channel (Weinshenker et al., 1999), clarifying why the serotonergic HSN neuron was not required for imipramine reinstatement of egg laying in egl-2 mutants. However, they fail to explain the actions of D2 antagonists, leaving open a role for DA in the egg laying circuit (Weinshenker et al., 1995). We will return to this topic following a review of DA receptors.

Defecation:

Application of exogenous DA decreases enteric muscle contractions in wild type worms resulting in slowed defecation (Weinshenker et al., 1995). The *egl-2 (n693)* mutant that originally was found to exhibit egg-laying defects also inhibits enteric muscle contractions (EMCs). This mutant is a gain of function mutation that displays enhanced potassium current at low voltages and that is expressed in *C. elegans* enteric muscles (Weinshenker et al., 1999). This suggests that DA normally enhances potassium channel activation and would explain why D2 antagonists such as chlopromazine, haloperidol, butaclamol, droperidol, and pimozide reinitiate defecation (Weinshenker et al., 1995). Since UNC-2 expression is also found in GABAergic DVB neurons, which work with AVL to control enteric muscle contractions (McIntire et al., 1993), it is not yet clear whether DA regulation occurs at the level of the AVL or on the enteric musculature itself. Regardless, DA modulation of potassium channels is also a critical facet in mammals of DA-mediated cortical plasticity (Dong et al., 2005) and thus further evaluation of the components supporting DA regulation of egl-2 in defecation circuits in the worm may shed light on pathways critical to higher brain function in man.

Movement:

Exogenous DA causes rapid and reversible paralysis in *C. elegans*. This behavior displays adaptation or desensitization involving the activity of the voltage gated calcium channel UNC-2 (Schafer and Kenyon, 1995). *Unc-2* mutants displayed a leftward shift in paralysis induced by DA indicating a greater sensitivity to DA induced paralysis

compared to wild type worms. Although this shift in DA potency was slight, the ability of *unc-2* mutants to adapt to DA was severely compromised to the point where the majority of *unc-2* animals display no spontaneous movement with prolonged DA exposure, whereas wild type animals regain movement after 3 to 4 hours in DA. Expression of unc-2 was noted in both the VC and HSN neurons (Schafer and Kenyon, 1995). This expression profile was extended to most motor neurons in the ventral nerve cord and the nerve ring motor neuron SDQR (Mathews et al., 2003). Expression was also seen in the head and tail region including in olfactory sensory cells AWC and the GABAergic tail neuron DVB.

As often happens, progress in one area (DA signaling) leads to insights in another (channel biology). Cloning of various *unc-2* mutations revealed that mutations sufficient to alter adaptation to DA reside in various locations in the UNC-2 protein, likely resulting in a loss of function of this channel (Schafer and Kenyon, 1995). Indeed, insertion of identified *unc-2* mutations into the rat voltage gated calcium channel alpha 1A subunit (the most homologous to UNC-2) and electrophysiological experiments revealed that mutations caused a variety of current defects from total loss of calcium current (e55 mutation), to rapid inactivation (ra612) or reduction of pre-pulse potential (Mathews et al., 2003). These studies underscore the opportunities available in combining forward genetic studies of model organisms with studies of mammalian channel orthologs (Weinshenker et al., 1999; Wei et al., 2005). Importantly, mammalian calcium channels are targets of DA modulation (Neve et al., 2004), and thus lessons learned in the effort to explore DA modulation of motor activity are likely to be relevant for the wide variety of actions of DA in the mammalian CNS.

Basal slowing response:

Besides its use for studies of the control of basal motor activity, the nematode model exhibits fine-tuning of motor plasticity that engages signaling pathways responsive to DA. *C. elegans* slow in the response to a bacterial lawn (Sawin et al., 2000). This response is mediated by either DA or 5HT depending on the dietary history of the animal. DA dictates basal slowing response in well-fed animals. Under these conditions, the TH mutant *cat-2(e1112)* shows no basal slowing response, indicating that this behavior is DA mediated (Sawin et al., 2000; Chase et al., 2004). Exogenous DA restores basal slowing response in *cat-2(e1112)* mutants as well as in the *cat-4(e1141);bas-1(ad446)* double mutant (an animal which lacks catecholamines altogether), indicating that a lack of endogenous DA is responsible for this behavior. Laser ablation of DA neurons has led to the identification of neurons that likely account for DA-mediated motor slowing in response to food (Sawin et al., 2000), specifically implicating actions of CEP neurons. Interestingly, double ablation of both the CEP and ADE neuronal cell groups restored the basal slowing response, suggesting more complex control of this behavior than initially recognized. Basal slowing was found to be a mechanosensory phenomenon as Sephadex G-200 beads could substitute for bacteria to elicit this response. Moreover, elimination of DA, using either the cat-2(e1112) mutant or by cellular ablation of all DA neurons in hermaphrodites, removed basal slowing in response to Sephadex beads (Sawin et al., 2000). Importantly, these studies reveal a role of DA in short-term motor plasticity reminiscent of actions the amine plays in fine-tuning the output of the motor program in vertebrates. Although the circuits that subserve motor

output in man are far more complex, lessons gathered regarding the neuromodulatory actions of DA in the *C. elegans* motor program can shed light on neuromodulatory integration just as studies of the modulation of the *Aplysia* gill reflex by 5HT have provided lessons relevant for learning and memory in man (Kandel and Schwartz, 1982).

Area Restricted Search:

An additional form of motor plasticity with DA support in the nematode is area restricted search (ARS) for food (Hills et al., 2004). Search behavior is displayed by organisms when food is encountered and is typified by an increase in turning behavior (Bell, 1991). This behavior is thought to arise from an organism's need to conserve energy in the search for food, with search area increasing over time once the local food source has been exhausted. This change from a focal to a more global search area results from a decrease in turns after food depletion. If initially exposed to a bacterial lawn, nematodes that are subsequently moved to a plate with no bacteria display a high number of acute-angled turns (< than 50°) in search of food. After 30 minutes without food, the number of these high angled turns is reduced, indicating that the worms are extending their search area (Hills et al., 2004), an activity that can be quantified using an ARS index determined by the number of turns observed in the first period divided by the number of turns observed in the last or test period. In contrast to the motor slowing response previously described, Hills and coworkers observed that changes in the ARSi were only seen in response to food and not in response to other sensory stimuli (Hills et al., 2004). Genetic ablation of all DA neurons resulted in an inability to change ARS after 30 minutes on plates lacking food, indicating that either synaptic DA action or humoral DA

provided from one or more of these sources is required for ARS. Ablation of either the CEP or ADE neurons alone had no effect on adaptation, whereas PDE ablation resulted in a reduction in habituation, suggesting that PDE signaling is required for learning to expand ARS and decrease turning behavior. Interestingly, ablation of both the ADE and PDE neurons results in a hyperturning phenotype that still habituates after 30 minutes off food, suggesting that multiple DA neurons coordinate to modulate ARS. Here, an intact CEP neuron may mediate hyperactive turning, an activity that is potentially opposed by ADE output. Because habituation is still seen in this experiment, DA release in the nerve ring by CEP may be sufficient for ARS. However, ADE inputs into the nerve ring are not sufficient to mediate ARS in the PDE/CEP double ablation implying that CEP-specific innervations are required. When both CEP and PDE neurons are ablated, habituation off of food is completely lost, implying that these two neurons work synergistically to mediate this behavior. One complication in this analysis is that there appears to be two distinct behaviors assayed in this experiment. The first is head turning frequency, and the second is ARS. Head turning frequency is increased by CEP neurons and appears to be inhibited by both ADE and PDE neurons. PDE neurons seem to be required for ARS because in the ADE/CEP double mutant ARS still occurs while in the genetic triple mutant habituation is lost while hyperturning is retained.

Interestingly, exogenous DA increases the number of high angle turns, implying that DA is sufficient to activate ARS. Endogenous DA was also shown to be required for ARS because *cat-2* (tyrosine hydroxylase, see below) mutants that contain little endogenous DA do not show increased frequency of head turning. Another interesting result of this research is the fact that movement through *E. coli* itself is required to

reinstate ARS (Hills et al., 2004), although it is not clear whether this activity engages food-source responsive circuits releasing endogenous DA or reflects an independent effect. Interestingly, animals that are allowed to feed display reduced ARSi scores, indicating habituation. Habituation is a common feature of the mammalian DA reward pathway and is thought to drive reinstatement of drug use (Gerdeman et al., 2003). As such, future investigations of DA support for habituation of the ARS pathway may provide useful clues to plasticities underlying drug abuse.

Another form of habituation that appears to involve DA is habituation to nose tap where, after a series of nose taps, worms will learn that the mechanical stimulation is non-threatening and will stop reversing (Rankin, 1991; Rankin and Broster, 1992; Rose and Rankin, 2001). Touch response requires five sensory neurons (ALMs, PLMs, and AVM) along with eight interneurons (AVAs, AVBs, AVDs, and PVCs) (Chalfie et al., 1985). The tap withdrawal response requires 3 additional neurons (PVDs and the DVA interneuron) (Wicks and Rankin, 1995). Mutants that cannot produce DA via tyrosine hydroxylase (*cat-2*, see below) are defective in normal habituation to non-generalized tap response but this response can be rescued with exogenous DA (Sanyal et al., 2004). Thus DA may play a more general role in habituation of motor responses, whether elicited by food, mates, or threatening stimuli. Although Sanyal *et al.* note that the CEP and PDE neurons do not synapse directly on neurons mediating the touch habituation response (Sanyal et al., 2004), this still leaves inputs from the ADE neurons which make direct synaptic connections on ALM, AVA, and AVD (Table 1) neurons (White et al., 1986) which are utilized in both touch (Chalfie et al., 1985) and tap habituation (Rose and Rankin, 2001). Work by Chase *et al*. underscores the likely long range, non-synaptic

actions of DA in the nematode (Chase et al., 2004), similar to the proposed role of DA in "volume transmission" in the mammalian CNS (Rice, 2000). Thus, although evidence of humoral signaling exists in the *C. elegans* literature (Chase et al., 2004), ADE inputs to these circuits need to be explored further.

C. ELEGANS DOPAMINE BIOSYNTHESIS AND STORAGE

Soon after the identification of nematode DA neurons, worm biologists implemented forward genetics to search for genes required for the production and storage of DA. Screening for mutations that produce a loss of FIF led to the identification of 6 independent catecholamine mutants (*cat-1* through *cat-6*) (Sulston et al., 1975). Cloning of several of these genes identified key proteins known to participate in either DA synthesis or storage. DA synthesis in mammalian neurons begins with the conversion of the amino acid tyrosine to 1-dihydroxypheny-l-alanine (l-DOPA), the immediate DA precursor, by the enzyme tyrosine hydroxylase (TH), a process that requires the co-enzyme tetrahydrobiopterin (THB). THB is regulated by GTPcyclohydrolase (GTPCH) activity and loss of GTPCH results in down regulation of THB, resulting in decreased DA synthesis (Kapatos et al., 1999). Finally, an efficient, and more widely expressed aromatic amino acid decarboxylase (AADC) converts l-DOPA to DA. Cytosolic DA is then rapidly packaged into synaptic vesicles by VMAT where DA is stored until secreted following neuronal depolarization. Intraneuronal metabolism occurs chiefly through the actions of mitochondrial MAO enzymes, although as will be noted below, DA reuptake is thought to play a more critical role in synaptic DA inactivation.

The first DA-related mutant identified (*cat-1*) displays a loss of punctate DA accumulation normally characteristic of DA nerve terminals (Sulston et al., 1975) and is considered likely to participate in the behavior or physiology of DA storage vesicles. This suspicion was validated in 1999 when Duerr and colleagues cloned the full length cat-1 gene and identified it as a VMAT homolog (Duerr et al., 1999). CAT-1 protein was found to localize to DA and 5HT neurons (Table 2) and to be 47% identical to human VMAT1 and 49% identical to human VMAT2. Importantly, CAT-1 supports time-dependent and saturable uptake of both [^{3}H]DA and [^{3}H]5HT in permeablized CV-1 cells, consistent with its role as a VMAT (Duerr et al., 1999). Original studies performed by Sulston *et al.* used the mammalian VMAT substrate reserpine to deplete these vesicles of catecholamines and eliminate FIF indicating that mammalian VMATs and CAT-1 share similar pharmacology (Sulston et al., 1975)**.**

In situ, indirect immunofluorescence studies using antibodies directed against CAT-1 sequence revealed punctate nerve ring fluorescence reminiscent of combined DA and 5HT FIF. *In vivo*, genomic cat-1 sequences (RM#424L) rescue the DA and 5HT-like FIF deficits of *cat-1* mutants (Duerr et al., 1999). The availability of antibodies specific for CAT-1 allowed for important insights into how VMAT proteins are localized to synapses. Although VMATs are located on synaptic vesicles, the trafficking determinants of VMAT had not been defined. Unc-104 is a kinesin motor protein that is known to traffic synaptic vesicles from the cell body to nerve terminals (Hall and Hedgecock, 1991). Loss of function of this protein leads to synaptic vesicle retention in the cell body and a decrease in synaptic signaling, supporting an uncoordinated (UNC) phenotype. When CAT-1 protein was visualized in *unc-104(e1264)* mutant animals using

Table 2. *C. elegans* DA Synthesis and Transport Proteins

Dopamine Synthesis and Transport Proteins

BAS-1	Mammalian Homolog	Aromatic Aminoacid Decarboxylase	Loer and Kenyon 1993
	Substrate	L-Dopa, 5-THP	Loer and Kenyon 1993
	Antagonist	?	
	Cellular expression	Dopamine and Serotonin neurons	Hare and Loer 2004
	Mutant Phenotype	Defective Basal slowing response	Sawin et al. 2000
		Defective male tail turning (mating)	Loer and Kenyon 1993
CAT-1	Mammalian Homolog	Vesicular Monoamine Transporter (VMAT)	Duerr et al. 1999
	Substrate	DA, Tyr >5HT>NE>Oct>>Histamine	Duerr et al. 1999
	Antagonist	Reserpine	Sulston et al. 1975
	Cellular Expression	Dopamine Neurons (ADE, CEP, PDE)	Duerr et al. 1999
		Serotonin Neurons (NSM, HSN, VC4,	Duerr et al. 1999
		VC5, ADF, RIH, AIM)	Duerr et al. 1999
		Unidentifed Amine (RIC, CAN)	Duerr et al. 1999
		Male Neurons	Duerr et al. 1999
	Mutant Phenotype	Defective Basal Slowing Response	Duerr et al. 1999
		Reduced Egg laying	Duerr et al. 1999
		Decreased mating efficiency	Duerr et al. 1999
		Decreased pharangeal pumping	Duerr et al. 1999
		Defective male tail turning (mating)	Loer and Kenyon 1993
CAT-2	Mammalian Homolog	Tyrosine Hydroxylase (TH)	Lints and Emmons 1999
	Substrate	Tyrosine	
	Antagonist	?	
	Cellular expression	DA neurons (CEPs, ADEs, PDEs)	Lints and Emmons 1999
		Male tail DA neurons (R5A, R7A, R9A)	
	Mutant Phenotype	Dopamine deficient	Sulston et al. 1975
		Defective Basal slowing response	Sawin at al. 2000
		↑ Tap Habituation	Sanyal et al. 2004
		Defective area restricted search	Hills et al. 2004
		Defective slowing in Sephadex beads	Sawin et al. 2000
DAT-1	Mammalian Homolog	Dopamine transporter	Jayanthi et al. 1998
	Substrate	DA > NE, Epi > 5HT	
	Antagonist	Imipramine, Desipramine, Nisoxetine, Mazindol, GBR 12909, Nomifensine, Cocaine.	Jayanthi et al. 1998
		Amphetamine‡	Nass et al. 2002
		Imipramine	Jayanthi et al. 1998
	Cellular expression	DA Neurons (CEP, ADE, PDE)	Nass et al. 2002
		R5A, R7A, R9A in male tail	
	Mutant Phenotype	?	

‡ Data implied from *in vivo* function studies.

immunofluorescence approaches, CAT-1 vesicles were found to accumulate in the cell body, consistent with VMAT employing machinery that traffics other synaptic vesicle proteins to the synapse.

Cat-2 has been identified as a TH homolog, with CAT-2 protein displaying 50% amino acid identity with both *Drosophila* and rat tyrosine hydroxylase (Lints and Emmons, 1999). GFP promoter fusions using cat-2 promoter sequences demonstrate that CAT-2 is expressed in all DA neurons of the nematode (Lints and Emmons, 1999). In addition, *cat-2* mutants display markedly reduced DA levels (9% compared to WT) as assessed by HPLC (Sanyal et al., 2004) (Table 2).

Cat-4 has features of a GTP cyclohydrolase enzyme suitable for production of the TH cofactor THB. While cat-4 has yet to be cloned and its mechanism of action has yet to be defined, predicted amino acid alignments reveal an 83.9% homology with the human splice isoform GCH-1 of GTP-cyclohydrolase (Wormbase, www.wormbase.org).

An aromatic AADC homolog (bas-1) has been identified and is required for 5-HT supported male mating behaviors but as yet has not been implicated in DA-mediated behaviors (Loer and Kenyon, 1993) (Table 2). Recently, Hare and Loer mapped the bas-1 (C05D2.4) gene and revealed that bas-1 indeed codes for an aromatic AADC homologue that is sufficient to rescue *bas-1* mutant lines for 5-HT immunoreactivity (Hare and Loer, 2004). Although the gene encoded by C05D2.4 (bas-1) rescues serotonin immunoreactivity, other potential homologs which could retain some AADC activity exist in *C. elegans* and a small amount of 5-HT persists in bas-1 mutant lines (Weinshenker et al., 1995). Two isoforms of bas-1 were identified, bas-1a, which displayed a 41% identity to human DOPA-decarboxylase (HsDDC), and bas-1b that

included a 27bp micro-exon inserted between predicted exons 2 and 3. Although more limited information is available concerning a role for bas-1 in DA synthesis, expression of GFP reporter constructs using the bas-1 promoter region reveals DA neuron expression as would be predicted for an aromatic AADC homolog.

Despite the presence of DA catabolites (DOPAC, 3-methoxytyramine, and homovalic acid) in whole worm extracts (Wintle and Van Tol, 2001), proteins important in the catabolism of DA have not been positively identified, although several MAO and COMT homologues exist in the genome (Wintle and Van Tol, 2001).

THE *C. ELEGANS* DOPAMINE TRANSPORTER

In mammalian systems, DA signaling is primarily terminated by presynaptic reuptake mediated by the DA transporter (DAT), with a contribution of DAT to presynaptic DA levels also evident (Gainetdinov et al., 2002). Studies using DAT KO mice (Giros et al., 1996) demonstrate that, after evoked DA release, extracellular DA levels remain elevated in the absence of DAT protein. The *C. elegans* DAT (dat-1;T23G5.5, originally termed CeDAT-1) was identified by searching *C. elegans* genomic sequences for genes homologous to mammalian SLC6 family members, including cocaine-sensitive DA, NE and 5HT transporters (Jayanthi et al., 1998), specifically targeting sequences bearing a highly conserved transmembrane (TM) 1 aspartate residue thought to interact with biogenic amine substrates. The identified DAT-1 protein bears 43% amino acid identity with mammalian DA transporters with the bulk of conservation localized to the transmembrane domains (TM).

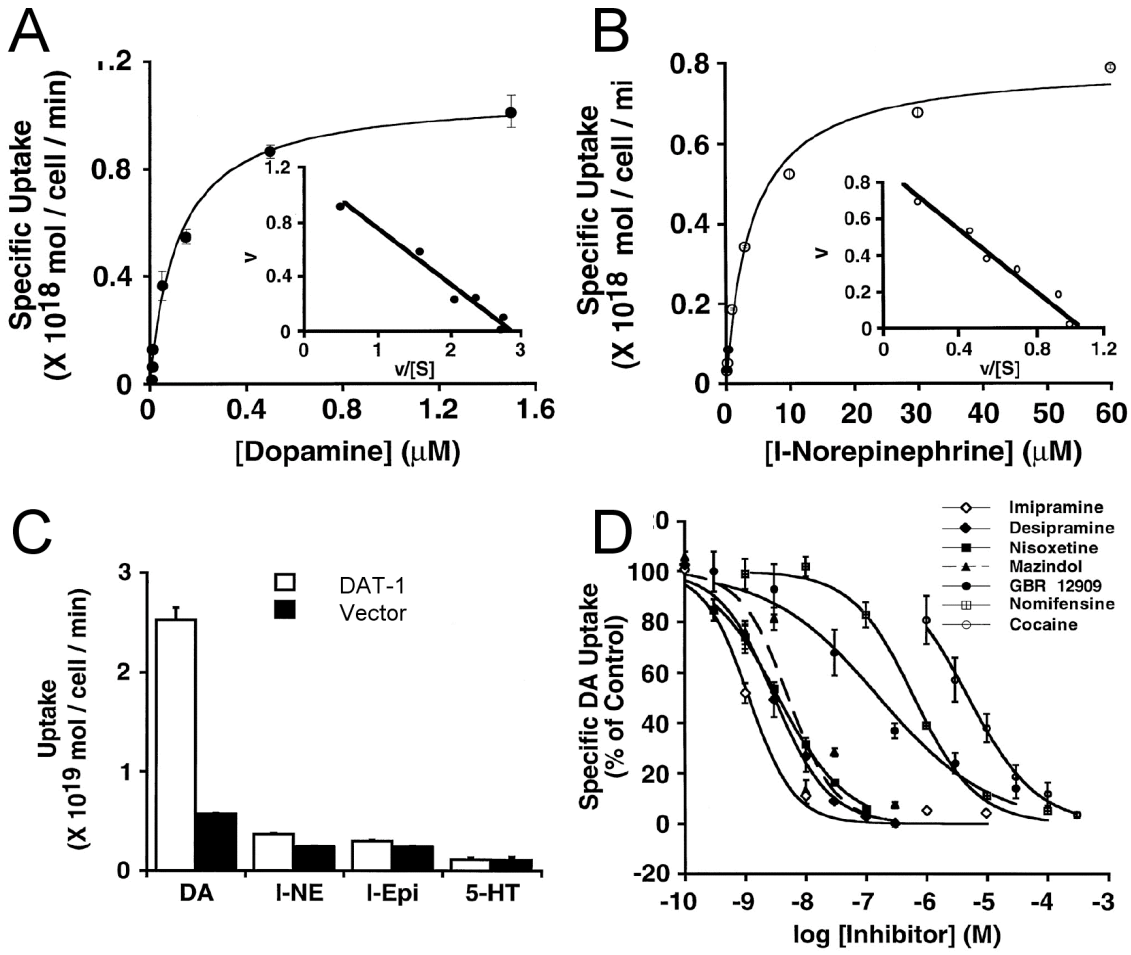

Figure 6. Validation that T23G5.5 Encodes a C. elegans DA Transporter.

A-B. Saturation kinetics of [3H]-DA (A) and [3H]-NE (B) uptake by DAT-1 in transiently transfected cells. Specific uptake was defined by subtraction of uptake activity obtained in vector-transfected cells assayed in parallel. Note the difference in axes values; ordinate legends reflect multiplication of data values by 1018 in order to obtain integer values on the y-axis. Insets, Eadie-Hofstee plots of saturation data (axis units, cell/min/liter x 1024) (figure adapted from Jayanthi et al., 1998). A. Specific uptake of 3H-DA by DAT-1. KM = 1.2 mM; Vmax = 1.08 pmol/106 cells/min. B. Specific uptake of 3H-NE by DAT-1. KM = 4.1 mM; Vmax = 0.79 pmol/106 cells/min. C. Substrate selectivity of DAT-1 uptake activity in DAT-1- or vector-transfected cells. All [3H]-labeled substrates were assayed at a saturating concentration of 20 nM. Values represent mean +/- standard deviation of three separate transfections. Ordinate legends reflect multiplication of data values by 1019 in order to obtain integer values on the y-axis. D. Inhibition of DAT-1 mediated [3H]-DA uptake by monoamine transporter antagonists. Points +/- standard deviation acquired from three separate competition experiments; nonlinear curve fits obtained using Kaleidagraph software (Synergy Software, Reading Pa)

Full length cDNA encoding the product of the dat-1 gene, when transfected into HeLa cells, supports transport of several different monoamines including DA, NE, Epi and 5HT but at distinctly different rates (Fig 6C). DAT-1 preferentially transports DA over other biogenic amines, with norepinephrine displaying reduced but detectable uptake (DA >> NE > Epi > 5HT). Given the absence of NE biosynthetic pathways in *C. elegans*, DAT-1 activity in the nematode is primarily responsible for the inactivation of released DA. Transport kinetics for both DA and NE was tested where DAT-1 displays saturable uptake kinetics with a K_m of 1.2μm for DA and 4.1μm for NE. When transporter specific antagonists were tested for inhibition of [^{3}H]DA uptake (Fig 6D), the most potent DAT-1 inhibitors were the tricyclic antidepressants imipramine and desipramine, compounds that in studies of mammalian transporters, target 5HT and NE transporters (SERT and NET, respectively). The mammalian NET inhibitor nisoxetine and the mixed DAT/NET antagonist mazindol also displays significant inhibition of DA uptake (Table 2). These studies established DAT-1 as a *bona fide* DA transporter but illustrate that pharmacological sensitivities are often distinct in comparing vertebrate and invertebrate orthologs.

To gain insight into the expression pattern of DAT-1 *in vivo*, Nass and coworkers (Nass et al., 2002) drove synthesis of cytosolic green fluorescent protein (GFP) using a 700bp DNA segment located immediately upstream of the *dat-1* transcription initiation site, resulting in fluorescence in all known DA neurons in the worm (Nass et al., 2002). *In vivo* function of DAT was established through accumulation of the DA neurotoxin 6-OHDA) (Nass et al., 2002). 6-OHDA treatments of animals wild type for the dat-1 allele expressing GFP in their DA neurons revealed loss of all DA head neurons with resistance

observed in the midline PDE neurons. DA neuron degeneration can be blocked by incubation of worms in DAT-1 transport antagonists such as imipramine. Importantly, neuronal susceptibility to 6-OHDA can be both blocked in DAT-1 deficient lines, and transferred by expression of dat-1 in cells that typically do not express the transporter (Nass et al., 2002). Features of this DA neuron degeneration, with its similarity to apoptotic versus necrotic cell death, offer insights into the pathophysiology of Parkinson's Disease (Nass and Blakely, 2003). In this regard, readily detectible DA neuron degeneration has also afforded adoption of the nematode model for studies of human alpha-synuclein mutants (Lakso et al., 2003) as well as the neuroprotective actions of torsin proteins (Cao et al., 2005).

The dependence of 6-OHDA induced degeneration of DA neurons on functional DAT-1 has permitted a forward genetic screen for suppressors that have the capacity to elucidate key features of DAT, its regulatory machinery, or facets of toxin-induced cell death. Indeed, Nass and coworkers (Nass et al., 2005) used this assay to identify three novel ethyl methane sulfonate- (EMS)-generated mutant alleles of *dat-1*. Two of the alleles identified resulted from point mutations in residues conserved across all known members of the SLC6 transporter gene family, suggesting a critical role for these residues in transporter structure and/or function. The third allele identified arises from a splicing defect altering the DAT-1 C-terminus by substituting an ectopic 15 amino acid sequence for the entire C-terminus. Each of these mutations resulted in a complete resistance to the effects of 6-OHDA *in vivo*. A fourth mutant was identified that also conferred complete resistance to 6-OHDA but which does not map to the dat-1 locus and remains unidentified. Translational fusions to the DAT-1 mutants were produced for *in vitro* and

in vivo expression to examine how these changes in DAT-1 protein lead to loss of function. The DAT-1 splicing mutant *(dat-1(vt4)* was found to be extremely defective for protein expression in transfected cells and demonstrated only weak expression *in vivo,* whereas the two point mutants displayed interesting trafficking and surface expression patterns, discussed in Chapter IV.

Mammalian DAT proteins exhibit multiple conductance states (Mortensen and Amara, 2003). Use of genetic/transgenic studies of DAT-1 in the nematode have been undertaken and have elucidated novel mechanisms that are relevant in terms of mammalian ion channel biology. Recently, Carvelli *et al*. took advantage of nematode primary cell culture techniques and obtained recordings from DA neurons isolated from various transgenic lines to monitor DAT-1 channel activity triggered by DA (Carvelli et al., 2004). Lines expressing wild type DAT-1 displayed DA-triggered inward currents like that reported for mammalian transporters featuring chloride ion dependence in the context of a lack of inward leak currents (Kilty et al., 1991; Ingram et al., 2002). Interestingly, lines over-expressing an N-terminal GFP:DAT-1 fusion in a wild type DAT-1 background increased the probability of detection of single channel events without changing channel amplitude compared to wild type lines alone, suggesting that N-terminal GFP tagging does not disrupt channel conductance *per se* but may affect channel gating. The current generated by individual DAT-1 channels was also sufficient to generate a macroscopic depolarizing current in whole cell recordings, indicating that the transporter may participate in DA neuron excitability *in vivo*. These studies lay the groundwork for genetic dissection of DAT-1 mediated currents and the role of DA neuron physiology in the nematode.

C. ELEGANS DA RECEPTORS

In mammalian systems, DA acts on 5 distinct G-protein coupled receptors (D1-5) that fall into two separate categories, being either D1-like or D2-like based on signaling specificities. These two classifications were originally assigned based on the receptor's effect on cyclic AMP levels (Spano et al., 1978). These two distinct classes are still recognized, the D1-like receptors positively coupling to adenylate cyclase (AC) increasing cAMP levels, and D2-like receptors inhibiting AC and cAMP formation, although additional second messengers and effector pathways are also recognized (Neve et al., 2004). Four DA receptors have been identified in *C. elegans*, specified as dop-1, dop-2, dop-3, and dop-4. Each receptor was originally identified by homology searches and has been subjected to both *in vitro* and *in vivo* analyses as noted below.

***Dop-1 DA receptors (F15A8.5)*:**

Suo *et al.* initially identified a D1-like DA receptor using comparison of mammalian DA receptor amino acid sequences to a translation of published *C. elegans* genome. The gene that displayed the highest homology, F15A8.5, was found to preferentially bind DA over other biogenic amines when expressed in COS-7 cells (Suo et al., 2002). RT-PCR studies revealed that the dop-1 gene encodes 3 distinct splice variants CeDOP1-L, CeDOP-1M, and CeDOP-1S. Differences in these three variants arise largely from differences in a 58 amino acid sequence within the receptor's third intracellular loop, which in mammalian G-protein coupled receptors has been shown to be important for G-protein coupling (Luttrell et al., 1993). The longest of these isoforms,

CeDOP-1L, retains this 58 amino acid insertion that also contains consensus phosphorylation sites for both PKC and PKA. CeDOP-1M lacks this sequence, but maintains PKC and casein kinase consensus sequence in the third intracellular loop. The CeDOP-1S isoform is almost identical to CeDOP-1M except for a deletion of 3 amino acids in the intracellular C-terminus that codes for another PKC consensus phosphorylation site (SSR). Four splice variants have been predicted by gene models including the three isoforms identified by Suo *et al.* and have subsequently been named dop-1a – d, according to worm nomenclature procedures (Horvitz et al., 1979; Hodgkin, 1995). The splice variant dop-1d has yet to be identified experimentally. Dop-1b was characterized pharmacologically in the initial report and displayed preferential displacement of [^{125}I]Iodo-LSD by DA (DA > NE > 5HT > Tyr = OA). Because there is no evidence of (nor)epinephrine in *C. elegans* (Horvitz et al., 1982; Sanyal et al., 2004), DA, 5HT, Tyr and OA profiles are the most physiologically relevant in considering potential endogenous agonists of these receptors *in vivo*.

In 2004, *Sanyal et al.* reported the cloning of a D1-like receptor using both *in silico* methods and mammalian D2 receptor sequences, followed by validation of expression and function using RT-PCR and GTPγS binding, respectively (Sanyal et al., 2004). These investigators again identified sequence encoded by the F15A8.5 gene as positive for DA mediated GTPγS binding in COS-7 cells. Only two isoforms of dop-1 were identified in this study (short and long splice variants), corresponding to the CeDop-1L and CeDop-1M transcripts described by Suo *et al.* Both isoforms stimulated an increase in cAMP production upon DA stimulation, verifying their role as bone fide D1-like receptors. Interestingly, co-expression of dop-1 with the *C. elegans* GTPγS isoform

(gsa-1) in conjunction with the G-protein coupled inwardly rectifying potassium (GIRK) channel (Kir3.2) resulted in a robust activation of a large potassium current (Sanyal et al., 2004). GIRK activation in mammalian systems typically results from activation of $G_o\alpha$ via D2 receptors (Missale et al., 1998), indicating that *C. elegans* DA receptors might signal differently than mammalian DA receptors.

Mammalian D1 receptor agonist and antagonists were assayed for functional coupling in culture on the DOP-1a isoform with mixed results (Table 3). The mammalian D1 receptor specific antagonist SCH23390 worked only as an agonist on dop-1 at high (1μm) concentrations. The D2 antagonists (+)-butaclamol and haloperidol, the mixed D1/D2 antagonist cis-flupenthixol, and octopamine displayed inverse agonist activity by decreasing the amount of basal cAMP activation (Sanyal et al., 2004). 5HT did not significantly activate dop-1a (in terms of GTPγS binding). Once again, although signaling pathways appear to overlap comparing mammalian and worm receptors, their pharmacologies are distinct and remain useful for receptor classification.

DA D1 receptors have been implicated in habituation to nose tap response (Rankin, 1991; Rankin and Broster, 1992; Rose and Rankin, 2001). Because dop-1 was found to be expressed in ALM and PLM neurons, tap habituation was tested in *dop-1(ev748)* mutants and habituation to non-localized tap response was tested (Sanyal et al., 2004). *Dop-1* knockout animals were found to habituate faster to this response than wild type animals implying that dop-1 is important for maintenance of the avoidance response. Expression of dop-1 in sensory neurons using the mec-7 promoter rescued tap habituation in *dop-1(ev748)* animals indicating that DA signaling via dop-1 in touch neurons is the

Table 3. *C. elegans* Dopamine Receptors

C. elegans Dopamine System Protein Characterization

D1-like Receptors

DOP-1	Gene Products	Dop-1a (L)	Suo et al. 2002
		Dop-1b (M)	Suo et al. 2002
		Dop-1c (S)	Suo et al. 2002
		Dop-1d[†]	Wormbase
	G-protein	Gs (gsa-1)	Sanyal et al. 2004
		Gq (egl-30)	Chase et al. 2004
	2nd Messenger	(↑) cAMP formation	Sanyal et al. 2004
	Effector	(↑) GIRK current	Sanyal et al. 2004
	Agonist	DA>NE>5HT.	Suo et al. 2002
		SKF38390, SCH23390.	Sanyal et al. 2004
	Inverse Agonist	Butaclamol	Sanyal et al. 2004
		Holoperidol	Sanyal et al. 2004
		Flupenthixol	Sanyal et al. 2004
	Cellular Expression	PLM Neurons	Sanyal et al. 2004
		PHC Neurons	Sanyal et al. 2004
		ALM Neuron	Sanyal et al. 2004
		RIM, AUA, and RIB	Sanyal et al. 2004
		Cholinergic cells in ventral nerve cord	Chase et al. 2004
	Mutant phenotype	↑ Tap habituation	Sanyal et al. 2004
DOP-4	Gene Products	dop-4 only	Sugiura et al. 2005
	G-protein	?	
	2nd messenger	(↑) cAMP formation	Sugiura et al. 2005
	Effectors	?	
	Agonist	DA	Sugiura et al. 2005
	Antagonists	?	
	Cellular expression	Pharyngeal neurons (I1, I2)	Sugiura et al. 2005
		ASG, AVL, CAN, and PQR neurons	Sugiura et al. 2005
		Vulva, intestine, rectal glands and epithelia, ray	Sugiura et al. 2005
		8 neurons (male tail)	Sugiura et al. 2005
	Mutant Phenotype	?	

D2-like Receptors

DOP-2	Gene Products	dop-2a (L)	Suo et al. 2003
		dop-2b (S)	Suo et al. 2003
	G-protein	?	
	2nd Messenger	(↓) cAMP formation	Suo et al. 2003
	Effector	?	
	Agonist (binding)	DA>5HT>Tyr>NE>Oct	Suo et al. 2003
	Antagonist (binding)	Butaclamol, Clozapine, CH23390, Haloperidol, Spiperone, Chlorpromazine, Sulpiride	Suo et al. 2003
	Antagonists (signaling)	Butaclamol	Suo et al. 2003
	Cellular Expression	Dopamine Neurons (ADEs, CEPs, and PDEs)	Suo et al. 2003
		Neurons in the male tail	Suo et al. 2003
	Mutant phenotype	?	
DOP-3	Gene Products	dop-3a[†]	Wormbase
		dop-3b	Chase et al. 2004
		dop-3c	Sugiura et al. 2005
		dop-3d	Sugiura et al. 2005
	G-protein	Go (goa-1)	Chase et al. 2004
	2nd messenger	(↓) cAMP formation	Sugiura et al. 2005
	Effectors	*DAG Kinase (dgk-1)*[‡]	Chase et al. 2004
		RGS protein (eat-16)[‡]	Chase et al. 2004
	Agonist	DA >> Tyr > Oct	Sugiura et al. 2005
	Antagonists	?	
	Cellular expression	PVD Neuron	Chase et al. 2004
		GABA neurons in ventral nerve cord	Chase et al. 2004
		Unidentified head neurons	Chase et al. 2004
		Unidentified tail neurons	Chase et al. 2004
		Body-wall muscle	Chase et al. 2004
	Mutant Phenotype	Defective Basal slowing response	Chase et al. 2004
		↓ DA induced paralysis	Chase et al. 2004

‡ Data implied from *in vivo* function studies.
† As listed by homology modeling in wormbase (www.wormbase.org)

critical determinant of nose touch habituation. Because ADE neurons synapse directly on a subset of these touch neurons (White et al., 1986) (ALM, AVA, and AVD) and ADE specific function was not tested in this study, it is difficult to determine whether ADE specific inputs or humoral DA reinstates this habituation.

***Dop-2 DA Receptor (K09G1.4)*:**

The *C. elegans* dop-2 receptor was originally identified by Suo *et al.*(Suo et al., 2003) by homology searches using the mammalian D2 receptor as a template. RT-PCR studies revealed two dop-2 gene products that differ by 135 amino acids in the third intracellular loop (CeDop2L and CeDop2S). These isoforms are the only two predicted splice variants for this gene in *C. elegans* and will be referred to as dop-2a (CeDop-2S) and dop-2b (CeDop2L) according to worm nomenclature (Horvitz et al., 1979; Hodgkin, 1995). Importantly, alternative splicing of the D2 receptor at this location is also noted for mammalian isoforms (Dal Toso et al., 1989; Giros et al., 1989; Monsma et al., 1989).

Pharmacologically, DOP-2 preferentially binds DA over other biogenic amines. Both the dop-2a and dop-2b isoforms were expressed in COS-7 cells and biogenic amines were assayed for their ability to displace [^{125}I]iodo-LSD. LSD displays high nM affinity for both isoforms (KD = 6.6 ± 0.6nM for dop-2b and 6.5 ± 2.1 nM for DOP-2a) with DA displacing [^{125}I]iodo-LDS with the highest potency (Ki = 2.98 ± .021 uM for DOP-2a and 2.24 ± .019um for DOP-2b). Displacement of [^{125}I]iodo-LSD for other biogenic amines tested followed the same pattern for both isoforms with a rank order of potency for displacement that followed 5HT > tyramine > NE > octopamine (Table 3). Antagonist profiles of [^{125}I]iodo-LSD displacement for the two isoforms are almost indistinguishable

with butaclamol showing the highest potency (~35nM for either DOP-2a or DOP-2b). To examine functional coupling to cAMP production, each of the two *C. elegans* dop-2 isoforms were transfected into CHO cells in combination with a commercially available vector (pCRE-Luc, Clontech) that displays increased luciferase activity in response to increase in cAMP levels. Addition of forskolin stimulated an increase in luciferase activity that could then be inhibited by DA (0.1μm). Both DOP-2a and DOP-2b isoforms decreased this forskolin-induced activation in CHO cells; the EC50 value for AC inhibition was reported to be ~74 nM for both dop2a and b, well below the K_i calculated for DA at these receptors and well within a physiological range. This inhibition by DA was reversed by the addition of 10μm butaclamol, consistent with binding inhibition studies (Suo et al., 2003).

Little is known of the behavioral contributions of dop-2. Exogenous DA increased the number of high angle turns. The mammalian D2 antagonist raclopride blocked this reinstatement of ARS, implying that DA is sufficient to activate this behavior. While raclopride is a specific D2 agonist in mammals, it is difficult to know what effect it may have on *C. elegans* receptors given the mixed pharmacology demonstrated by the cloned DOP receptors in response to mammalian antagonists (Suo et al., 2004). Future studies using *dop-2* mutants may help clarify *in vivo* roles.

***Dop-3 DA Receptor (T14E8.3)*:**

A novel D2-like receptor was identified by Chase and colleagues based on sequence similarity to human D2 receptors (Chase et al., 2004). Initially, several potential genes with high homology to the human D2 receptor were identified. To

narrow their search, TM domains from the human DA, 5HT, and muscarinic acetylcholine receptors, along with the already identified DOP-1 and DOP-2 protein sequences, were aligned and compared to BLAST-based alignments of uncharacterized nematode homologs. Three genes clustered with both the human and *C. elegans* DA receptors (T14E8.3, C24A8.1, and C02D4.2) with T14E8.3 displaying the highest homology to the known *C. elegans* D2 receptor dop-2. T14E8.3 was therefore targeted for investigation and subsequently renamed dop-3. Isolation of the full-length clone using RT-PCR revealed that DOP-3 protein is most similar to human D2 receptors with 51% identity in putative transmembrane spanning domains and 38% identity overall. Alignment with the human D1 and D2 receptors reveals a large 3rd intracellular loop and a small C-terminal tail, consistent with D2-like receptors. Four isoforms for dop-3 are predicted for the T14E8.3 locus (DOP-3a-d, see Table 3). Comparison of the predicted amino acid sequences for each of these variants reveals that the isoform identified by Chase *et al.* most resembles DOP-3b. No splice variants were reported in this original publication however recent work reveals at least one more splice isoform is coded for by *C. elegans*.

Shortly after Chase *et al.* published their findings on dop-3b, Suguira and colleagues reported two novel DOP-3 splice variants, one which encoded a 590 amino acid receptor and another that encoded a truncated DOP-3 receptor (DOP-3nf) which lacked the sixth and seventh transmembrane domains normally predicted for the full length DOP-3 receptor (Sugiura et al., 2005). The first of these receptors coded for sequence predicted for DOP-3c and is 18 amino acids shorter than the receptor reported

by Chase and colleagues. The second truncated isoform coded for a 245 amino acid receptor that corresponds to the length of the predicted DOP-3d isoform.

To determine whether either of these proteins encoded a *bone fide* DA receptor, the individual isoforms were transfected into CHO cells in conjunction with a cAMP responsive luciferase reporter gene. The ability of different biogenic amines to reduce forskolin activated luciferase activity was tested on cells expressing the full-length DOP-3c isoform. DA displayed the most potent attenuation of forskolin induced luciferase expression, with an EC_{50} value of 5.57 ± 0.13μm. Tyramine and octopamine also decreased luciferase expression but at much higher concentrations. When DA was tested on cells expressing the truncated DOP-3d receptor isoform, no DA dependent inhibition of luciferase expression was reported indicating that this product may not function via adenylate cyclase and cAMP pathways. Instead co-transfection of DOP-3d with DOP-3c reduced the EC_{50} value for DA, indicating that DOP-3d may act to blunt signaling by coupling to DOP-3c.

The intrinsic pharmacology of DOP-3b has not been characterized, instead elegant genetic experiments have been conducted on knockout strains to determine the effects of dop-3 on DA-mediated behavior as discussed in more detail below. These behavioral experiments revealed that dop-1 and dop-3 expressed by cholinergic neurons work antagonistically to mediate DA-induced paralysis, utilizing different G-proteins to mediate their effects. Genetic dissection of DA signaling indicates that the dop-3 pathway includes activation of the $G_o\alpha$ protein goa-1, the RGS protein eat-16 (with its beta subunit gpb-2) and a diacylglycerol kinase (dgk-1). In these studies, Chase and coworkers isolated a *dop-3* mutant line that displays reduced paralysis in response to

exogenous DA (Chase et al., 2004). Expression of dop-3 was observed in both cholinergic and GABAergic cell bodies and paralysis in response to DA was rescued when dop-3 was expressed in cholinergic neurons using the acr-2 promoter (Chase et al., 2004). Screening for mutants with reduced paralysis in response to DA yielded 4 additional mutants including novel alleles of *goa-1, dgk-1, eat-16,* and *gpb-2*. Importantly, all of these genes function as downstream effectors of $G_o\alpha$ and have been shown to negatively modulate $G_q\alpha$ responses in *C. elegans* (Hajdu-Cronin et al., 1999; Miller et al., 1999). These studies reinforce recent diversification of DA signaling pathways beyond simply modulation of cyclic nucleotides (Beaulieu et al., 2005).

To examine potential DA receptor interactions in the worm, *dop-1* and *dop-3* double mutants were generated. The *dop-1;dop-3* double mutants paralyzed in DA, suggesting that the *dop-1* knockout should be hypersensitive to DA in terms of slowing, a trend that was noted by Chase *et al.* (Chase et al., 2004). Expression of dop-1 using acr-2 in the *dop-3;dop-1* double mutant partially restored *dop-3* resistance to paralysis, indicating that these receptors likely work antagonistically in cholinergic neurons to mediate DA effects. The fact, however, that the double mutant was still responsive to DA paralysis suggests that there is most likely another DA receptor in this pathway that acts via goa-1 that has yet to be identified (Jorgensen, 2004). Regardless, these studies were the first to demonstrate DA signaling in *C. elegans* modulating behavior mediated by two antagonistic DA receptors via differential G-protein coupling, underscoring further similarities to mammalian actions of DA. With respect to other DA-supported behaviors, *dop-3* but not *dop-1*or *dop-2* receptor knockouts alter basal slowing response *in vivo* suggesting that basal slowing mechanisms may engage signaling pathways similar to

those engaged for modulation of basal motor activity (Chase et al., 2004). Chase and co-workers also remind us that actions of DA in the motor slowing circuit may arise from humoral actions of DA rather than from direct synaptic contacts (Chase et al., 2004).

Dop-4 DA Receptors (C52B11.3):

A novel D1 like DA receptor (*dop-4*) was cloned by Sugiura *et al.* using sequence homology to human DA receptors (Sugiura et al., 2005). RT-PCR using a C52B11.3 specific anti-sense primer coupled with splice leader sequence 1 (SL1) sense primer amplified a single transcript of 1.7bp. HEK293 cells co-expressing this dop-4 cDNA with a cAMP responsive luciferase reporter construct was tested for alterations in luciferase levels in response to several biogenic amines. Only DA produced a significant increase in luciferase expression, indicating that this receptor acts to increase cAMP levels specifically upon DA stimulation. The increase in cAMP levels is consistent with D1-like activity, making DOP-4 the second D1-like DA receptor identified in *C. elegans* (Table 3). Although this receptor was originally identified using homology searches to mammalian DA receptors, it clusters most with invertebrate DA receptors and may represent an invertebrate specific DA receptor. More pharmacology on this receptor should be pursued to determine differences and similarities between DOP-4 and mammalian D1-like receptors in terms of G-protein coupling and down stream effectors before this conclusion is solidified.

The expression of dop-4 was determined by fusing a 6.1kb promoter sequence including sequence up to the middle of exon 2 with GFP. Fluorescence was noted in several pharangeal neurons (I1 and I2), and head neurons including ASG, AVL, CAN,

and PQR. There was also reporter expression in vulva, intestine, rectal glands, and rectal epithelial cells. Expression was also seen in neurons projecting into ray 8 in the male tail. This expression profile suggests that this receptor may play a role in the regulation of pharyngeal pumping, chemosensation, defecation, oxygen sensing and male mating behavior (Sugiura et al., 2005).

Still More C. elegans DA Receptors?

Studies of receptor involvement in egg-laying behaviors noted above also suggest a role of as yet uncharacterized DA receptors. The D2 antagonists chlorpromazine, butaclamol, and haloperidol increase egg laying in wild type and egl-1 mutants but not in animals lacking DA and 5HT (*cat-4(e1141)*), implying that DA antagonism at a D2 like receptor may play a role in activation of egg laying behavior (Weinshenker et al., 1995). This DA receptor would have to reside in vulval muscle and effect potassium conductance through egl-2. Although dop-2 is inhibited by chlorpromazine, it is unlikely that the dop-2 receptor mediates DA dependent inhibition of egg-laying since evidence indicates it is not expressed in any of the neurons that mediate egg-laying responses, nor is it found in muscle (Suo et al., 2003). Haloperidol acts as an inverse agonist on dop-1 (chlorpromazine was not tested), however, dop-1 does not appear to be expression muscle cells (Chase et al., 2004; Sanyal et al., 2004). As dop-3 is expressed in muscle, this receptor becomes an interesting candidate; however dop-3 does not appear to be expressed in vulval muscle cells and no constitutive egg-laying was noted in the *dop-3* mutants identified by Chase (personal comm., D. Chase). These findings suggest the

existence of an unidentified DA and chlorpromazine/haloperidol-sensitive receptor that is linked to the egg-laying circuit.

CONCLUSION

The past fifty years of discoveries in catecholamine science has provided a rich literature, which to this day, provides a platform for novel catecholamine research. As new technologies and models are explored, such as the *C. elegans* system described here, answers to old questions give rise to yet more possibilities. Catecholamine biologists now have an impressive tool kit, enhanced by the utilization of powerful genetic models that, in the coming years, will reveal novel partners and pathways supporting DA signaling and stimulate our thinking about DA disorders and therapies in man. Utilizing this system, we will examine the localization and function of both the endogenous DAT-1 protein but also use GFP:DAT-1 fusion proteins to determine *in vivo* movements and describe mutants which impact DAT-1 function.

CHAPTER III

ANTIBODY PRODUCTION AND *IN SITU* VISUALIZATION OF THE *C. ELEGANS* DA TRANSPORTER (DAT-1)

INTRODUCTION

Sulston and colleagues first described a DA nervous system in the adult hermaphrodite of *C. elegans* supported by 8 DA containing neurons (Sulston et al., 1975). The development of FIF techniques (Falck et al., 1962) allowed for visualization of a DA signal from specific neurons within fixed *C. elegans*. Six of these neurons reside in the hermaphrodite head and were called the CEP and ADE cell groups. Taking advantage of serial electron micrographs, Sulston *et al*, reconstructed the wiring of this DA nervous system in the head, reporting both axonal and dendritic like projections for each of the 6 head neurons. The four CEP neurons send long dendritic projections to the nose of the worm with several small axonal projections into the nerve ring, while the two ADE cell bodies alternatively send small dendritic projections to body wall muscles with longer axonal projections to a ventral ganglion, which synapse into the nerve ring.

Another cell group, the PDE cells, were located in the mid-body of the worm and sends long projections project ventrally from the PDE cell body, which run both anteriorally and posteriorally along the ventral nerve cord. Little is known about the synaptic connections made by the PDE neurons.

Although promoter fusions provided evidence of DAT-1 expression in these neurons, visualization of DAT-1 protein distribution in the various DA cell groups have not been explored, and specific localization of endogenous DAT-1 protein remained

unknown. A COOH-terminal GFP fusion to DAT-1 (DAT-1:GFP) was reported to rescue 6-OHDA toxicity in the *dat-1(ok157)* KO strain but localization *in vivo* was never discussed (Nass et al., 2002). Given known COOH-terminal interactions with mammalian DAT-1 proteins, we re-examined these proteins *in vivo* to reveal significant intracellular accumulation (Chapter IV).

To advance studies of DAT regulation in a genetically-tractable model system, we have established the cellular localization of the *C. elegans* DAT-1 protein using newly developed DAT-1 antibodies. Affinity-purified DAT-1 antibodies directed against the transporter's COOH terminus specifically stained both DAT-1 transfected COS-7 cells and wild type (N2) nematode DA neurons and processes. Native DAT-1 protein was detected at moderate levels within DA neuron cell bodies and was enriched in axon terminals, with low but detectible expression along dendrites.

The function of the synaptic vesicle motor protein UNC-104, which is essential for the targeting of proteins that reside on synaptic vesicles to synapses, was also examined. Localization of native DAT-1 protein in a mutant UNC-104 background (*unc-104(e1265)*) reveals that DAT-1 localization to either the nerve ring or elaboration along dendrites is independent of UNC-104 function, revealing a heretofore unrecognized mode of delivery of DAT-1 protein to these cellular compartments.

MATERIALS AND METHODS

Plasmid Constructs

Bacterial expression vectors were created for the production of GST:COOH-terminal fusion peptide for use in antibody production against the cytosolic C-terminus (C-term)

of DAT-1. cDNA encoding the DAT-1 COOH-terminus was amplified from full length *dat-1* cDNA (pRB235) using oligonucleotides that encoded a 5' BamHI and 3' EcoRI restriction sites suitable for cloning into pGEX5x3 expression vectors (Pharmacia Biotech, Milwaukee, WI) (TCA sequence was added 3' of either sequence and just 5' of EcoRI sites to create a stop codon and have been underlined in the oligo sequences). The COOH-terminal peptide was amplified using oligos RB 1402 (5' – CGC CGG ATC CTC TAC AAA TTC GTC AAT GCG AGG – 3') and RB 1403 (5' – CGC CGA ATT CCT TCA TAG CAT TAT GTC AGA GTG CGG – 3'). The resultant cDNA fragments were cloned into pGEMT-easy vectors and sequences verified by di-deoxy nucleotide sequencing (Center for Molecular Neuroscience, Neurogenomics Core). Correct clones were subcloned into the bacterial expression vector pGEX5x3 (Promega, Madison WI) to create the final pBY633 vector.

Peptide and Antibody Production

Polyclonal antibodies were generated against a GST fusion protein consisting of the entire DAT-1 intracellular COOH-terminus. The NH2 terminal GST fusion protein expression vector (pBY633) was transformed into BL21(DE3) cells for bacterial expression. Individual colonies were picked and grown in 40mL of liquid broth (LB) overnight at 37°C under selection. The 40mL LB/bacteria media was added to 400mL of LB with 2% glucose and agitated for 1 hr at 37°C. Chemical induction of bacterial expression was initiated using isopropyl-beta-D-thiogalactopyranoside (IPTG) and protein purification was performed as previously described (Ferguson et al., 2003), except purified extract was visulized on an 10% SDS-PAGE gel via Zinc staining and the

full-length fusion protein was extracted by gel electroelution (Pierce, Rockford IL) . The resultant purified full-length fusion protein was then dialyzed to a final concentration of 1mg/mL and used for immunization into rabbits with emulsification adjuvent (Prosci, San Diego, CA). Serum obtained from two different rabbits (RB1565 and RB1566) was first pre-absorbed against a fixed and permeabilized (Ruvkun fixation protocol (Finney and Ruvkun, 1990)) DAT-1 deficient *C. elegans* strain (*dat-1, ok157*) to remove any non-specific antibodies generated by a previous nematodal infection in the rabbits as well as epitopes unrelated to the DAT-1 protein. This *dat-1* cleared antiserum was then used in all immunofluorescent experiments.

Mammalian Cell Culture and Immunofluorescence

In order to test the specificity of our antibodies for immunofluorescence, HEK-293T cells were transfected with DAT-1 cDNA and probed with our purified DAT-1 antisera. Cells were plated at 60,000 cells/dish in γ-irradiated 35mm glass bottom microwell poly-d-Lysine coated dishes (MatTek Cultureware, Ashland, MA) and allowed to attach for 24 hr prior to transfection. The cells were transfected with 200ng of either DAT-1 cDNA (pRB454, (Jayanthi et al., 1998)) or an empty vector (pcDNA3, Invitrogen, Carlsbad, CA) using TransIT-LT1 (Mirus, Madison, WI) as the transfection vehicle. At 48hr post-transfection, the cells were washed once with room temperature phosphate buffered saline (PBS). The cells were then fixed with 2mL of Prefer fixative (ANATECH LTD., Battle Creek, MI) for 15 minutes at room temperature and washed twice with TRIS buffered saline (TBS). Cells were blocked for 1 hr in TBS containing 2% Normal Goat Serum (NGS) (Jackson Immunoresearch, West Grove, PA) and 0.2% IGEPAL CA-630

(Sigma Aldrich, St. Louis, MO). DAT-1 cleared serum diluted 1:100 in blocking agent was added to the cells and incubated for 2 hours at room temperature. The cells were washed three times with TBS/0.2%IGEPAL CA-630 then stained for one hr at room temperature in a 1:5000 dilution of Goat anti-Rabbit CY3 labeled secondary antibody (Jackson ImmunoReseach) and finally washed two times with room temperature TBS and suspended in room temperature PBS for imaging.

Confocal Imaging

Indirect immunofluorescence images for both cell culture and nematode staining experiments were taken using an LSM510 confocal microscope (Vanderbilt Cell Imaging Core). Either a single confocal image plane (1.2uM) or a series of 1.2uM image planes were obtained, creating a "Z stack". Z stacks were used to create 3D reconstructions of images and have been noted in the figure legends.

C. elegans Fixation and Immunofluorescence

Animals were fixed using 1% formaldehyde following a modified Finney/Ruvkun fixation protocol (Finney and Ruvkun, 1990) as adapted by C. Niemeyer and D. Miller (Miller and Niemeyer, 1995). After fixation, animals were additionally permeabilized by adding 500μL of collagenase solution (2mg/mL collagenase type I, Sigma, 100mM TRIS pH 7.4, 1mM $CaCl_2$) to 50μL of fixed strain. Animals were shaken vigorously for 30 minutes on a VWR mini-vortexer at high speed in a 1.5mL microcentrifuge tube and then pelleted at 2,000g on a Sorval Biofuge Fresco for 5 minutes. The collagenase solution was then aspirated off and 500μL of antibody buffer A (AbA) was added to the worm

pellet. Animals were washed in AbA 2 times. Both antiserum from RB1565 and a Cy3 conjugated goat anti-rabbit secondary antibody (Jackson ImmunoReseach) were exposed to fixed permeabilized *dat-1* animals for 24 hr at 4°C to remove any non-specific antibodies. Preabsorbed RB1565 was used at a concentration of 1:500 in AbA and exposed to permeablized animals for 16 hr at 4°C. Animals were washed 6 times (3 quick, and 3, 15 minute washes) in AbB. The Cy3 preabsorbed secondary Ab was used at a concentration of 1:1000 in AbB.

C. elegans Strains

All strains were derived from the wild-type N2 Bristol isolate and maintained at 14 to 25°C using standard methods (Brenner, 1974). The *unc-104 (e1265)* line was obtained from the *Caenorhabditis* Genetics Center (University of Minnesota, Minneapolis). The *dat-1(ok157)* strain was a gift of J. Duerr and J. Rand (Oklahoma Medical Research Foundation, Oklahoma City). The BY250 strain which expresses GFP in all DA neurons was a gift from G Wong (A. I. Virtanen Institute, Kuopio University, Finland).

RESULTS

DAT-1 COOH Terminus Peptide Expression and Purification

Bacterial expression of the GST:COOH-terminal DAT-1 fusion was initiated by IPTG induction of BL21(DE3) cells. Pre- and post- induction bacterial lysate was analyzed on a 12% acrylamide gel and protein was visualized by GelCode Blue staining (Pierce, Rockford, IL). Protein staining revealed induction of GST:COOH-terminal peptide that was absent in the pre-induction lane, with a higher molecular weight than

purified GST alone (Fig. 7A). The post-induction bacteria were then lysed and the GST:COOH-terminal fusion was purified on glutathione beads. Purified product was again tested for purification using SDS-PAGE and revealed protein bands consistent with both a full length fusion protein as well as several degradation products which migrated at a lower molecular weight (Fig 7B).

To obtain a full length GST:COOH-terminal peptide, glutathione purified peptide was analyzed on a 10% polyacrylamide gel and zinc stained to isolate full length product (Fig. 7B). The highest molecular weight product that had a mobility consistent with our full length GST:COOH-terminal fusion was extracted and electro-eluted to obtain a purified full length fusion peptide. This purified product was again analyzed on a 12% polyacrylamide gel and visualized, revealing only full-length fusion peptide (Fig. 7C). This material was then used as an immunogen for DAT-1 antibody production in rabbits.

Immunoreactivity of DAT-1 Antibodies via Western Blot Analysis

Two separate rabbits (PAS 1565 and PAS 1566, ProSci, Poway CA) were immunized with the GST:COOH-terminal DAT-1 peptide and serum collected from both was tested by ELISA to assay immunoreactivity. The antiserum, now named RB1565 and RB1566, showed evidence of a high specific ELISA titer (RB1565 > 1:75,000, and RB1566 > 1:50,000) and thus immunoblotting of purified DAT-1 protein was tested.

Both antisera were tested for immunoreactivity against GST, the GST:COOH-terminal fusion peptide, and COS-7 cell extract expressing DAT-1 protein. Only the antiserum from RB1565 showed high molecular weight product, consistent with the full

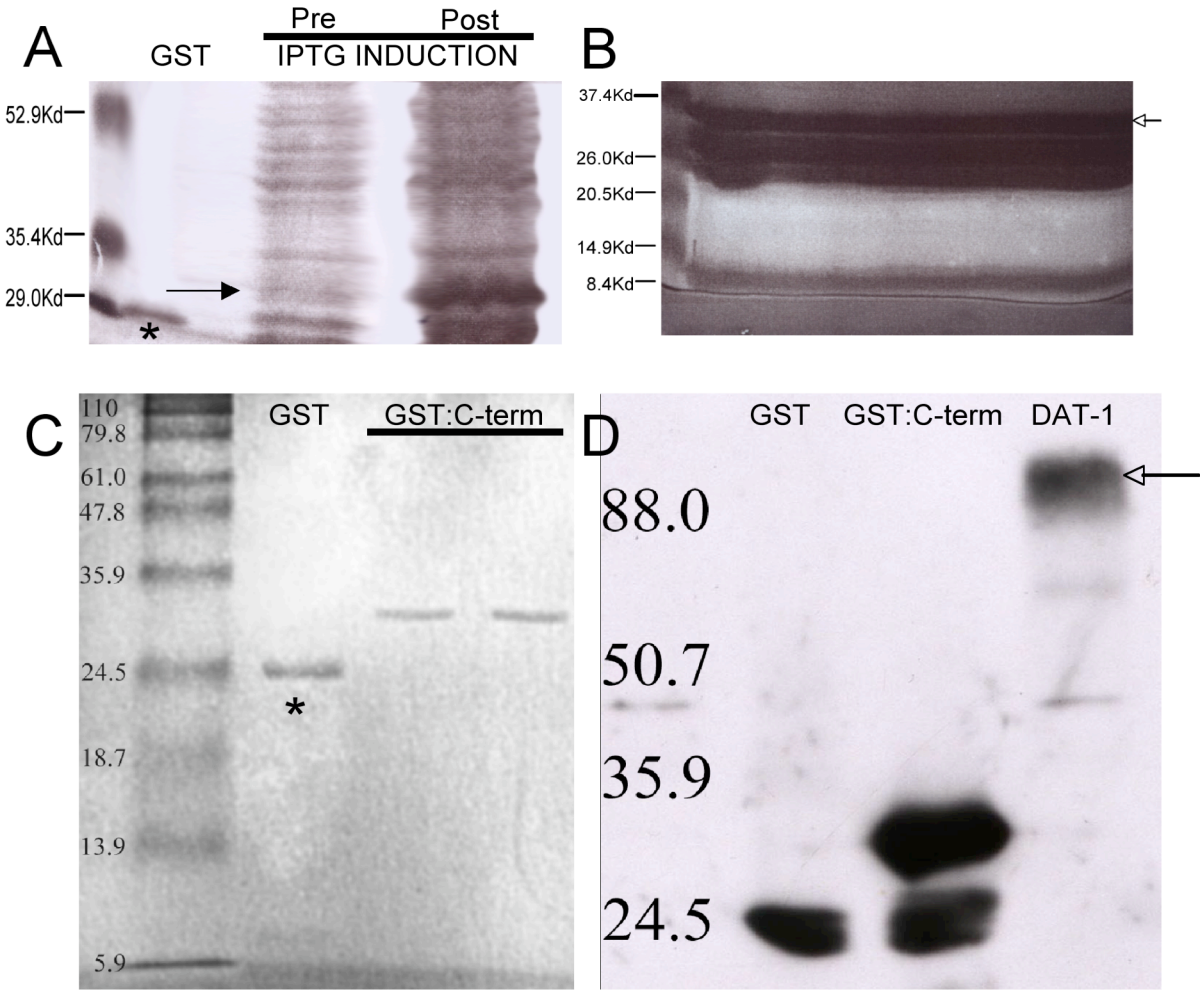

Figure 7. Peptide Purification and Antibody Recognition of DAT-1 by Western Blot Analysis.

A. Bacterial lysate from BL21(DE3) cells transfected with the pBY633 GST:COOH-term fusion vector. Lane 1 contains purified GST (asterisk) while lane 2 and 3 contain bacterial lysate. Pre-induction lysate is analyzed in lane 2 and compared with post-induction lysate in lane 3. Significant GST:COOH-terminus expression can be seen in the post induction lane (arrow). **B**. Zinc staining of post glutathione purified fusion protein. Several background or degraded bands are seen below the highest full length protein band (arrow) which was selected for gel purification and ellectroelution. **C**. Post-purified and full length peptide were analyzed in comparison to GST alone (asterisk). All background and degredation products were removed by previous gel purification (in B) and lanes 3 and 4 reveal full length fusion protein product used to inoculate rabbits. **D**. Western blot analysis of GST, fusion peptide, and full length DAT-1 using RB1565 antisera. The antisera recognizes GST, the fusion peptide, and full length and glycosylated DAT-1 from COS-7 cell extracts (arrow).

length DAT-1 protein (Fig 7D) and was therefore tested in immunofluorescence experiments on fixed *C. elegans* strains.

DAT-1 Antibodies Recognize DAT-1 in Transfected Cells

Antisera RB1565 and RB1566 were assayed for DAT-1 immunoreactivity and specificity using HEK293T cells transfected with either a plasmid containing DAT-1 cDNA (p235) or an empty vector (pBluescriptII). Cells transfected with p235 (Fig. 8A & B), but not empty vector (Fig. 8C & D), showed specific periplasmic staining with the RB1565 antibody (and to a lesser degree with the RB1566 antisera, data not shown). Ab RB1565 was therefore used in immunofluorescence experiments using either DAT-1 knockout (*dat-1(ok157)*) or wild type (N2) *C. elegans* strains.

DAT-1 Antibodies Define DAT-1 Expression in Fixed C. elegans In Situ

N2 and *dat-1* lines at mixed stages were washed off a small NA22/OP50 plates and fixed using a modified Finney Ruvkin fixation procedure. Fixed animals were incubated in RB1565 antisera and subjected to indirect immunofluorescence using a goat anti-rabbit CY3 secondary antibody. A majority of the N2 animals displayed staining in all the DA head neurons, including the four CEP and two ADE neurons (Fig 9A). The majority of the Cy3 secondary signal emanated from the ADE and CEP cell bodies (small dots represent cell somas, 9A) and in areas consistent with synaptic terminals innervating the nerve ring (asterisk, 9A) and the ventral ganglion (Fig. 9A, arrow). There was also reduced signal along dendritic projections from the CEP cell bodies (arrowheads, 9A). Identification of the PDEs was rarely noted. DAT-1 specific staining was absent in the

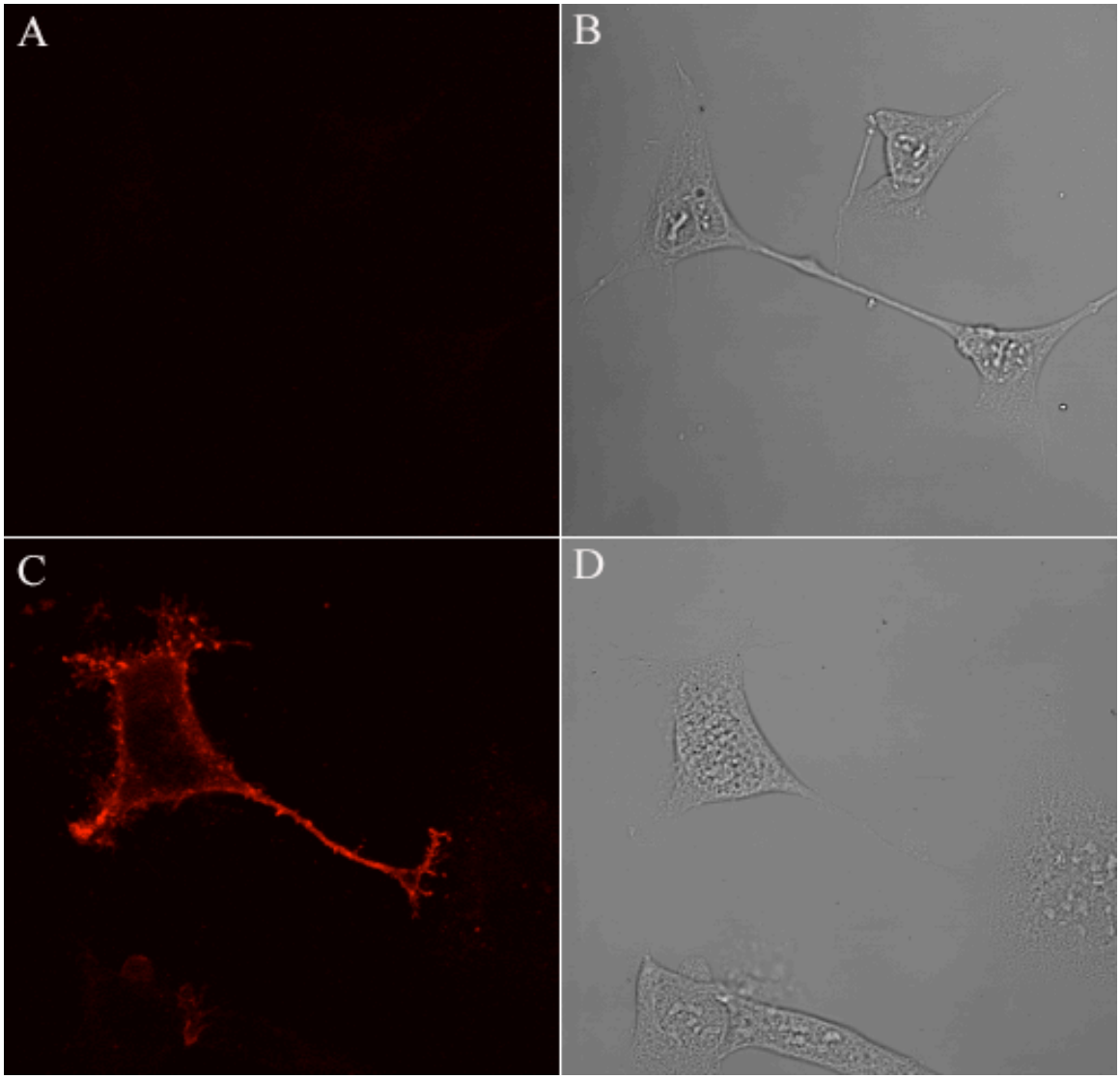

Figure 8. Antibody RB1565 Reveals DAT-1 Protein Expression in HEK Cells.

A. HEK cells transfected with pBlueScript cDNA and probed with RB1565 display no detectible RB1565 immunoreactivity. **B.** DIC images taken simultaneously during the CY3 scan reveal the presence of multiple HEK cells in the field of view. **C.** CY3 imaging of RB1565 and CY3 secondary antibodies recognizing DAT-1 protein expression in DAT-1 expressing HEK cells. **D.** DIC images taken simultaneously during the CY3 scan reveal differential expression in multiple cells in the field of view.

dat-1(ok157) KO strain (Fig. 9C). It should be noted that the greatest intensity of DAT-1 specific staining was obtained using young animals, with a reduction in staining progressively occurring over the lifetime of the animal (data not shown). Similar results were noted with our GFP:DAT-1 fusion protein and transcriptional regulation of the DAT-1 promoter region was tested and will be discussed in Chapter IV.

The UNC-104 mutant unc-104(e1265) displays normal DAT-1 staining in situ.

The kinesin motor protein UNC-104 has been shown to traffic synaptic vesicle proteins directly to the synapse (Hall and Hedgecock, 1991). To test whether DAT-1 synaptic localization is dependent upon a functional UNC-104 protein, a mutant line (*unc-104(e1265)*), which has been shown to be sufficiently defective in VMAT localization (Duerr et al., 1999). Unc-104 animals were selected based on their overall UNC phenotype and were fixed and subjected to indirect immunoflurescence assays using the RB1565 antibody. Significant immunoreactivity was maintained in nerve ring structures (Fig. 9B, asterisk) including the ventral ganglion projection from the ADE cell bodies (Fig. 9B, arrow). Immunoreactivity was also detected in CEP projections up to the nose of the animal (Fig 9B, arrowheads) indicating that dendritic expression was maintained in this mutant line. No significant cell body accumulation was noticed in this line (Fig. 9B, dot) suggesting that UNC-104 plays little role in DAT-1 synaptic localization.

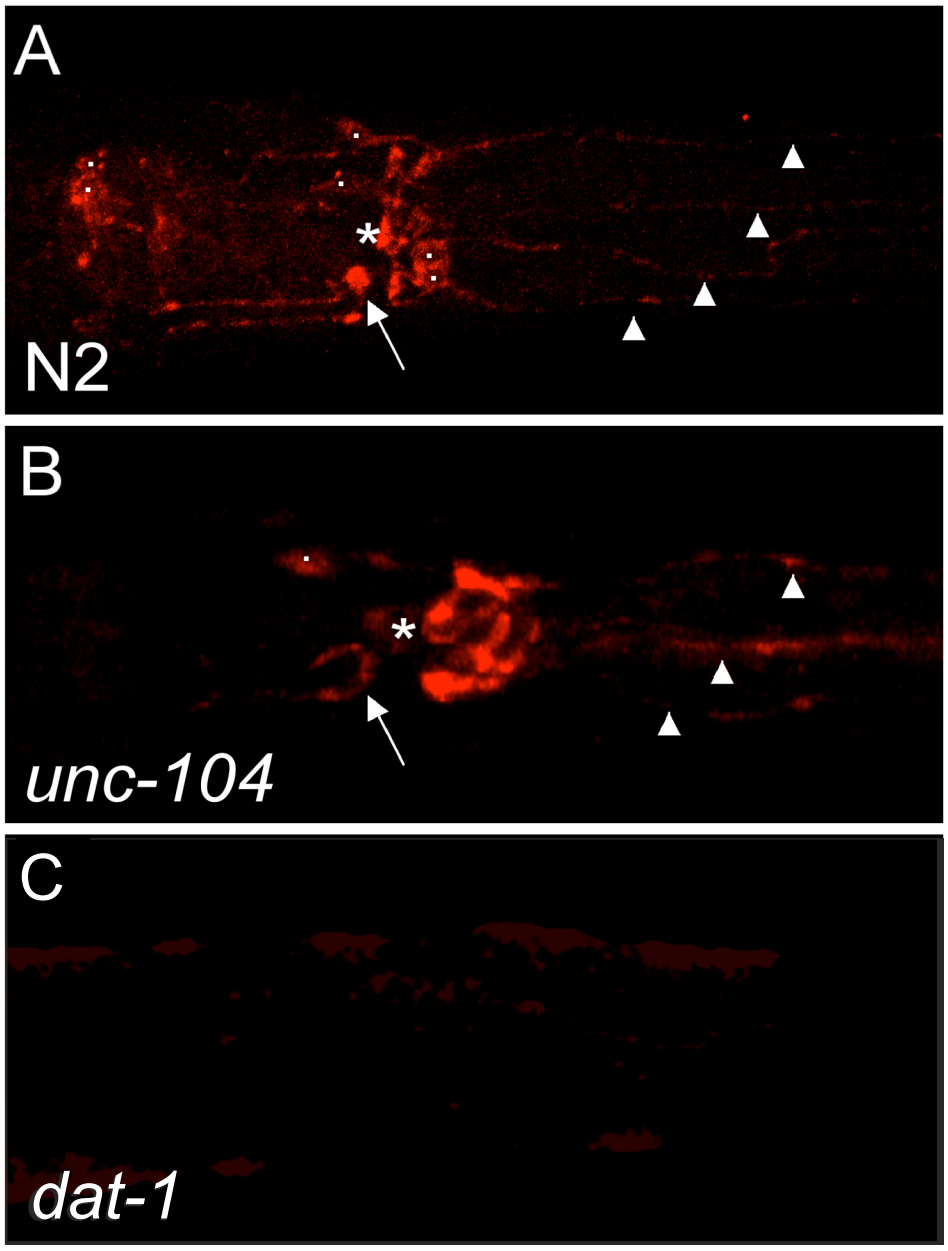

Figure 9. DAT-1 Antisera RB1565 Reveals DAT-1 Localization *In Situ*.

A. N2 animals stained with RB1565 followed by a CY3 secondary demonstrate cell body (dots), synaptic (asterisk, arrow) and dendritic localization. DAT-1 immunoreactivity in cell bodies is restricted to the perinuclear zone and specific accumulation can be noted in the nerve ring (asterisk). There is also faint but specific staining out along dendritic projections from the CEPs to the nose. **B.** Mutant *unc-104* animals display similar staining patterns as noted in N2 animals including ventral ganglion (arrow), nerve ring (asterisk) and dendritic expression(arrowheads). **C.** DAT-1 knockout animals display no specific anti-DAT-1 staining.

DISCUSSION

Indirect immunofluorescence using the newly developed RB1565 antibody reveals that the *C. elegans* DA transporter (DAT-1) is expressed in all cellular specializations of the *C. elegans* DA neurons. Expression of DAT-1 is enriched in locations described as nerve terminals by Sulston (Sulston et al., 1975), in the ventral ganglion projection from the ADE cells, and in cell bodies, with reduced immunoreactivity in dendritic projections from the CEPs. This staining is consistent with DAT immunostaining in higher organisms including rat and human studies, where DATs have been reported to be located in dendrites, cell bodies, with accumulation at terminals (Hersch et al., 1997; Nirenberg et al., 1997).

Cell body, dendritic, and synaptic localization of DAT-1 is consistent with antibody studies performed on mammalian DATs. Studies performed by Nirenberg and colleagues on rat midbrain tissue using both immunohistochemistry and immunogold techniques revealed a high density of rDAT in nerve terminals of the striatum where it obtained a "peri-synaptic" localization (Hersch et al., 1997; Nirenberg et al., 1997). An enriched synaptic density and peri-synaptic localization was also confirmed for hDAT in striatal tissue from post mortem brains (Ciliax et al., 1999). These results are consistent with our findings in *C. elegans* fixed strains, where an increase in immunoreactivity is noted in areas consistent with synaptic localization.

Substantia nigra cell bodies from rat midbrain also revealed significant immunoreactivity for DAT antibodies (Nirenberg et al., 1996; Hersch et al., 1997), with higher resolution immuno EM revealing DAT in structures consistent with Golgi body

and endoplasmic reticulm (ER), consistent with DAT-1 maturation and glycosylation via these pathways. DAT was also found in tubuolovesicular bodies near the plasma membrane and inserted in dendrites (Nirenberg et al., 1996; Nirenberg et al., 1997). Again, we find striking similarities using our DAT-1 specific antibodies to studies performed in mammals. DAT-1 signal is significant in the cell body, although it is apparently excluded from intracellular structures consistent with Golgi and ER membranes. This exclusion could be due to the fact that our antibody detects COOH-terminal epitopes whereas the previous studies used either NH2-termial or second loop directed antibodies.

Studies on the human DA transporter (hDAT) reveal that different DA projections (Nigralstriatal v. mesocortical) contain a varying density of hDAT in terminal fields (Ciliax et al., 1999). We report a similar finding in the *C. elegans* DA nervous system with CEPs expressing the highest about of immunolabeling followed closely by the ADE cell groups. In all of our studies, there was no distinguishable PDE immunoreactivity, suggesting a very low level of DAT-1 is maintained in these cells.

The kinesin motor protein UNC-104, which traffics synaptic vesicles and associated proteins to synaptic targets, is not responsible for DAT-1 localization to nerve ring structures. Examination of DAT-1 localization using the RB1565 antibody reveals a localization pattern that is strikingly different from synaptic vesicle proteins visualized using similar fixation and visualization methods and GFP fusion techniques (Nonet et al., 1993; Duerr et al., 1999; Nonet, 1999). The fact that DAT-1 is not loaded onto transport vesicles and directly targeted to the synapse indicates a yet unknown mechanism for DAT-1 synaptic targeting and accumulation. Recent findings of non-SNARE dependent

trafficking of the rat gamma-aminobutyric acid transporter (rGAT-1) supports a role for the Exocyst complex proteins may be important for transporter budding from the Golgi/ER complex and subsequent plasma membrane localization/insertion (Farhan et al., 2004).

The Exocyst complex was originally identified in yeast and involves at least 15 gene products which are specifically involved in vesicular transport from the Golgi to the plasma membrane (TerBush et al., 1996). A member of the Exocyst complex, Sec-5, was shown to effect neuronal outgrowth without effecting synaptic release in drosophila, suggesting that the Exocyst complex does not effect synaptic vesicle targeting but does localize proteins important for neuronal growth to the plasma membrane (Murthy et al., 2003). This model of Exocyst mediated transporter localization supports a non-UNC-104 dependent localization process that should be examined further.

This study highlights *C. elegans* DAT-1 steady state localization in fixed and permeabilized wild type strains using newly developed C-terminal antibodies. These antibodies recognize full length DAT-1 in both transfected cells and in native wild type tissues, demonstrating utility as an immunohistochemical reagent. RB1565 also recognized full length DAT-1 protein via western blot analysis, making this antisera a potential biochemical reagent. Examination of the UNC-104 mutant line suggests that DAT-1 is not trafficked by this kinesin motor protein but might use a heretofore unrecognized localization strategy, potentially via exocyst machinery as is suggested for rGAT-1.

CHAPTER IV

LOCALIZATION AND TRAFFICKING OF *C. ELEGANS* DAT-1 *IN VIVO*

INTRODUCTION

Reuptake of DA through DAT is the primary mechanism by which DA signaling is terminated at the synapse (Gainetdinov et al., 1998; Benoit-Marand et al., 2000). Either genetic or pharmacological ablation of DAT leads to a marked increase in DA clearance time, with clearance rate in the synapse diminishing to diffusion (Giros et al., 1996). This data implies a specific need for DAT to govern both the spatial (synaptic) and temporal (rapid termination) clearance of DA. It is therefore important to understand mechanisms by which DAT is trafficked and retained at the synapse in order to better understand DA signaling in the nervous system.

Electron micrographs using gold labeled antibodies directed against the rat DAT (rDAT) revealed that rDAT is located at the plasma membrane and on tubulovesicular structures near the soma of cell bodies. It is also localized to plasma membranes in intermediate and distal dendrites in the Ventral Tegmental Area (VTA) and Substantia Nigra (SN), with the majority of rDAT localizing on either side of the active zone in a perisynaptic zone at the synapse (reviewed in Chapters I and III). These studies give a static image of DAT localization in fixed and sectioned tissue. Several *in vivo* imaging studies including imaging in rhesus monkeys using radiolabeled ligands specific for DAT show a high density of DAT in the striatum (Fischman et al., 1997). Although these studies are consistent with an accumulation of plasma membrane elaborated DAT at

nerve terminals observed in the high resolution immuno EM antibody studies (Hersch et al., 1997; Nirenberg et al., 1997), they are of insufficient resolution to ascertain subcellular localization patterns in the same cell.

The discovery of a bioluminescent protein that can be genetically encoded revolutionized the study of protein trafficking both *in vitro* and *in vivo*. Publication of the primary sequence of the green fluorescent protein (GFP) from the jellyfish *Aequorea victoria* enabled biologist, for the first time, to encode genetically a fluorescence molecule (Prasher et al., 1992) and examine gene expression, protein trafficking and protein-protein interactions in real time, *in vivo*.

The cloning of various DATs combined with the publication of the GFP sequence made translational fusions of DATs that could report DAT localization a possibility. An NH2-terminal GFP fusion to hDAT was first utilized in 1999 when Daniels and Amara examined PMA induced internalization of hDAT in Madin-Darby canine kidney (MDCK) cells (Daniels and Amara, 1999). Discussion of PMA-induced internalization of the transporter were emerging in the literature and various kinetic and biochemical studies had supported the idea of hDAT internalization upon PMA stimulation (Pristupa et al., 1998). Using the GFP:hDAT fusion, regulated internalization upon PMA activation could be both qualitatively and quantitatively assayed in living cells, bypassing the dependence of molecular biologists on fixation and use of fluorescently labeled antibodies. Fluorescently labeled DATs have since been used as tools to examine cellular localization, oligomerization, and movement of DAT in response to various stimulus in real time, demonstrating the utility of such fusions for elucidating DAT regulation (Sorkina et al., 2003; Kahlig et al., 2004; Garcia et al., 2005).

Torres *et al.* identified PICK1 as a modulator of DAT localization to the plasma membrane, suggesting that there exists proteins which mediate DAT localization in the membrane. PICK1 was originally identified as a PKC interacting protein and was subsequently named for this interaction (protein that interacts with C kinase or PICK1) (Staudinger et al., 1995). PICK1 contains a PDZ (PSD-95, dishevelled and ZO1) motif which is a molecular protein interaction domain and was found to be the mediator of PICK1/PKC binding (Staudinger et al., 1997). This PDZ domain is promiscuous and can interact with several different tripeptide binding motifs including a type I (S/TxV, where x is any amino acid) and type II (ϕXϕ, hydrophobic, x, hydrophobic) interaction domain usually located at the distal COOH-terminus of proteins (Staudinger et al., 1997).

Investigation of DATs reveals a conserved type II PDZ binding motif in the distal COOH-terminus. When the COOH-terminal peptide was used as bait in a yeast-two-hybrid screen, PICK1 was identified as a DAT interacting protein (Torres et al., 2001). Truncation of the PDZ binding domain revealed that it is important for DAT maturation in the Golgi, plasma membrane retention, and function (Torres et al., 2001; Bjerggaard et al., 2004). Evidence from Torres *et al.* suggested that this binding domain might mediate synaptic targeting of DAT in midbrain cultures. Bjerggaard *et al*. found, however, that in cell culture, interfering with the PDZ binding domain by addition of an alanine to the PDZ binding sequence (which has been shown to disrupt PDZ interactions) did not interfere with plasma membrane expression. However, ablation of the PDZ recognition motif correlates with a decreased protein expression and results in intracellular accumulation.

To advance studies of DAT regulation in a genetically tractable model system, we previously established the cellular localization of the *C. elegans* DAT-1 protein using

DAT-1 specific antibodies. In the current study, we take advantage of facile *C. elegans* transgenic techniques to examine the localization of a green fluorescent protein (GFP) fused to the NH_2-terminus of DAT-1, creating a GFP:DAT-1 translational fusion protein. This protein is expressed specifically in nematode DA neurons *in vivo* in an attempt to establish a platform for studies of GFP:DAT-1 distribution and examine effects of mutations, including truncation of this conserved PDZ binding domain.

The distribution of NH_2-terminal-tagged GFP:DAT-1 matches that expected from native DAT-1 expression, including synaptic co-localization with monomeric red fluorescent protein (mRFP)-tagged vesicular monoamine transporter (VMAT). Whereas mRFP:VMAT targeting to synapses is lost in the synaptic vesicle motor mutant *unc-104*, GFP:DAT-1 (as well as native DAT-1 protein (described in Chapter III)) synaptic localization is unaffected, revealing a heretofore unrecognized mode of delivery of DAT-1 protein to synapses.

To date there is no model for the study of biogenic amine transporter localization to synaptic regions in an intact nervous system *in vivo* achievable at single neuron resolution. In this study we present efforts to quantitate the localization of the *C. elegans* DA transporter (DAT-1) in different compartments of single dopaminergic neuron *in vivo*, and examine the impact of various perturbations linked to altered transporter trafficking, including the study of DAT-1 mutants identified in a forward genetic screen for 6-OHDA resistance, DAT-1 localization in an UNC-104 (microtubule based transport) deficiency line, and alteration of a canonical PDZ binding domain that is conserved in DAT-1.

MATERIALS AND METHODS

Plasmid Construction

P_{dat-1}::GFP:DAT-1 vector constructs

In order to establish localization of a GFP:DAT-1 fusion protein *in vivo*, a GFP:DAT-1 *C. elegans* expression vector was generated. Creation of the P_{dat-1}::GFP:DAT-1 fusion vector pPM005 (pBY538) was described previously (Carvelli et al., 2004). The PDZ deletion mutant was created using oligo RB2004 (5' – CGG AAG ATC TTC AGT CAG AGT GCG GTT GAG TGG – 3') and RB1241 described previously (Carvelli et al., 2004). Amplification of *dat-1* cDNA using antisense oligo RB2004 deletes the final 9 nucleotides from the distal COOH-terminus, creating a premature stop and ablating a PDZ motif (IML*) upon translation. This ΔPDZ fragment was sub-cloned into pGem2T-easy and the entire *dat-1*ΔPDZ cDNA was sequenced. A correct clone was identified and sub-cloned into pBY538 replacing the full-length *dat-1* cDNA and creating pBY814 (P_{dat-1}::GFP:DAT-1ΔPDZ). The COOH terminal fusion construct was created as described previously (Nass et al., 2002).

P_{dat-1}::CAT-1:mRFP vector constructs.

To establish synaptic areas in DA neurons, we created the DA neuron specific vector driving the monomeric Red Fluorescent Protein (mRFP) fused to the C. *elegans* VMAT homolog CAT-1. mRFP was amplified from a pRSETv containing mRFP1 (Campbell et al., 2002) using oligos RB1957 (5' – GGC GCG CCA TGG CCT CCT CCG AGG ACG – 3') and RB1958 (5' – GGC GAG ATC TTT AGG CGC CGG TGG AGT GG – 3'). RB1957 contains an *AscI* site just 5' of the mRFP ATG and RB 1958 contains a *BglII* site in place of the TAG stop codon. *C. elegans* vesicular monoamine transporter (VMAT or

CAT-1) was amplified from N2 genomic DNA using RB2010 (5' – CGC CTT AAT TAA TGT CGT ACA TTC TTG ATT GG – 3') containing a 5' *PacI* site and RB2011 (5' – GGC GCG CCT AAA TGC ACT GGT TGC AG– 3') containing a 3' *AscI* site. Both mRFP and CAT-1 products were cloned into pGEM2T-easy creating pPM023 and pPM024 respectively. Both clones were sequenced as above. The *dat-1* sequence from pBY538 was removed and replaced with mRFP isolated from pPM023 using *AscI* and *BglII*, enzymes creating pPM023.1. The GFP sequence from pPM023.1 was removed and replaced by *cat-1* isolated from pPM024 using PacI and AscI enzymes to create P_{dat-1}::CAT-1:mRFP (pBY813).

Mammalian Cell Culture and Immunofluorescence

Methods for cell expression and imaging were described previously in Chapter III.

C. elegans Fixation and Immunofluorescence

Analysis of DAT-1 specific antibodies and strain preparation were described previously in Chapter III.

Sample Preparation for Imaging

In order to visualize fluorescent fusion proteins *in vivo*, gravid adults from either the BY250 (cytosolic GFP in all DA neurons), BY312 (GFP:DAT-1 fusion in all DA neurons), or the BY350 (GFP:DAT-1(ΔIML)) lines were picked to small NA22/OP50 plates and allowed to lay eggs. After 48hr at 20°C, small L2/L3 animals were collected using water and pelleted for 1 min at 2,000 x *g*. Alternatively, synchronized L1s were

plated on small NA22/OP50 plates and collected with water 24 hr after plating. Water was then decanted and anesthetic (.02% tetramisol, .2% Tricane in H_2O) was added to the animals. Animals were then allowed to paralyze in the anesthetic for 10 minutes before being mounted on a 2% agarose pad. Animals prepared for immunofluorescence studies were directly mounted on 2% agarose after final antibody wash was completed. Cover slips were then placed onto the sample and imaged within 30 minutes of original anesthetic exposure.

C. elegans Strains

All strains were derived from the wild-type N2 Bristol isolate and maintained at 14 to 25°C using standard methods (Brenner, 1974). The *unc-104 (e1265)* line was obtained from the *Caenorhabditis* Genetics Center (University of Minnesota, Minneapolis). The *dat-1(ok157)* strain was a gift of J. Duerr and J. Rand (Oklahoma Medical Research Foundation, Oklahoma City). The BY250 strain expressing cytosolic GFP driven by the DAT-1 promoter in DA neurons produced as described by Lakso and colleagues (Lakso et al., 2003) and was a gift from G. Wong.

C. elegans Genomic Preparation

Genomic preparation was carried out as describe previously (Nass et al., 2005).

C. elegans dat-1 Genotyping

In order to determine *dat-1* alleles, *dat-1* knockout (*dat-1(ok157)*) and wild type (*dat-1*) DNA was obtained and used to determine the genotype of lines after husbandry

experiments. Oligonucleotides directed against a 30 base sequence 200 bp 5' of the *dat-1* ATG (RB 1731 5' – GGC ACA CAT ACA CCG GAA TAT TCG ACA TGC – 3') and a 27 base sequence 15 bp 3' of the *dat-1* stop codon (TGA) (RB 817 5' – CGA GTG AAA CTA GGA TAA TGA AAG TGG – 3') amplify a 4 kb fragment in N2 animals. Mutant *dat-1(ok157)* animals contain a truncation midway through exon 4 that leads to a functional null (Nass et al., 2002). Amplification of the *dat-1* allele in this strain leads to a 1.8kb fragment. DNA from genomic preps was used at a concentration of 1ng/μL. PCR based analysis was performed using Advantage 2 PCR kit from BD Biosciences with 1ng of DNA, 50pM of RB 1731 and RB 817 in a total reaction volume of 25μL. PCR was performed in a Peltier thermal cycler (PTC-200 from MJ Research) using an initial "hot start" of 94°C for 2 minutes then followed by 30 cycles of 94°C melting for 15 seconds, 60°C annealing for 30 seconds, and 68°C extension for 6 minutes. Samples were then analyzed via agarose gel electrophoresis.

Construction of Transgenics and Stable Integrants

Stable transformants were created by co-injection of plasmid constructs with a marker plasmid using standard methods (Mello et al., 1991). Transgenic animals containing the GFP:DAT-1 translational fusion (pBY538) were obtained after co-injection of a final concentration of 15ng/μL of pBY538, 60ng/μL of pRF4[*rol-6(su1006)*], 50ng/μL of carrier DNA (pBluescript), and 2μL of 10x injection buffer into the *dat-1* strain. Transgenic animals containing the CAT-1:mRFP translational fusion (pBY813) were obtained after co-injection of a final concentration of 15ng/μL of pBY813, 60ng/μL of pRF4[*rol-6(su1006)*], 60ng/μL of carrier DNA (pBluescript), and 2 μL of 10x injection

buffer into *dat-1* strain. L4s from lines containing extrachromasomal arrays that conveyed low penetrance were exposed to 50ug/ml trimethyl Psoralen for array integration as previously reported (Clark and Chiu, 2003). All integrated lines were then outcrossed 4 times to *dat-1* animals unless otherwise noted.

C. elegans Husbandry

Previously we had acquired a strain that was genetically wild type for *dat-1* but contained GFP in all DA neurons (BY250) (gift from G. Wong). BY250 was crossed to *dat-1(ok157)* strains creating a new BY326 line that expresses soluble GFP in DA neurons but is in the DAT-1 KO backgound. To examine GFP:DAT-1 fusion function *in vivo*, BY312 animals integrated for the GFP:DAT-1 allele, were then crossed to strains carrying cytosolic GFP in the *dat-1(ok157)* background (BY326) strains creating BY329. The rest of the transgenic animals created were injected directly into *dat-1(ok157)* and outcrossed to *dat-1(ok157)* to preserve the *dat-1(ok157)* locus. These lines were then crossed to BY326 for use in the toxicity assays. All strains used in 6-OHDA toxicity assays were then genotyped to confirm the *dat-1* allele.

6-OHDA Toxicity Assay

The 6-OHDA toxicity assay was performed as described previously (Nass et al., 2002) with slight modifications. Animals were synchronized and plated as described previously (Carvelli et al., 2004). After 24 hours at 20°C, plates were screened for older L4 animals that had not been destroyed as L1s by the bleaching procedure. These animals were removed and the remaining L2/L3 animals were washed off of large 8P/NA22 plates

using sterile H_20. Animals were washed four times in H_2O to remove all bacteria. Animals were pelleted and moved to a 1.5mL microcentrifuge tube and the total volume of the worm/water slurry was resuspended to a total of 500µL. An initial stock of 100mM 6-OHDA in 20mM ascorbic acid was alliquoted and kept at -80°C and used in all experiments to reduce variability. An appropriate amount of the 100mM 6-OHDA in 20mM ascorbic acid stock was added to the 500µL worm slurry making the final concentration either 50mM 6-OHDA in 10mM ascorbic acid (AA) or 25mM 6-OHDA in 5mM AA. Animals were then rocked gently on a Nutator at room temperature for 1 hour. After treatment, animals were spread on a large 8P/NA22 plate without removal of the 6-OHDA. After 72 hr at 20°C, animals were washed off plates using H_2O and individual strains were placed onto separately prepared 2% agarose pads on slides for visualization. Strains were blinded for scoring and animals were scored on a 4 point scale with 4 = no intact neurons and 0 = all intact neurons. A total of 3 groups with 50 animals in each group made up the score for each strain. The total toxicity scored was determined as % toxicity using the total number of neurons ablated for the group divided by 200 (total number of neurons in group).

C. elegans Biochemistry

Strains were grown on large 100mm 8P/NA22 plates until gravid. Eggs were then harvested from adults by sodium hypocholirite treatment to synchronize strains (see above) and isolated in 35% sucrose by centrifugation for 10 min at 2,000 x *g* (Sorval). This purified egg population was then washed 3x in H_2O and 2x in M9 solution. Eggs were incubated at RT for 24 hours and allowed to hatch in M9 solution. After 24 hours

in M9, L1 larvae were plated on large 8P/NA22 plates and incubated at 20°C for 48 hr. Animals were then harvested using H_20 and then separated from bacterial contaminants using 35% sucrose flotation at 2,000 x *g* for 10 minutes (Sorval). The top layer containing L2/L3 animals was harvested and animals were washed 2x in H_20. After the second wash, protease inhibitor cocktail (Sigma) was added to the worm slurry and worms were quick frozen in liquid nitrogen. Frozen strains were then ground to a powder using mortar and pestle and kept at -80°C until ready for western blot analysis.

Western Blot Analysis

To each tube containing the worm slurry preps described above, 500µl of Radioimmunoprecipitation Assay Buffer (RIPA) containing a 1:200 dilution of Protease Inhibitor Cocktail (Sigma Cat#P8340) was added. The tubes were rocked on a Nutator at 4^0C for 2 hr. Post incubation, extracts were spun at 6,000 x *g* for 10 minutes to pellet undissolved worm debris. The supernants were then transferred to 1.7ml microcentrifuge tubes where they were centrifuged at 16,000 x *g* rpm for 20mintues to further remove debris. After centrifugation, samples were transferred to fresh 1.7ml centrifuge tubes and placed on ice. The total protein concentration of each sample was assayed using a BCA Protein Assay kit (Pierce Cat#23250) and analyzed on a SmartSpec 3000 (Bio-Rad). An equivalent amount of total protein from each sample was calculated and 35µg of total protein from each worm line, with the exception of BY250 where only 7µg of total protein was used to reduce the signal, was transferred to a new microcentrifuge tube then treated with 4X Lammuneli Sample Buffer for 30 min at 25^0C. The samples were run on a 4-20% Tris SDS-Page Ready Gel (Bio-Rad Cat# 161-1105) then transferred overnight

to an Immobilon-P PVDF membrane (Millipore Cat# IPVH00010). The membranes where blocked for one hour in Phosphate Buffered Saline (PBS) containing .5% Tween20 and 5% instant nonfat dried milk. After blocking, the membranes were incubated for one hour with a 1:1000 dilution in blocking solution of a primary Mouse anti-GFP antibody (Clontech BD Living Colors A.v. Monoconal Antibody (JL-8)). The membranes were then washed three times for 10 minutes with PBS containing .5% Tween 20. After washing, the membranes were incubated for one hour with a 1:15,000 dilution in blocking solution of a secondary Goat anti-Mouse peroxidase-conjuated antibody (Jackson ImmunoResearch Laboratories Cat# 115-035-062). The membranes were again washed three times for 10 minutes with PBS containing .5% Tween 20. The peroxidase was activated using Western Lightning Chemiluminescence Reagent Plus (Perkin Elmer Cat# NEL105) and exposed for 15 min to Hyperfilm ECL (GE Healthcare Biosciences Cat# RPN3114K).

To examine the accuracy of the protein loading equivalency, the membranes were stripped by rocking them in a 2% SDS, 62.5mM Tris-HCL pH6.8, and 0.7μl/ml b-mercaptoethanol stripping buffer at 50^0C for 30 min. The membranes were rinsed with deionized water then reblocked and blotted as described above but using a 1:1000 dilution of a primary Mouse monoclonal anti-Actin antibody (MP Biomedicals Cat# 69100) instead of the anti-GFP antibody.

Band densities were analyzed using NIH image and average band density values (±S.E.M) were imported into Excel. Each of the actin bands was normalized to the hightest intensity actin band and then used to normalize the band density recorded for the

GFP band density in that lane. Density values were then imported into GraphPad Prism (GraphPad, San Diego, CA) and used to generated density bar graphs.

Confocal Imaging

Imaging was performed as described previously (See Chapter II).

Quantitative Imaging

In order to determine relative amount of GFP:DAT-1 in different neuronal compartments within a single neuron, single confocal image planes (1.2µm) containing both cell body and synaptic regions of selected strains were imaged and used to determine the relative amount of GFP signal in the different cellular compartment. Each sample was scanned and saturation of pixels was monitored and digital gain was reduced until all pixels contained in the image plane were within linear range of the detector (0 – 255 AFU). A single image was then scanned using 4x averaging, containing a 1.2µm section that included both the synaptic and cell body regions of a single neuron (and when possible, the dendrite). Pixel intensity was determined using either a line scan over the surface of the cell body or synapse with the peak intensity value being used to calculate the overall intensity amounts. Alternatively, pixel density was calculated in Metamorph™ by selecting either an area of interest that included the entire cell body, to obtain a total cell body fluorescence measure, or a 15 unit radius circle was used to collect data from the synaptic region. Both methods yielded similar results and the specific method used is noted in the results. To ensure consistency, each image was examined non-biasly for a maximum pixel intensity level above 220 AFU. Any images that did not contain at least

one pixel above a threshold level of 220 AFUs (as measured by examining the "maximum" pixel intensity for the whole image in Metamorph™) were eliminated from the data set.

RESULTS

A GFP Fusion Protein Recapitulates DAT-1 Staining and Rescues 6-OHDA Sensitivity

To obtain data for DAT-1 localization and function in living animals, we fused GFP to the NH_2 terminus of DAT-1 and expressed the fusion protein in all DA neurons of a *dat-1* (KO) strain using the DAT-1 promoter. Microinjection of pBY538 (15ug/μL) with the rol-6 dominant plasmid (pRF4) and carrier plasmid (pBSKII) created transgenic animals containing an extrachromasomal array that were positive for GFP signal. Several lines displaying >90% penetrance were selected for imaging. All lines showed expression in all of the DA neuron head groups (ADEs and CEPs). GFP:DAT-1 expression was only observed in the posterior neurons (PDEs) in higher expressing lines (>15ng/μL/injection). Because these lines showed a high degree of mosaicism, we integrated the array into the genome to create four stably expressing lines. Of these four lines, the lowest expressing line, as assessed by fluorescent imaging (BY312), was used to examine GFP:DAT-1 localization and function in the DA neurons.

Confocal imaging of BY312 revealed detectable levels in all aspects of the 6 head DA neurons (Fig 10D) with no detectable GFP signal in the PDE neurons. The highest level of GFP expression localized to discrete swellings along the axonal projections and at the nerve terminals projecting into the nerve ring (Fig 10D, asterisks). All of the DA head neurons displayed a high level of GFP:DAT-1 expression in cell bodies, which was

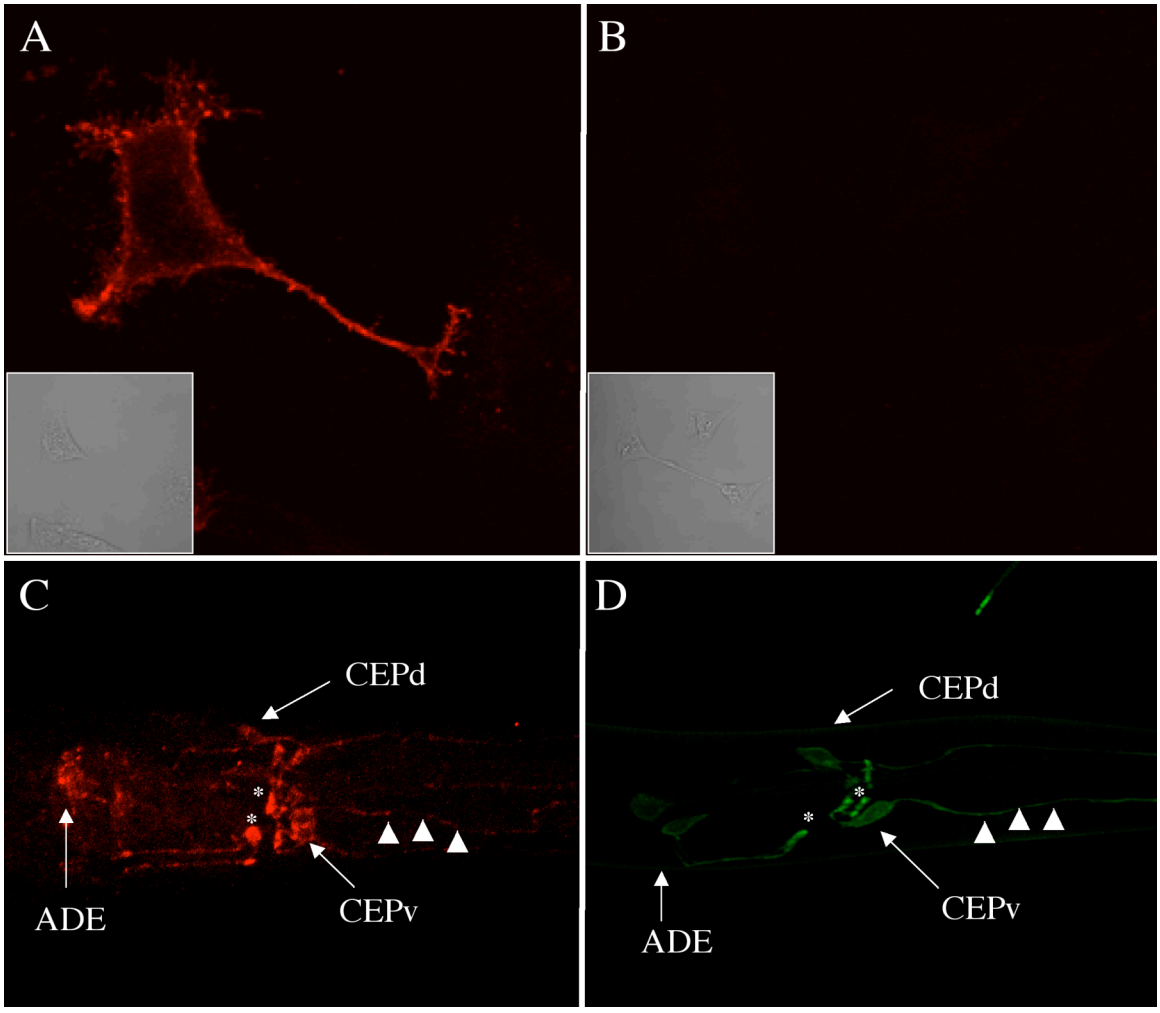

Figure 10. A GFP:DAT-1 Fusion Protein Recapitulates Native DAT-1 Staining.

Antibodies generated against the COOH-terminus of DAT-1 were first tested on HEK cells transfected with dat-1 cDNA. Specific staining of DAT-1 in transfected cells (**A**) but not in cells transfected with an empty vector (**B**) display specificity of DAT-1 antibodies. Antibodies were then used on wild type (N2 strain) animals and displayed a specific staining pattern for the 6 known DA head neurons (**C**). A GFP:DAT-1 fusion protein recapitulates this native staining pattern (**D**) with expression in the cell bodies (arrows) at terminals (asterisks) and in dendrites (arrowheads).

excluded from the nucleus and elaborated near the plasma membrane. The four CEP cells showed reduced but consistent expression out along dendritic processes (10D, arrowheads).

To test the function of the GFP:DAT-1 fusion protein *in vivo*, 6-OHDA toxicity studies were performed. Toxicity of DA neurons depends upon uptake of 6-OHDA via a functional, plasma membrane inserted DAT (Nass et al., 2002; Nass et al., 2005). Various lines expressing cytosolic GFP in all DA neurons were used to monitor this toxicity. These lines expressed either the wild type dat-1 allele (BY250), the genetically null allele (BY326), or the GFP:DAT-1 fusion protein in the null *dat-1*(*ok157*) background (BY329, Table 4). All three strains were synchronized and L2 animals were exposed to a high concentration (50mM) of 6-OHDA. This concentration was sufficient to lead to 81.1% toxicity of DA neurons in wild type DAT-1 expressing strains (BY250) with marked blebbing and loss of GFP fluorescence in all dendritic processes (Fig 11A, arrowheads). In control animals, only 10.6% of the *dat-1* knockout lines (BY326) showed any dendritic blebbing or toxicity, with the majority of animals showing no effects of the toxin (Fig. 11C). The introduction of GFP:DAT-1 into the genetically null background (BY329) substantially rescued 6-OHDA induced sensitivity to 67.3%, with animals showing a range of ablation of the dendritic processes (Fig. 11B, arrowheads). This level toxicity was significantly reduced compared to wild type (81.1% v. 67.3%, Students t-test) but provided sufficient rescue over the genetically null *dat-1* strain (Fig. 11D).

Table 4. DNA Plasmids Used for GFP:DAT-1 Experiments.

DNA Plasmids	Constructs	
pRF4	Expression	*C. elegans*
	Translated protein	*rol-6(su1006)*
pRB235	Parental Vector	pBlueScript II
	Expression	Cell Culture
	Vector Insert	dat-1 cDNA
	Translated Protein	DAT-1
pBY538	Parental Vector	pFA6
	Expression	*C. elegans*
	Vector Insert	$P_{dat\text{-}1}$::GFP:dat-1
	Translated Protein	GFP:DAT-1 fusion
pBY633	Parental Vector	pGEX-5x3
	Expression	Bacterial
	Vector Insert	dat-1 C-terminus
	Translated Protein	GST:DAT-1 C-term
pBY813	Parental Vector	pBY538
	Expression	*C. elegans*
	Vector Insert	$P_{dat\text{-}1}$::cat-1:mRFP
	Translated Protein	CAT-1:mRFP
pBY814	Parental Vector	pFA6
	Expression	*C. elegnas*
	Vector Insert	$P_{dat\text{-}1}$::GFP:dat-1(ΔIML)
	Translated Protein	GFP:DAT-1(ΔIML)

GFP:DAT-1 Co-localizes with the Synaptic Marker Protein VMAT:mRFP In Vivo.

The distribution of GFP:DAT-1 in the DA neurons revealed accumulation at regions consistent with presynaptic DA terminals innervating the nerve ring (Sulston et al., 1975). To better define the synapse, a known synaptic protein, the vesicular monoamine transporter (VMAT or CAT-1) was tagged and used for co-localization studies with GFP:DAT-1 *in vivo*. Specifically, a P_{dat-1}::CAT-1:mRFP line was created using vector p813 and expressed in the DAT-1 KO background (*dat-1(ok157)*). Expression was restricted to the DA neurons in *C. elegans* and displayed a punctate distribution, with the majority of the fluorescent signal emanating from the area of the nerve ring. These lines were then integrated and outcrossed 4x to the DAT-1 knockout line (*dat-1(ok157)*), to eliminate any mutations that might be caused the integration procedure, creating BY346. BY312 (GFP:DAT-1:*dat-1(ok157)*) animals were then crossed to BY346 animals to create a two color animal for use in co-localization studies.

The VMAT:mRFP signal displayed a distinctively different localization pattern compared to GFP:DAT-1 in the DA neurons *in vivo*. The VMAT:mRFP signal was split between unidentified punctate structures within the cell body (Fig 12B, arrowhead) and labeling of terminals projecting into the nerve ring (Fig 12B, arrow). Expression of another synaptic vesicle fusion protein, snaptobrevin (SNB-1) fused to mRFP, leads to a similar expression pattern in these same neurons (data not shown) leading us to believe that cell body accumulation is not an expression artifact, but rather a feature of synaptic vesicle associated protein expression and trafficking. Areas of highest GFP:DAT-1 fluorescence signal (Fig 12A, arrow) co-localized with VMAT:mRPF at terminals in the DA neurons (Fig 12C, arrow), providing evidence of synaptic enrichment of GFP:DAT-1

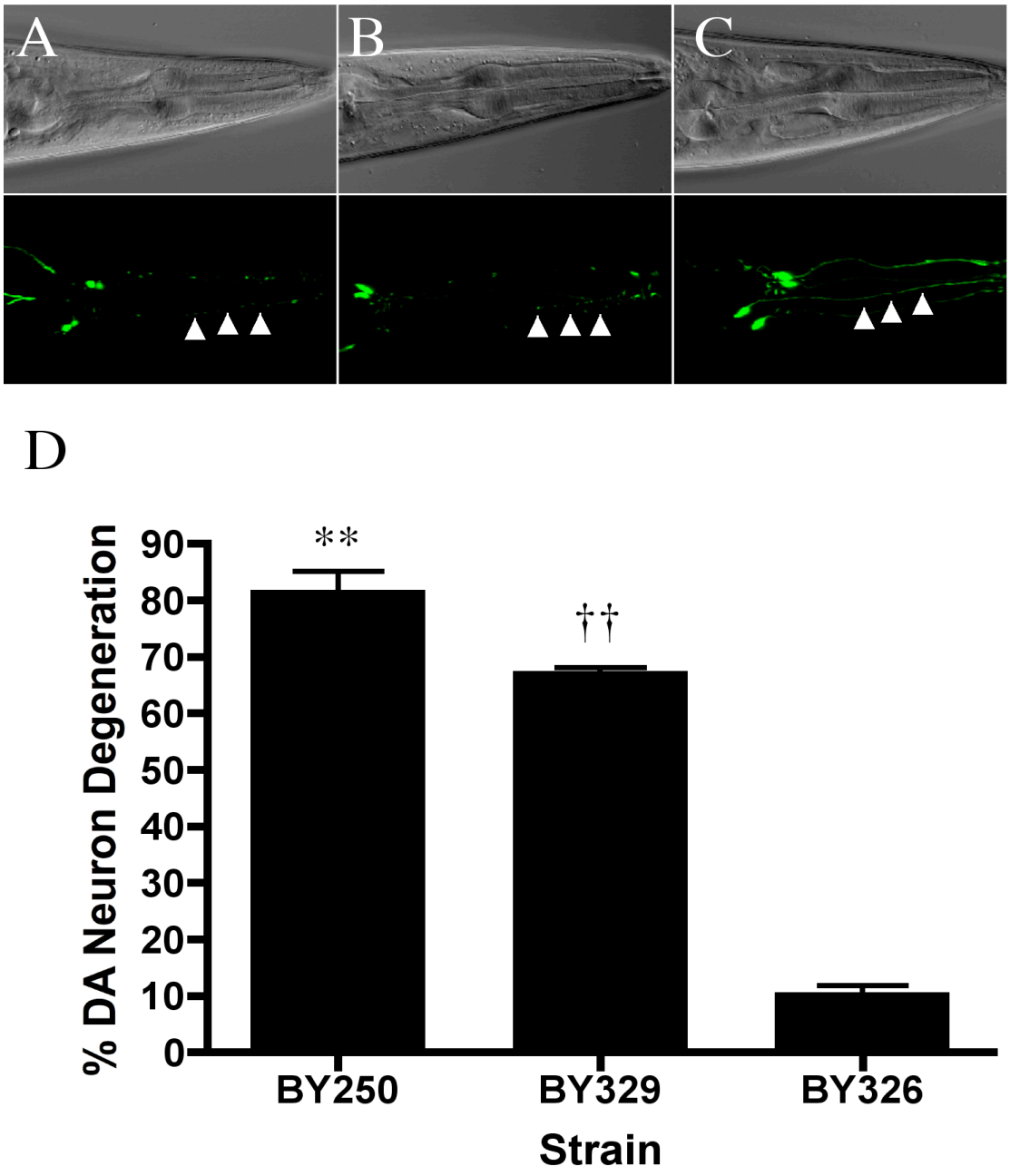

Figure 11. A GFP:DAT-1 Fusion Protein Restores DAT-1 Function *In Vivo*.

Animals expressing cytosolic GFP in all DA neurons were subjected to the DA specific neurotoxin 6-OHDA. Animals expressing endogenous DAT-1 (N2) were highly susceptible to 6-OHDA toxicity (**A** and **D**) compared to DAT-1 knockout lines (*dat-1*) (**C** and **D**) with fragmented dendrites (arrows). Animals that were genetically null for DAT-1 but expressed the GFP:DAT-1 fusion protein in all DA neurons (GFP:DAT-1;*dat-1*) rescued 6-OHDA sensitivity to near wild type levels (**B** and **D**).

in vivo. Occasionally, mRFP signal could be observed in dendritic projections that co-localized with GFP:DAT-1 accumulation at dendritic swellings, potentially displaying potential sites of *en passant* or dendro-dendritic signaling (see Fig. 12C, inset arrow).

GFP:DAT-1 Fusion Protein Accumulates at the Synapse In Vivo.

Having defined areas of GFP:DAT-1 accumulation as synaptic, we quantified DAT-1 distribution in different cellular compartments of individual DA neurons *in vivo*. Single 1.2μm confocal image planes containing cell body, synaptic regions, and occasionally dendrites of a single DA neuron in BY312 animals *in vivo*, were captured and used to determine the relative amount of GFP signal in different cellular compartments. Pixel intensity was determined using a line scan over the surface of either the synapse (Fig 13A), cell body (Fig 13B), or dendrite (not shown) with the peak intensity value being used to calculate the max intensity values. A representative intensity line scan reveals the Gaussian and punctate nature of the synaptic region (Fig 13C), while a representative scan from the cell body reveals a bi-modal distribution with most of the fluorescence falling along the perimeter of the cell body, within or near the plasma membrane (Fig 13D). Synaptic regions were found to have an average maximal fluorescence intensity value of 217.5 ± 6.7 AFU, while maximal cell body fluorescence was found to be 41.6% lower (127.0 ± 6.0 AFU) when compared to synaptic fluorescence (Fig 13E). Fluorescence in dendrites had the lowest value with an average fluorescence of 76.9 ± 8.5 AFUs or 65% less fluorescence compared to synaptic regions (Fig 13B). In contrast, expression of a cytosolic fluorophore (pTimer), resulted in a predominant accumulation of fluorescent signal in the cell body, with little export into the synaptic or

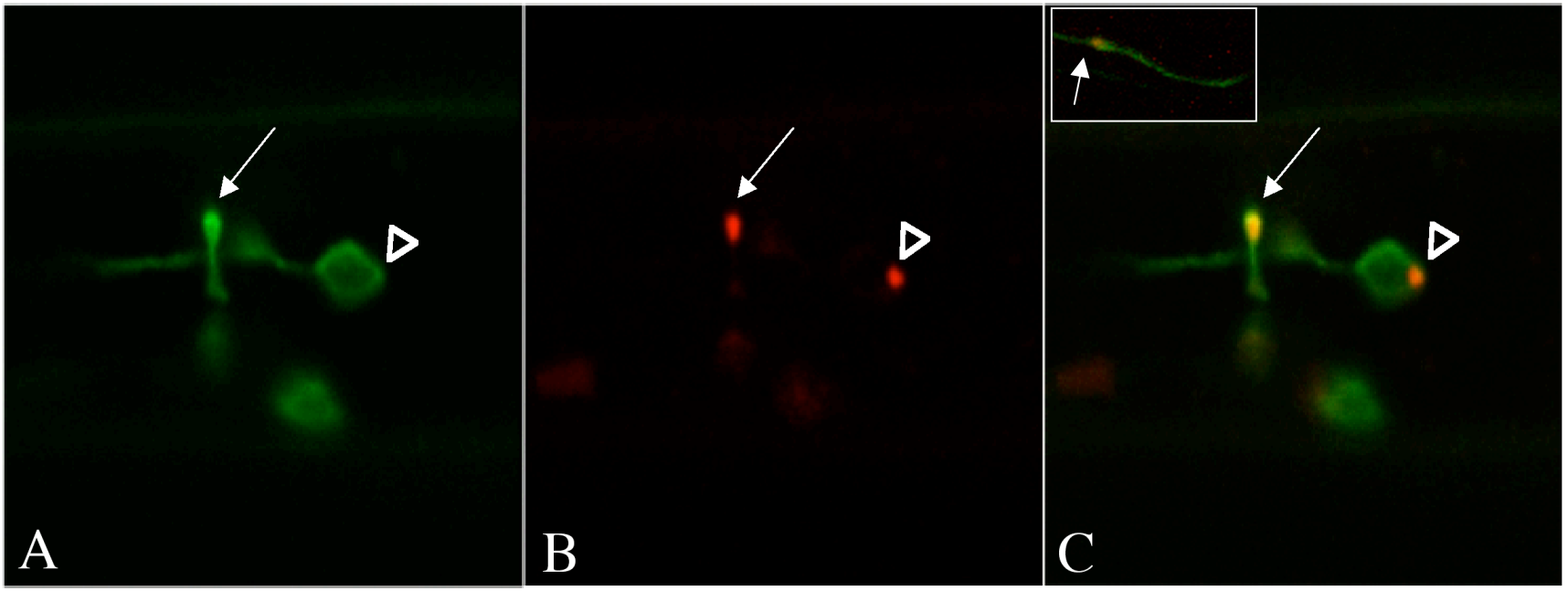

Figure 12. GFP:DAT-1 Co-localizes with VMAT:mRFP at the Synapse *In Vivo*.

Co-expression of GFP:DAT-1 and VMAT:mRFP in DA neurons *in vivo* reveals that GFP:DAT-1 accumulation at specific locations (**A**, arrow) are consistent with VMAT:mRFP synapses (**B**, arrow). There are also sites of VMAT:mRFP accumulation in the cell body which are independent of GFP:DAT-1 accumulation (**C**, arrowhead). VMAT;mRFP signal could also be visualized in swellings along dendrites (**C**, inset) suggesting en passent synaptic signaling in the dendrites.

dendritic regions (Fig. 14F & H). This data indicates that GFP:DAT-1 is not evenly distributed within the cell but rather accumulates at synaptic locations, suggesting either an active transport mechanism to the synapse or a passive retention of DAT-1 leading to accumulation at the synapse.

DAT-1 Does Not Traffic to the Synapse on Synaptic Vesicles

As noted in chapter II, synaptic vesicle associated proteins are delivered to the synapse via the kinesin motor protein UNC-104 (Hall and Hedgecock, 1991). Included in this list of UNC-104 dependent proteins is the VMAT2 homologue CAT-1 (Duerr et al., 1999). Several hypomorphic alleles of *unc-104* have been identified which display an overall uncoordinated phenotype resulting from cell body retention of synaptic vesicle precursors and their proteins, leading to a reduction in synaptic transmission. To determine UNC-104's role in GFP:DAT-1 synaptic accumulation, BY312 and BY250 lines were crossed to the *unc-104(e1265)* strain which carries an UNC-104 hypomorph, creating BY330 and BY354 respectively. VMAT:mRFP localizes to puncta in the nerve ring in a wild type (N2) strain (Fig 14B, arrow), but the mRFP signal is restricted to the ADE and CEP cell bodies in the *unc104* mutant line (Fig 14D, arrows). This is consistent with previously reported studies using CAT-1 antibody staining (Duerr et al., 1999), and confirms that the *e1265* allele is sufficiently hypomorphic to mislocalize VMAT:mRFP *in vivo*.

Examination of the BY330 lines revealed that reduced function of UNC-104 has no effect on overall GFP:DAT-1 distribution (Fig. 15B). GFP:DAT-1 distribution in the *unc-104* background did not effect accumulation of GFP signal into the nerve ring (Fig.

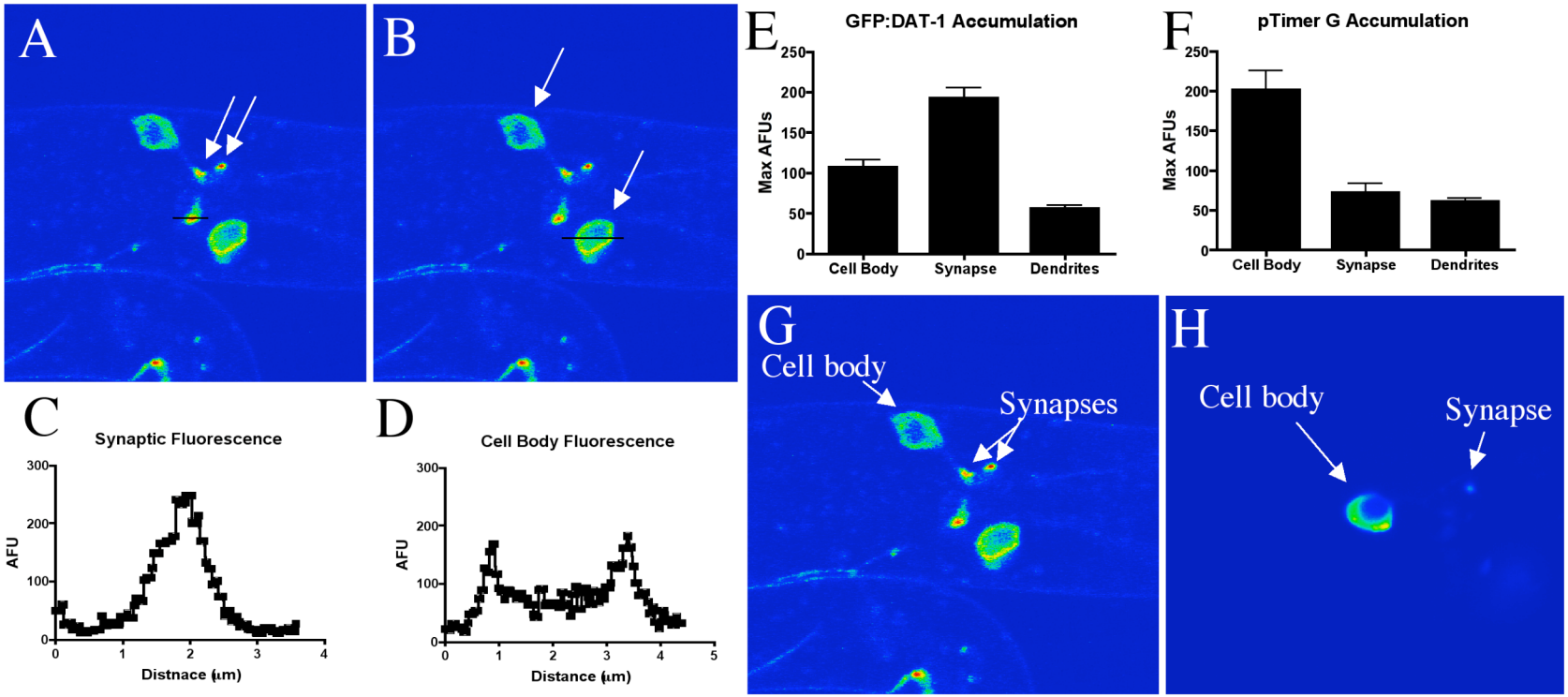

Figure 13. GFP:DAT-1 Accumulates at DA Neuron Presynaptic Terminals *In Vivo*

Pseudocolored single confocal images reveal that areas of highest GFP intensity (red) occur at synaptic areas (**A**, arrows). Line scans over either the presynaptic terminal or cell body reveal a punctate accumulation of signal at the synapse (**C**) v. a broad bi-modal distribution in the cell body (**D**). This synaptic accumulation is specific for the GFP:DAT-1 fusion (**G**) as a cytosolic fluorophore (pTimer) is retained predominatly in the cytoplasm (**H**). Quantification of signal from the various cellular compartments of individual neurons displays a differential distribution of GFP:DAT-1 with presynaptic terminal > cell body > dendrite (**E**). This distribution is different that that noted in the cytosolic pTimer lines ($p < .05$, Two-way ANOVA genetic line v. subcellular localization) (**F**).

15B, asterisk) nor out into dendrites (Fig. 15B, arrowheads). To ensure this was not an artifact of the GFP tag on DAT-1, the *e1265* strain was permeabilized and indirect immunofluorescence assays was performed to examine native DAT-1 localization in this strain. Consistent with the GFP fusion data, this hypomorphic allele had no effect on DAT-1 distribution *in situ* (See Chapter III). To test *in vivo* function of native DAT-1 in the *unc-104(e1265)* background, BY354 animals (Table 5) were subjected to 25mM 6-OHDA and assayed for DA neuron toxicity. Animals carrying the *e1265* allele showed a slight and insignificant increase in toxicity induced by 6-OHDA (Fig 19). Consistent with imaging studies, these data indicate that reduction of UNC-104 kinesin motor function has little or no effect on DAT-1 localization or function *in vivo*.

Animals Carrying the unc-104 Hypomorphic Allele Display Reduced Synaptic Accumulation In Vivo

Whereas VMAT:mRFP signal is entirely retained in the DA cell bodies in the (*e1265*) mutant background, GFP:DAT-1 expression extends both into the axons and dendrites, indicating that UNC-104 is not required for somatic export *in vivo*. Although the *unc-104(e1265)* background does not alter DAT-1 synaptic localization, *per se*, synaptic density in the *unc-104(e1265)* background is reduced (Fig 18, G). Accumulation of GFP:DAT-1 in nerve terminals of BY312 animals, not in the (*e1265*) backgournd, display a significantly higher density of GFP:DAT-1 signal (one-way ANOVA, $p < .05$). Because a consistent area measure is taken for each synapse (15 unit radius), and maximal pixel intensity within this region is calculated to be > 220 AFU for

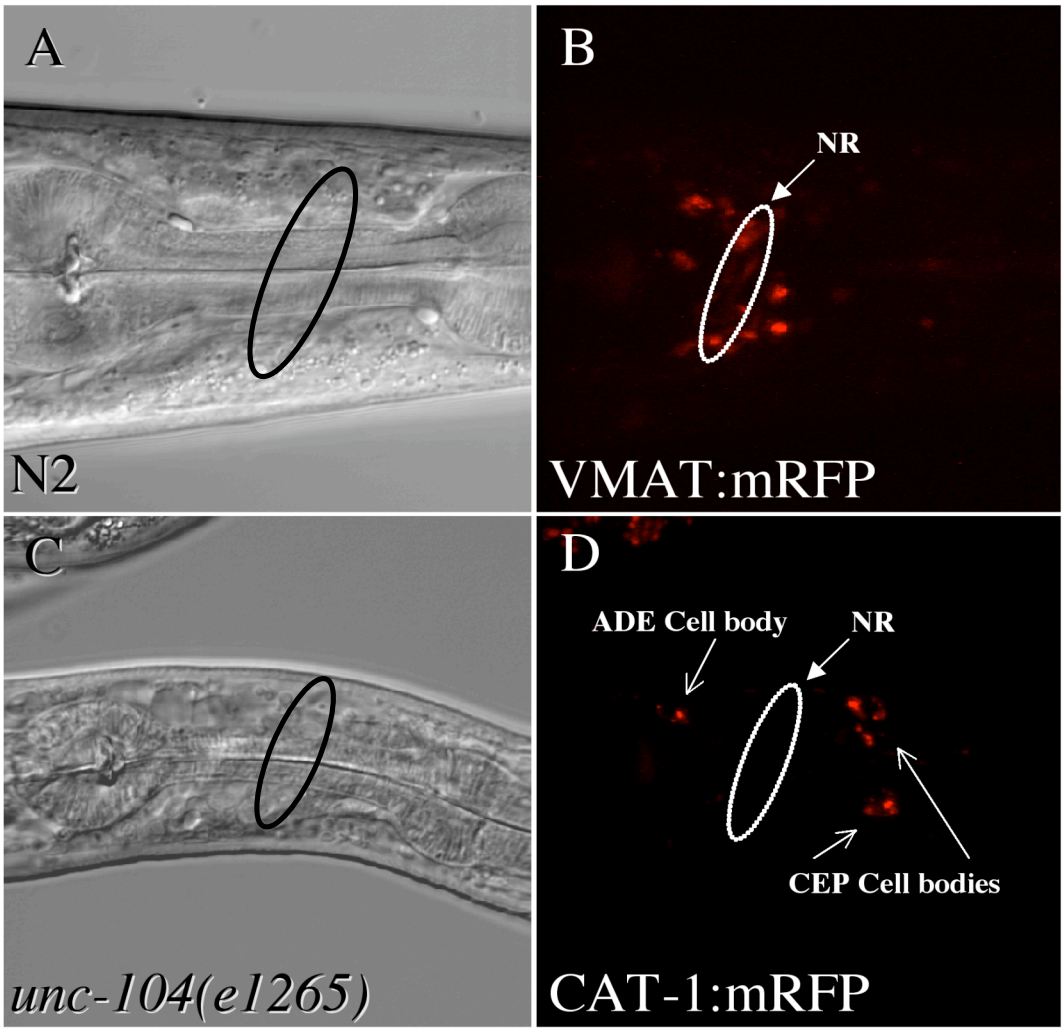

Figure 14. VMAT:mRFP is Retained in Cell Bodies in an UNC-104 Mutant.

VMAT:mRFP predominantly localizes to the nerve ring (NR) when expressed in a wild type (N2) strain *in vivo* (**B**, NR arrow). Outcrossing VMAT:mRFP to the e*1264* allele of unc-104 leads to cell body retention (**D**, ADE and CEP cell bodies, arrows).

each sample (see Methods), this result would indicate a decrease in synaptic density in these mutants.

Examination of Novel DAT-1 Mutant Alleles in C. elegans in vivo.

A genetic screen for mutants resistant to the DA specific and DAT-1 dependent toxin 6-OHDA was conducted and novel DAT-1 alleles were isolated (Nass et al., 2005). Three novel alleles were identified in this screen, two of which confered missense mutations, and a third that resulted in mis-splicing event which results in a neomorphic COOH-terminal tail. The two point mutations recovered result in a glycine to a glutamine amino acid substitution at positions 55 and 90 (G55E and G90E respectively). The third allele, a splicing mutation, results in a novel reading frame at the beginning of exon 12, resulting in a 13 amino acid substitution that replaces a 32 amino acid sequence normally coding the remainder of the DAT-1 COOH-terminus.

To determine the impact of DAT-1 mutations *in vivo*, we generated transgenic nematodes expressing either wild type or mutant GFP:DAT-1 fusion proteins in all DA neurons of the worm. Animals expressing the wt GFP:DAT-1 (GFP:DAT-1_{WT}) fusion displayed a readily detectible level of expression in all DA head neurons (CEP, ADE). We observed expression of GFP:DAT-1_{WT} primarily along the plasma membrane of the CEP and ADE cell somas, out along dendrites, and in terminals as described above, consistent a synaptic localization in the nerve ring (Fig 16A).

Examination of the expression pattern of animals expressing the G55E mutant (GFP:DAT-1_{G55E}) revealed little effect on the global distribution of the transporter. Overall GFP expression did appear reduced in these lines relative to the wild type

Table 5. *C. elegans* Strains Used to Test GFP:DAT-1 Function in *vivo*..

C. elegans Strains Created or Used		
N2	Genotype	Wild Type Strain
dat-1(ok157)	Genotype	dat-1 translocation mutation
	Protein expression	DAT-1 loss of function
unc-104(e1265)	Genotype	unc-104 mutant
	Protein expression	UNC-104 hypomorph
	Phenotype	Uncoordinated coiler
BY250(vtIs7)	Genotype	N2 background P_{dat-1}::GFP integration
	Protein expression	GFP in all DA neurons
BY312(vtIs6)	Genotype	*dat-1(ok157)* background P_{dat-1}::GFP:dat-1 integration pRF4 integration
	Protein expression	GFP:DAT-1 fusion in DA Neurons (low) *rol-6(su1006)* in cuticle
	Phenotype	Roller
BY320(vtIs13)	Genotype	*dat-1(ok157)* background pBY538 integration pRF4 integration
	Protein expression	GFP:DAT-1 fusion in DA Neurons (high) *rol-6(su1006)* in cuticle
	Phenotype	Roller
BY326	Genotype	vtIs7 in *dat-1(ok157)* background
	Protein expression	GFP in all DA neurons
BY329	Genotype	vtIs6; vtIs7; in *dat-1(ok157)* background
	Protein expression	GFP in all DA neurons GFP:DAT-1 fusion in all DA neurons *rol-6(su1006)* in cuticle
	Phenotype	Roller
BY330	Genotype	vtIs6 in *unc-104(e1265)* background
	Protein expression	GFP:DAT-1 in all DA neurons
	Phenotype	Uncoordinated
BY350(vtIs12)	Genotype	*dat-1(ok157)* background pBY814 integration pRF4 integration
	Protein expression	GFP:DAT-1(ΔIML) in all DA neurons *rol-6(su1006)* in cuticle
	Phenotype	Roller
BY351	Genotype	vtIs12; vtIs7; in *dat-1(ok157)* background
	Protein expression	GFP:DAT-1(ΔIML) in all DA neurons GFP in all DA neurons *rol-6(su1006)* in cuticle
BY352(vtIs13)	Genotype	*dat-1(ok157)* background pBY813 integration pRF4 integration
	Protein expression	CAT-1:mRFP fusion in all DA neurons *rol-6(su1006)* in cuticle
	Phenotype	Roller
BY353	Genotype	vtIs13 in *unc-104(e1265)* background
	Protein expression	CAT-1:mRFP fusion in all DA neurons *rol-6(su1006)* in cuticle
	Phenotype	Uncoordinated
BY354	Genotype	vtIs7 in *unc-104(e1265)* background
	Protein expression	GFP in all DA neurons
	Phenotype	uncoordinated

construct, suggesting an alteration in the overall amount of protein synthesized or retained within DA neurons (Fig 16B).

Transgenic lines carrying the G90E (GFP::DAT-1_{G90E}) mutation exhibited both a reduction in protein expression as well as an altered pattern of localization. In all lines examined, mutant expression was evident in the ADE and CEP cell bodies but was notably absent from either axonal or dendritic processes (Fig 16C). This distribution is consistent with both a protein trafficking/processing defect and enhanced degradation or reduced synthesis.

No appreciable GFP signal could be detected in lines injected with the COOH-terminal splice mutant (ΔK584R, GFP:DAT-$1_{\Delta K584R}$) mutation, despite clear evidence of successful transgene expression as indicated by *rol-6*(d) (+) phenotype. Only when the mutant DNA concentration was increased to over 3x the gene dosage used to create the other transgenic lines (50ng/μL compared to 15ng/μL), weak expression was evident, and in these cases, restricted to ADE and CEP cell bodies (Fig 16D).

Ablation of the COOH-terminal PDZ Binding Domain (IML) of DAT-1 Reduces DAT-1 Stability and Results in Inntracellular Retention.

Findings that elimination of the DAT-1 COOH-terminus in (GFP:DAT-$1_{\Delta K584R}$) leads to loss of synaptic localization encouraged us to further investigate elements in the DAT-1 COOH-terminus responsible for somatic export and synaptic localization. Several investigators have shown that the conserved COOH-terminal PDZ binding domain of several biogenic amine transporters is important for membrane insertion, and when deleted, leads to a decrease in maximal uptake (V_{max}) without a change in uptake

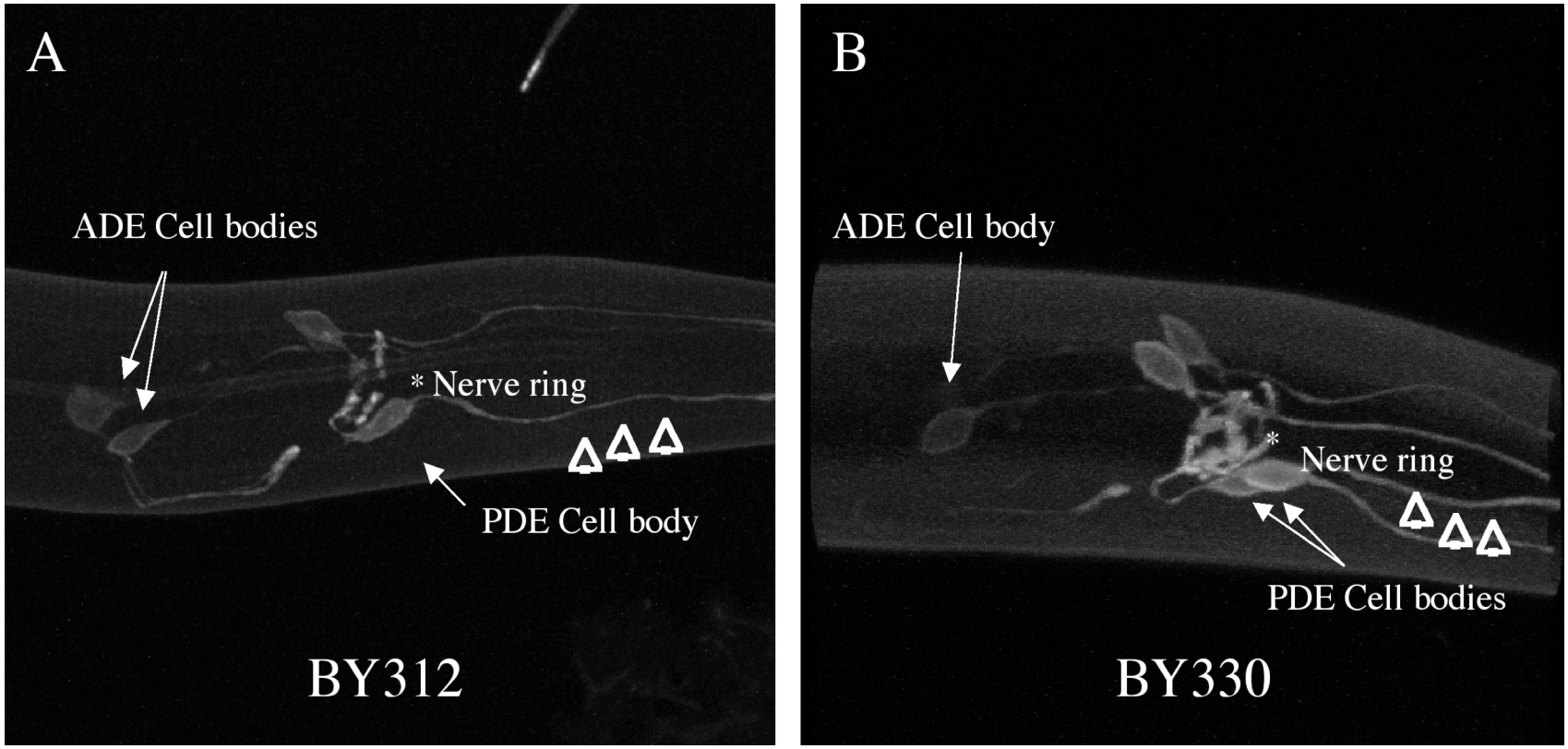

Figure 15. GFP:DAT-1 Distribution is Normal in the *unc-104(e1264)* Background.

GFP:DAT-1 expressed in wild type (N2) strains displays cell body (**A**, arrows) and dendritic expression(**A**, arrowheads), with accumulation at nerve terminals (**A**, asterisk). GFP:DAT-1 in the *e1264* background retains this distribution with full cell body (**B**, arrows), dendritic (**B**, arrowheads), and nerve terminal accumulation (**B**, asterisk).

kinetics (K_m) (Torres et al., 2001; Bjerggaard et al., 2004; Farhan et al., 2004). Torres *et al.* demonstrated that transfection of the hDAT lacking the PDZ binding domain into midbrain neurons results in cell body accumulation with a lack of synaptic targeting. To determine whether this conserved binding domain alters synaptic enrichment in *C. elegans in vivo*, a mutant GFP:DAT-1 construct lacking the last 3 amino acids (GFP:DAT-1(ΔIML)) was injected into *dat-1* strains.

Low concentrations of GFP:DAT-1(ΔIML) DNA (15ug/μL) initially used to create transgenic lines lead to stable transgenic strains (as measured by ROL-6 dominant phenotype) but displayed no detectible GFP signal. This concentration of wild type GFP:DAT-1 has been previously shown to yield high expression of GFP:DAT-1 in all head DA neurons (Nass et al., 2005). DNA was therefore injected at increasing concentrations (30, 60, and, 90 μg/μl) until a stable transgenic line could be obtained that displayed consistent GFP signal in all DA head neurons (at 90μg/μl).

Imaging of animals showing >90% penetrance for our injection marker (*rol*-6) revealed intracellular retention of some of the GFP:DAT-1(ΔIML) protein compared to wild type GFP:DAT-1 (See Fig 17A & B, arrows). This intracellular accumulation was never observed at any concentration in wild type GFP:DAT-1 expressing lines. Consistent with the intracellular accumulation observed in the ΔIML line, addition of COOH-terminal GFP (DAT-1:GFP), which occludes PDZ interactions (Bjerggaard et al., 2004; Madsen et al., 2005), recapitulates this intracellular accumulation (Fig 17C). These findings indicate that an intact and/or available DAT-1 COOH terminal sequences support efficient protein export and cell body export.

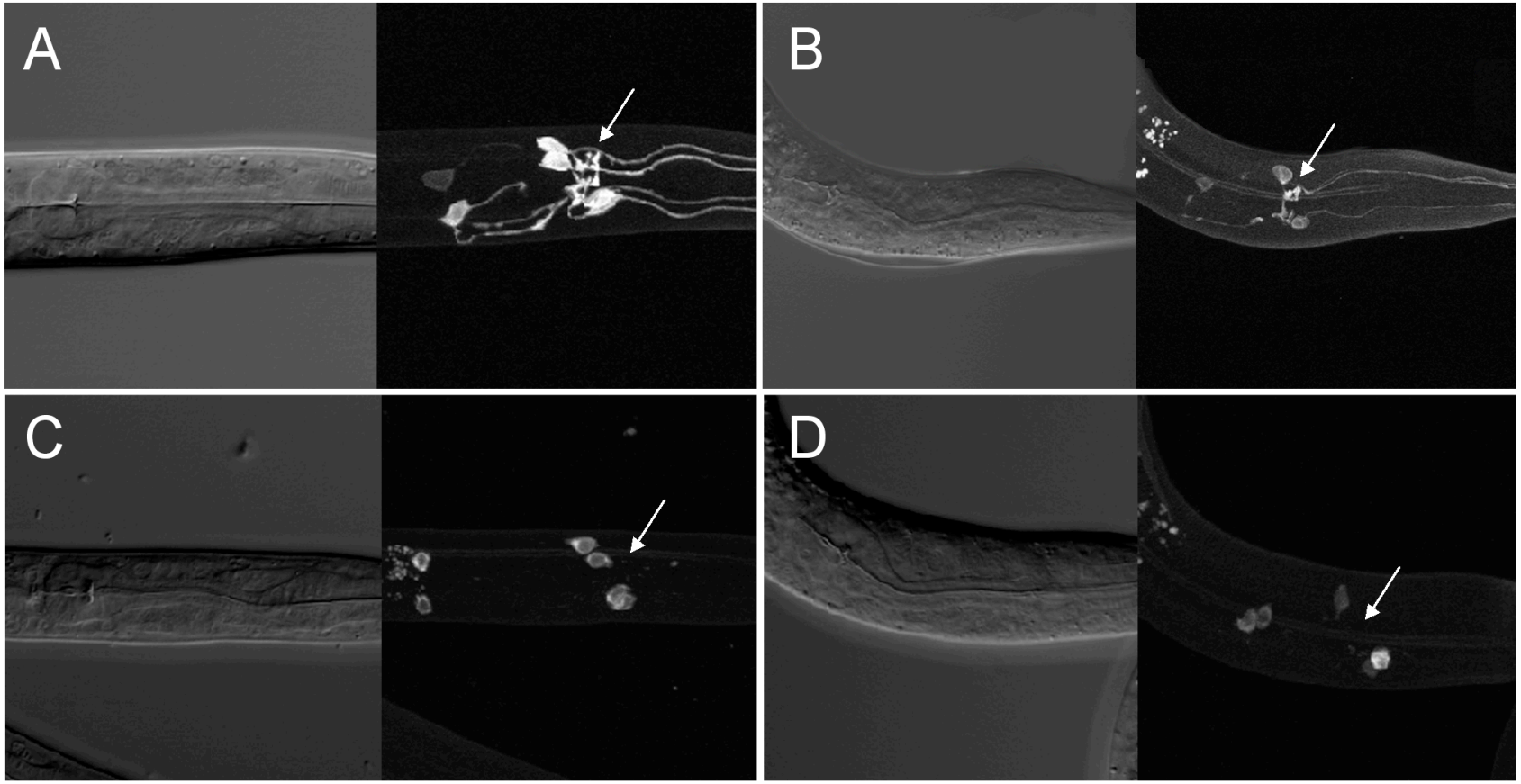

Figure 16. Altered Expression and Localization of DAT-1 Mutants.

A. Expression of wild type GFP:DAT-1 fusion with enhanced expression into the nerve ring (arrow). **B**. The G55E mutation leads to a decrease in overall expression but retains cell body and nerve ring expression (arrows). **C** and **D**. Both the G90E (**C**) and DK584R (**D**) expression is exclusive to the cell bodies with lack of nerve ring localization (arrows).

Neither PDZ Binding Domain Truncation Nor COOH-terminal Addition of GFP Effect Synaptic Localization In Vivo

The creation of an integrated ΔPDZ line (BY350) reduced the amount of GFP:DAT-1(ΔIML) expression and resulted in loss of cell body retention described above. GFP:DAT-1(ΔIML) cell body elaboration became indistinguishable from non-mutant GFP:DAT-1 protein cell body localization (Fig. 17A). There was no overall change in cellular distribution for the different DAT-1 strains (BY312, BY350, and DAT-1:GFP) with the PDZ mutant lines accumulating a majority of their fluorescence in the nerve ring (Fig 18B, C, & F, arrows).

To quantify subcellular localization among the different lines, fluorescence density measurements were made in the different neuronal compartments and compared across strains. Consistent with our earlier data regarding BY312 accumulation at synaptic regions, density measures were consistent with peak fluorescent values measured previously (Max AFU v. AFU/μm^2, Fig 13E v. Fig 18A). A significant increase in both cell body fluorescence and synaptic density is observed in the DAT-1:GFP strain (Fig 18E, asterisks) most likely as a result of significant transporter over-expression (Fig 18F). This visible increase in accumulation is not observed in the BY350 line, which maintains expression at levels comparable to both BY320 and BY312 (Fig 18C).

DA Uptake and 6-OHDA Sensitivity is Unaffected in Delta PDZ Strains

Although trafficking of GFP:DAT-1(ΔIML) to synaptic structures appears to be unaffected *in vivo,* these assays do not permit conclusions related to plasma membrane insertion. Therefore, we sought to determine the effect of this mutation on

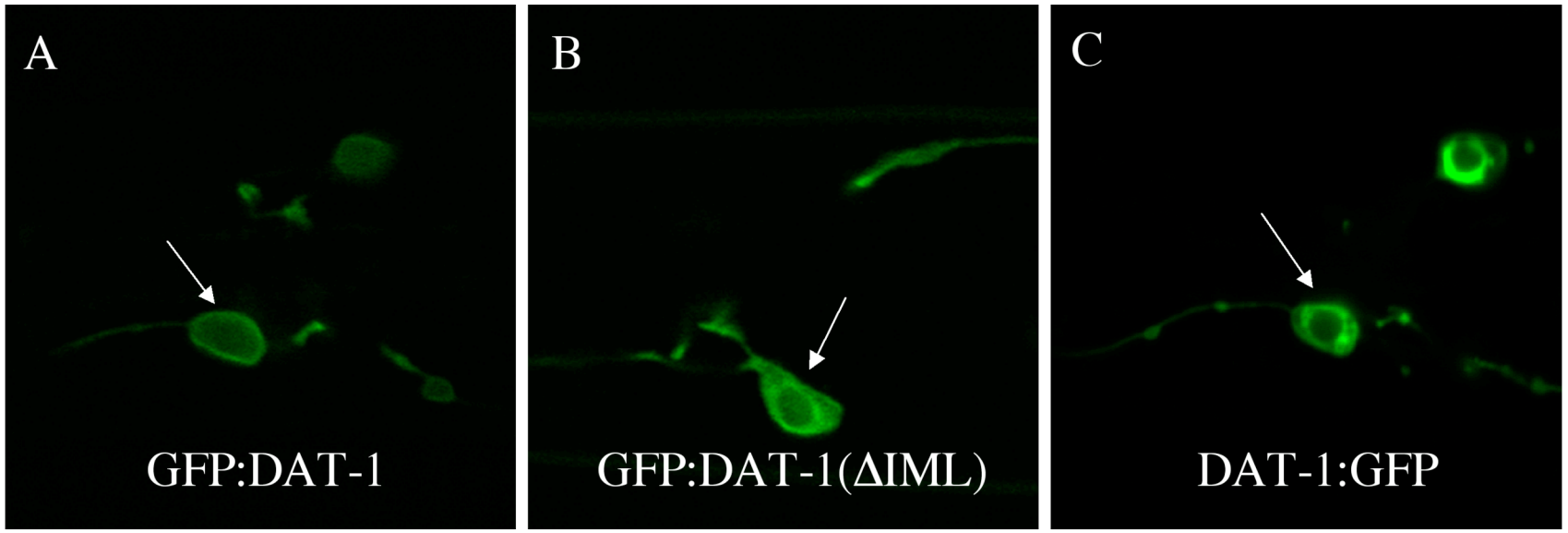

Figure 17. Disruption of the PDZ Binding Domain of DAT-1 Results in Intracellular Retention *In Vivo*.

GFP:DAT-1 in DA neurons displays a plasma membrane accumulation with no accumulation of intracellular signal *in vivo* (**A**, arrow). Truncation of the PDZ binding domain produces labeling of both plasma membrane as well as intracellular accumulation (**B, arrow**). Physical disruption of PDZ binding with the addition of a C-terminal GFP results in a cellular distribution that is similar to the truncation mutant, with marked intracellular accumulation (**C**, arrow).

DAT-1 transporter uptake capacity both *in vivo* and *in vitro*. It had previously been reported that a COOH-terminal DAT-1:GFP fusion rescued 6-OHDA sensitivity at a high 50mM concentration (Nass et al., 2002). To determine the functional significance of the PDZ binding domain truncation, the integrated the GFP:DAT-1(ΔIML) line (BY350) was crossed to a line expressing soluble GFP in the *dat-1(ok157)* background (BY326) to create BY351 for use in 6-OHDA experiments.

In an attempt to differentiate subtle differences between the strains, a 25mM concentration of 6-OHDA was used, which results in a 60% loss of neurons in the wild type DAT-1 expressing line (BY250). Consistent with data from higher 50mM studies, the BY329 line restores 6-OHDA sensitivity to the *dat-1* strain at levels which are mildly, but significantly, reduced compared to wild type (BY250) (Fig 11 and Fig 19). The BY351 strain displayed similar reduction in overall toxicity level compared to the BY250 line that was insignificantly different than toxicity observed in the BY329 line (Fig 19).

In vivo quantitiation using GFP fluorescence was used for relative comparisons between strains (see methods). GFP:DAT-1(ΔIML) in the BY350 line is expressed at a level that is intermediate to both the GFP:DAT-1 expressing lines (BY312 and BY320, Fig 20A). Western blot data of integrated lines using polyclonal GFP antibodies normalized to actin confirm these relative expression levels (data not shown).

Neurons cultured from the BY350 line display an intermediate level of uptake capacity, which is consistent with expression data (Fig 20A and B). Maximal uptake (V_{max}) suggests that PDZ truncation does not effect DA uptake in these cells (Fig 20B). To rule out contributions from a wild type dat-1 allele that may have contaminated these lines, genotyping for the *dat-1(OK157)* (KO) allele or dat-1 (N2) allele was performed on

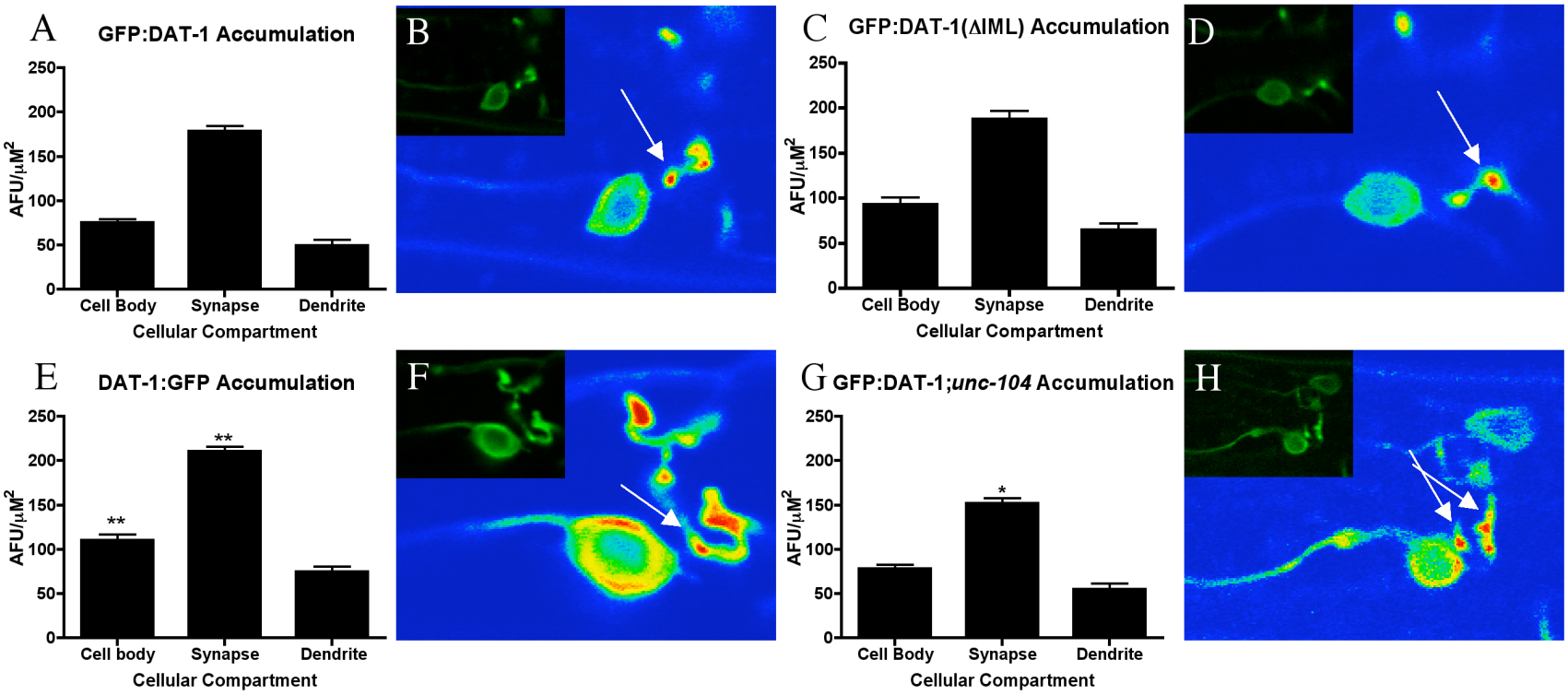

Figure 18. Despite Intracellular Accumulation, PDZ Disruption Does Not Effect Synaptic Accumulation.

Density of GFP signal in the different cellular compartments of the DA neurons *in vivo* reveals a synaptic accumulation phenotype for GFP:DAT-1 (**A & B, arrow**). This distribution is retained in either the PDZ truncation mutant (GFP:DAT-1 (ΔIML)) or the PDZ binding disruption line (DAT-1:GFP) (**B** and **C**). Significant accumulation of the GFP signal can be seen in the DAT-1:GFP line (**A** cell body v. **C** cell body, Student's t-test) however, the overall distribution is preserved. All regions tested against GFP:DAT-1 to generate statistical analysis. One-way ANOVA analysis was performed with ** being $p < .001$ (v. GFP:DAT-1 cell body or synapse) and * $p < .05$ (v. GFP:DAT-1 synapse)

the lines used for both uptake and 6-OHDA experiments. No wild type dat-1 contamination was found, indication that GFP:DAT-1(ΔIML) expression is sufficient to rescue both 6-OHDA sensitivity and DA uptake in the dat-1 background (Fig 20D).

Examination of DA uptake efficiency (uptake/DAT protein) suggests that the lowest expressing line (BY312) is capable of higher levels of DA uptake per unit transporter (Fig. 20C). As expression level increases, efficiency decreases suggesting the existence of a saturable process, limiting DAT-1 *in vivo* activity.

DISSCUSSION

This is the first demonstration of localization of a GFP-tagged biogenic amine transporter in an intact nervous system *in vivo*. Important in this study is the comparison of the NH_2-terminal GFP:DAT-1 fusion protein distribution to antibody visualized native proteins, as the NH_2-termius is a site of known protein interactions. Our previous antibody staining localizing native DAT-1 protein is recapitulated by GFP:DAT-1 fusions (both BY312 and BY320), including cell body elaboration and targeting of DAT-1 to synaptic regions within the nerve ring. GFP:DAT-1 expression was consistent with antibody staining of native DAT-1 expression in all compartments examined, including a low level of dendritic elaboration of both signals. Globally, antibody immunoreactivity was preferentially detected in the CEP neurons, followed by ADE and rarely seen in PDEs. The antibody data suggests that our GFP:DAT-1 fusion is fidelitus to native DAT-1 DA neuron expression.

The NH_2-terminal GFP:DAT-1 fusion allows for a more dynamic imaging modality for DAT-1 steady state localization in DA neurons of the nematode *C. elegans*

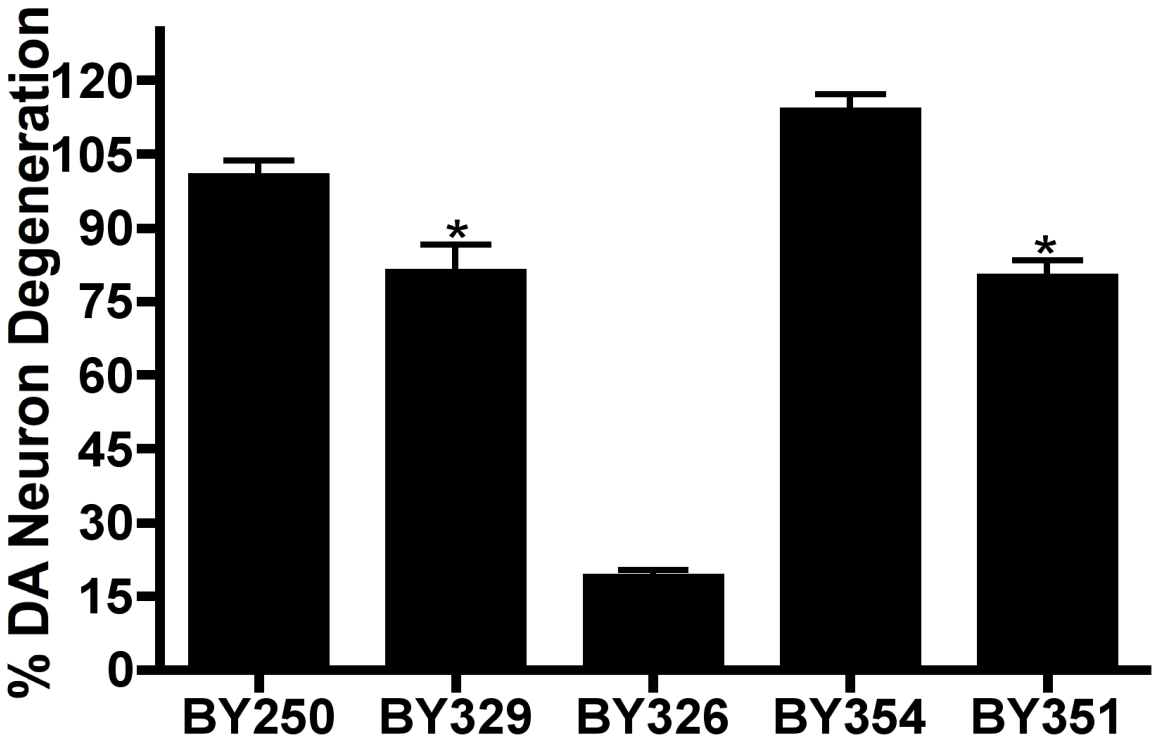

Figure 19. 6-OHDA Toxicity of Various DAT-1 Expressing Lines.

Both GFP:DAT-1 (BY329) and GFP:DAT-1(ΔIML) (BY351) rescue 6-OHDA sensitivity in a *dat-1(ok157)* knockout background. This rescue is significantly reduced compared to wild type (BY250) suggesting an effect of NH_2-terminal tagging. The *unc-104*(*e1264*) line expressing a wild type dat-1 allele shows robust toxicity with a trend toward an increase in toxicity (BY250 v. unc104). * $p < .05$ Student's t-test.

in vivo. Overall expression levels differed in the 3 sets of DA neurons in the worm with the greatest expression observed in the four neurons of the CEP cell group with a slightly lower level of expression in the two ADE cells and much lower level of expression in the 2 PDE neurons (CEP > ADE >> PDE), implying that there may be different regulatory elements in these cells. This differential expression level is consistent with native DAT-1 staining using immunofluorescence assays. The differential DAT-1 density in these neuronal groups may account for their differential susceptibility to 6-OHDA toxicity (Nass et al., 2002). Originally noted by Nass and colleagues (but also seen in our experience), the CEP cell group, which in our experience displays the highest level of both DAT-1 immunoreactivity and GFP:DAT-1 expression, is preferentially susceptible to the effects of this toxin. The ADE cell groups rarely display any notable toxicity as is true for the PDE neurons.

Examination of DAT-1 immunoreactivity at different stages of the worm's lifecycle was explored using DAT-1 specific antibodies and preliminary results indicate that DAT-1 immunoreactivity decreases precipitously between L4 and adult. Our GFP:DAT-1 fusion protein also demonstrated age specific expression, with highest expression observed in young L2/L3 animals. Synchronization of GFP:DAT-1 strains and preliminary examination of GFP expression over the lifetime of the animal indicates that GFP:DAT-1 fusion expression decreases after L4. Expression of the fluorescent molecule which changes its spectral profile as it ages, pTimer, indicates that the promoter is turned off near the transition from L4 to adult.

Differential cellular expression levels seen for DAT-1 in both the antibody experiments and with the GFP:DAT-1 fusion proteins is consistent with mammalian data

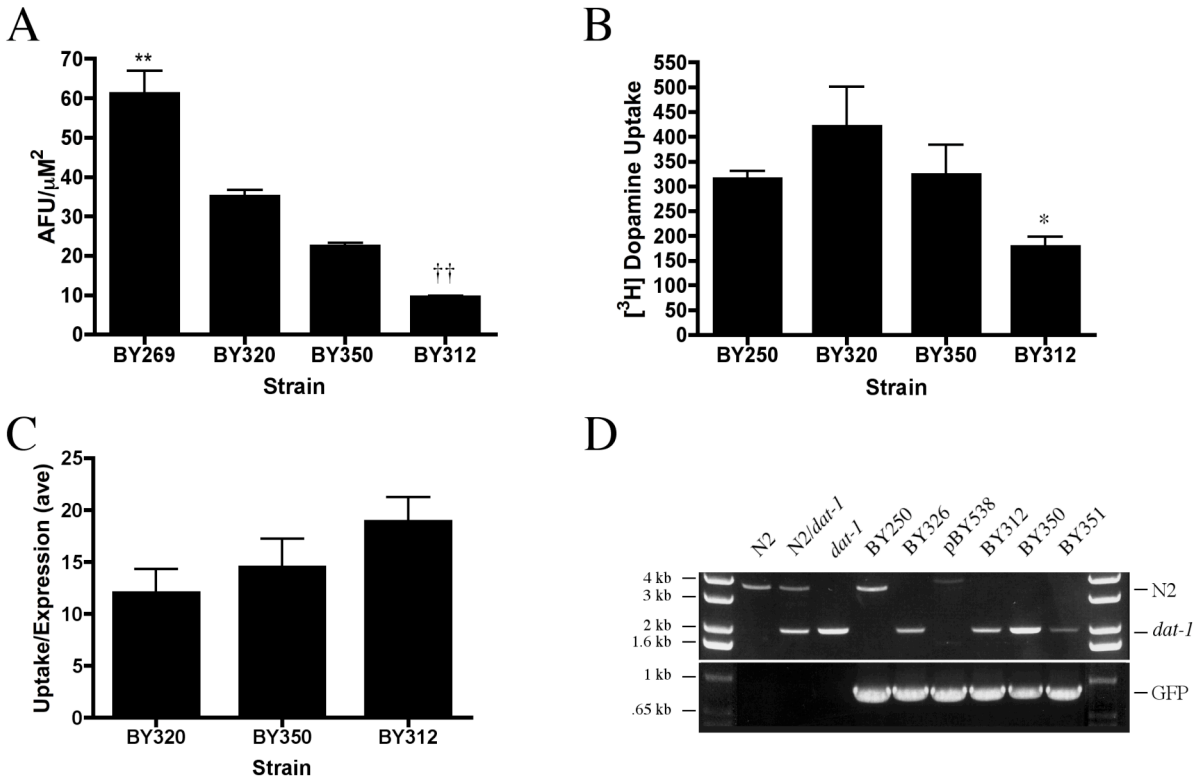

Figure 20. Strain Genotyping, Fusion Protein Expression Levels, and Uptake.

A. GFP expression density measures were taken from the cell body of different transgenic strains. The COOH-terminal fusion line displayed the highest expression level which was significantly different than BY320, 350, and 312 ($p < .01$, one-way ANOVA). There was no detectible difference between the GFP:DAT-1 high expression line (BY320) and the PDZ truncation line (BY350). The GFP:DAT-1 low expression line (BY312) was significantly lower than the BY320 line but not significantly different than the BY350 line. **B**. [^{3}H]Dopamine uptake experiments performed on cultures derived from the different integrated strains reveals that uptake follows a similar pattern as the expression seen in **A**. None of the strains tested were significantly different from the wild type stain (BY250). BY312 was significantly lower than BY320 ($p < .05$, one-way ANOVA). **C**. Normalizing DA uptake to expression reveals that there is no significant difference between strains. However, there is a trend for increased efficiency in the lower expressing line (BY312). To eliminate the possibility that the wild type dat-1 allele may contribute to the uptake noted in the delta PDZ lines, genotyping experiments were conducted (**D**). Amplification for the wild type (N2), heterozygote (N2/*dat-1*), and pure dat-1 KO allele (*dat-1*) and our experimental strains, reveals no dat-1 wt contamination in our expected KO lines (BY326, 312, 350, and 351). As a control, the vector originally used to create the transgenics (pBY538) was used and produced a faint band that ran higher than the 4.0 Kb WT band. Robust GFP amplification was seen for all GFP bearing lines.

where DATs are expressed at varying levels in different DA neuron groups. Highest levels of mammalian DATs is reported in substantia nigra neurons (in the nigrostriatal pathway) with lower expression observed in ventral tegmental neurons (in the mesocortical pathways) and scant expression in DA neurons of the arcuate nucleus (in the tuberoinfundibular pathways) (Hoffman et al., 1998; Ciliax et al., 1999), presumably reflecting differential needs for DA clearance in these pathways.

Despite consistencies between the wild type DAT-1 immunostaining localization and the GFP:DAT-1 fluorescence, there is a slight and significant decrease in 6-OHDA sensitivity between the native and GFP fused DAT-1. This difference may reflect a difference in copy number or disruption of N-terminal binding partners important for transport efficiency, which may be lost in the GFP fusion. We have previously shown a biophysical difference between the wild type DAT-1 protein and the N-terminal fusion, which results in an increase in open probability for the tagged transporter (Carvelli et al., 2004). The SNARE protein syntaxin 1A has been shown to interact with the NH_2-terminus of several biogenic amine transporters including the human DAT (hDAT) (Lee et al., 2004), the human norepinephrine transporter (hNET) (Sung et al., 2003), the rat serotonin transporter (rSERT) (Haase et al., 2001), and the GABA transporter (GAT-1) (Deken et al., 2000). These interactions are reported to change the conducting state of the respective transporters, altering ion permeation from coupled to uncoupled ion flux (SERT (Quick, 2003) as well as GABA and NE transport rates (Sung et al., 2000; Hansra et al., 2004)). Cumulatively, our data suggests that although a free NH_2-terminus is not required for DAT-1 synaptic accumulation, once localized, NH_2-terminal interactions may be required for appropriate transporter function.

The accumulation of GFP:DAT-1 at the synapse is independent of the function of the kinesin motor protein UNC-104, suggesting that DAT-1 is transported to terminals via mechanisms distinct from transport of synaptic vesicle precoursors. All synaptic vesicle proteins tested to date in *C. elegans*, require a functional UNC-104 (Hall and Hedgecock, 1991; Nonet et al., 1993; Nonet et al., 1998; Duerr et al., 1999). The fact that DAT-1 targets to synapses independently suggests that DAT-1 maybe loaded onto constitutive secretory vesicles rather than synaptic vesicles. This has recently been suggested for the GABA transporter GAT-1 where non-SNARE mediated exocytosis and trafficking is mediated by Exocyst proteins and is PDZ binding domain-independent (Farhan et al., 2004). Interestingly, synaptic density of GFP:DAT-1 is modestly reduced in the *unc-104(e1265)* background (Fig 19G), suggesting that UNC-104 dependent cargo or DA signaling itself may be important for establishing synaptic density of DAT-1.

Examination of mutant DAT-1 alleles illustrates that transgenic expression of GFP-tagged transporters in *C. elegans in vivo* is an amenable approach to investigate otherwise intractable questions about somatic export and synaptic targeting in an intact nervous system. As an initial example of the use of this system, we examined several DAT-1 alleles recovered from a forward screen using DAT-1 dependent 6-OHDA toxin accumulation and subsequent DA degeneration.

Biochemical experiments using an N-terminal, HA tagged version of these mutants revealed initial biosynthesis defects of these mutants, which tracked with the *in vivo* deficits reported here. The G55E mutant when expressed in COS-7 cells revealed reduced expression of full-length transporter that fails to express wild type levels of transporter on the plasma membrane and induces no detectable [^{3}H]DA uptake (Nass et

al., 2005). Expression of an NH_2-terminal GFP tagged version of the this mutant *in vivo* reveals an overall reduction of GFP signal with no detectable difference in overall localization. Loss of DA uptake activity in the face of relatively normal patterns of trafficking suggests that the G55 residue is likely to play an important role in the structural organization of DAT-1 protein and transporter surface insertion/stability but may also indicate actions of this residue in the DA transport process. The *dat-1(vt2)* allele, located in TM1, changes a conserved glycine residue to a glutamate (G55E) (Fig 21).

The G90E *dat-1* point mutation recovered in this screen, *dat-1(vt3)*, induces a conversion of a conserved glycine at position 90 in TM2 to a glutamate (G90E, Fig 21). The G90E mutation demonstrates a shift in the ratio of mature to immature protein such that there is a resultant accumulation of immature protein in COS-7 cells (Nass et al., 2005). Uptake of DA by this mutant was either just above or equivalent to that achieved with non-transfected cells, suggesting a significant impact on the DA transport process. *In vivo* GFP imaging indicates somatic retention with an accumulation of intracellular signal at opposing aspects of the cell bodies. While it does appear that some of the transporter resides at or below the cell surface, it is clear that no protein is trafficked out to synaptic or dendritic areas (Nass et al., 2005).

The recent publication of a high-resolution structure of a DAT-1 homolog, a leucine transporter ($LeuT_{Aa}$) from *Aquifex aeolicus* (Yamashita et al., 2005), adds new dimensions to interpreting the physical impact of DAT-1 mutations. Mapping of the DAT-1 Gly55 and Gly90 residues onto the $LeuT_{Aa}$ structure (in which these glycines are conserved) demonstrates that G55E mutation lies in close proximity to the proposed

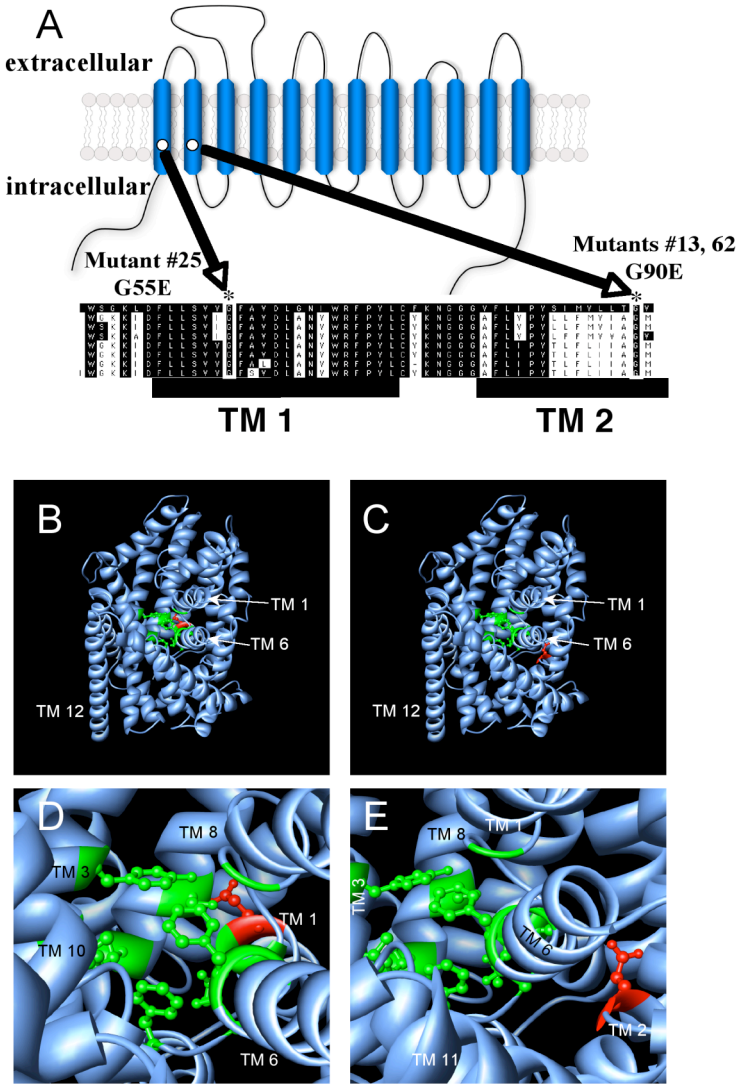

Figure 21. Structure Modeling of DAT-1 Mutations.

A. Schematic of DAT-1 membrane topology. The two mutations, G55E and G90E, occur at positions entirely conserved across eight species variants of dopamine, norepinephrine, and epinephrine transporters as well as most other SLC6 family members including $LeuT_{Aa}$. **B - E**. Side view of $LeuT_{Aa}$ crystal structure (PDB accession number 2A65.Q9). Proposed ligand-binding residues highlighted in green; DAT-1 mutations highlighted in red with glutamate side chain substituted for that of glycine. Amino acid substitutions introduced and images generated using UCSF Chimera software (http://www.cgl.ucsf.edu/chimera). **B.** $LeuT_{Aa}$ protein with the binding pocket (green) and the G55E mutation (red) highlighted. **C.** $LeuT_{Aa}$ protein with the binding pocket and the G90E mutation highlighted. **D**. Higher magnification of the proposed $LeuT_{Aa}$ binding pocket with the G55E mutation highlighted in red. **E.** Higher magnification of the proposed $LeuT_{Aa}$ binding pocket with the G90E mutation highlighted in red. (Figure courtesy of Ms. Julie Field, Vanderbilt, TN)

substrate binding site, engaging residues in TMs 1, 3, 6, and 8 (Yamashita et al., 2005). The substitution of a large, acidic side chain in this area likely results in a deformation of the ligand binding pocket, potentially changing the rotation or helix packing of TM1 that may serve a dual role in transporter assembly and function. In addition to the introduction of bulk at this site, the introduction of a charged side chain, and a new hydrogen bonding partner, in the bottom of the ligand binding pocket may disrupt the favorable binding orientation of DA or its co-transported ions, thereby reducing transport efficiency.

The TM2 mutation, G90E, introduces change in a region of the protein distal to the substrate binding site. However, the addition of increased bulk as well as the introduction of a charged side chain in a protein region likely isolated from the aqueous permeation pathway may significantly impact the helix packing of TM2 with its TM1 and 6 neighbors that support substrate interactions. Review of the $LeuT_{Aa}$ structure suggest that the G90E mutation may impact the structure specifically of TM6, a helix proposed to participate in ligand binding as well as the gating mechanism of transport (Yamashita et al., 2005). Given that the G90E mutant reported by Nass et al. 2005 exhibits a reduction in transport V_{max} but no change in DA K_m, it seems likely that alterations in helix packing of TMs 1, 2, and 6 induces significant adverse changes linked to the translocation of DA rather than compromising DA recognition. Like the G55E mutant, the decreased efficiency of helix packing of TMs 1, 2 and 6 may also induce global protein misfolding, resulting in trapping of immature DAT in the ER (Nass et al., 2005). In COS-7 cells, the G55E mutant demonstrates modestly diminished levels of both mature and immature DAT-1 protein, implying that this mutation does not affect maturation of dat-1 through the glycosylation pathway (Nass et al., 2005). *In vivo*, the G55E mutation yields an

overall diminished GFP signal relative to wild type DAT-1 suggesting this mutation leads to a diminished capacity of overall DAT-1 protein expression. The fact that significant quantities of DAT-1 G55E appear in the axons and dendrites of DA neurons coupled with the almost complete loss of surface expression observed in the COS-7 cell experiments suggests that this mutation may disrupt surface trafficking or retention, a measure that is likely indeterminable using *in vivo* imaging techniques currently utilized.

The most severe phenotype was evident for the COOH-terminal splice mutant (ΔK584R) where 32 amino acids from the DAT-1 COOH terminus were removed and replaced with an ectopic sequence unrelated to any sequences known in the gene family. Given both the removal of significant COOH-terminal sequences and the addition of ectopic COOH-termianal sequence, it is difficult define the exact mechanism supporting the loss of DAT-1 in these neurons. Regardless, the findings do underscore and important role of the native COOH-terminal sequences in DAT-1 biosynthesis and trafficking. In COS-7 cells, small amounts of immature protein and no mature protein were evident in total extracts, and surface fractions were devoid of DAT-1 protein (Nass et al., 2005). Similarly we could visualize no GFP signal *in vivo* until the DNA injection concentration was significantly increased (by over 3 fold). Even at 50 ng/μL (as compared with 15 ng/nL), only a few weakly visible soma were evident and no process expression could be visualized.

Recent studies have revealed that the COOH-terminal domain supports multiple protein-protein interactions and appears to be essential for transporter biosynthetic progression. The mammalian DAT COOH terminus has been found to interact with PICK-1 (Torres et al., 2001), α-synuclein (Lee et al., 2001; Lee et al., 2004), and Hic-5

(Carneiro et al., 2002). A *C. elegans* α-synuclein ortholog is not evident in a BLAST search of genomic sequences whereas multiple PICK-1 and Hic-5 related genes exist. Hic-5, a multiple LIM domain protein that may serve as a scaffold to link DAT to other modulators supporting DAT localization and/or function, interacts with the juxtamembrane regions of the human DAT COOH terminus, a region not highly conserved in *C. elegans* DAT-1, but nonetheless interrupted by alterations in DAT-1 COOH terminal sequences.

Several authors have investigated the effects of the DAT PDZ binding domain and have reported similar results as those presented here. Torres *et al*. first characterized an interaction with hDAT and the PKC interacting protein PICK1 that depended upon the type II PDZ binding domain located at the distal C-terminus of hDAT (Torres et al., 2001). In their study, co-expression of PICK1 with hDAT increased V_{max} for hDAT without affecting DA K_m values. This increase in DA transport activity was lost when the PDZ binding domain was ablated (-KLV), with a trend towards a decreased V_{max} for the truncated protein. Bjerggaard *et al.* provided a further characterize this interaction and also reported a significant decrease in V_{max} with the PDZ truncated transporter (-KLV*).

Intracellular retention in of hDAT PDZ truncation lines was initially reported by Torres *et al.*, who argued that this sequence may also play an important role in synaptic targeting for the rDAT (Torres et al., 2001). Bjerggaard *et al* also reported an intracellular retention observed for the PDZ truncated hDAT, coupled with an overall reduction in expression level for this mutant (Bjerggaard et al., 2004). Addition of even a single alanine to this sequence (LKV**A***), shown to interfere with PDZ binding, rescued

intracellular accumulation suggesting that the PDZ binding domain is not important for cell surface targeting but rather may be important for protein stability and/or expression.

In our study, the PDZ mutant lines were capable of rescuing both 6-OHDA sensitivity and uptake in cultured cells in the *dat-1(ok157)* KO background. Nass *et al.* previously reported that a COOH-terminal fusion rescues 6-OHDA sensitivity *in vivo* (Nass et al., 2002), indicating that PDZ ablation by sequence addition did not effect DA uptake capacity using this measure. In the current study, elimination of the PDZ binding domain (IML) is consistent with this finding, where 6-OHDA toxicity levels for transgenic GFP:DAT-1(ΔIML) line is similar to the full length GFP:DAT-1 fusion. Cultured neurons from this line also demonstrated substantial DA uptake capacity, consistent with total expression levels as observed by fluorescence and western blot analysis, indicating functional rescue is not limited to the substrate 6-OHDA toxicity assays.

Although DA uptake appears to be unaffected by PDZ disruption, loss of the PDZ binding domain leads to a decrease in overall expression, coupled with intracellular cell body accumulation. The intracellular retention observed with the PDZ ablation mutants, coupled with lack of expression evident in the ΔIML lines at low DNA concentrations, indicate multiple problems with overall stability and biosynthesis of the ΔIML construct. Interestingly, integration and decreased expression of the ΔIML construct resulted in rescue of this retention, which was not observed in high expressing WT lines (BY320), indication that PDZ binding may be secondary to another primary export/recycling process *in vivo*.

In contrast to Bjerggaard *et al* (2004), we find that masking of the PDZ binding domain with the addition of GFP to the COOH-terminus does not relieve the intracellular accumulation observed with the PDZ truncation, indicating that PDZ binding partners may be important for intracellular trafficking. Our data also conflicts with the findings of Torres *et al.* (2002) in that disruption of the PDZ binding domain did not affect synaptic accumulation *in vivo*. We are not the first to report a lack of effect examining PDZ binding domain ablation *in vivo*. Despite evidence that disruption of PDZ binding domain interactions blocks synaptic delivery of AMPA receptors and LTP induction *in vitro* (Hayashi et al., 2000), *in vivo* expression of a PDZ ablated GluR1 receptor, which replaced the endogenous GluR1 gene, failed to effect either synaptic localization or LTP induction (Kim et al., 2005). It is also unlikely that truncation of the IML sequence for DAT-1 reveals amino acids capable of maintaining PDZ interactions as the three amino acids proximal to this deletion are HSD, which are not recognized as a PDZ binding motif. Although interaction with a specific PDZ containing proteins has not been shown for DAT-1 *per se*, complete ablation of this conserved interaction domain would indicate that the IML sequence is not utilized for DAT-1 localization in *C. elegans*.

Given the role of DAT in the termination and modulation of DA signaling in the brain, motifs within DAT and proteins that determine DAT localization become important targets for drugs that aim to alter DA signaling. Here we present a novel system that illustrates the localization of the *C. elegans* DA transporter DAT-1 and use this sytem to explore the impact of DAT-1 mutations as well as manipulations of potential DAT-1 regulators. Our work establishes a pattern of synaptic enrichment

tractable for phramacological or genetic manipulations that define key determinants of presynaptic transporter function *in vivo*.

CHAPTER V

USING FLUORESCENCE RECOVERY AFTER PHOTOBLEACH (FRAP) TO MONITOR DAT-1 MOVEMENTS *IN VIVO*.

INTRODUCTION

Perhaps the earliest example of protein movement in a fluid membrane came from studies by Frye and Edidin who examined integral membrane protein movements using indirect immunofluorescence (Frye and Edidin, 1970). In these experiments, human and mouse heterokayrons were exposed to either primary antibodies directed against human cell antigen (polyclonal antibodies from rabbit directed against whole human cell membrane) or mouse antibodies directed against the H-2 alloantigen. Goat anti-mouse and goat anti-rabbit secondary antibodies were then conjugated to different fluorescent dyes and antigen mobility assayed after heterokaryons fusion was induced by Sendai virus infection. Frye and Edidin then described a re-distribution of both epitopes across the newly fused membrane and reasoned that this re-distribution occurred via diffusion in the membrane, setting the stage for examination of membrane fluidity and protein mobility in the plasma membrane.

A formal model of plasma membrane fluidity and protein mobility was popularized in 1972 when Singer and Nicolson published their fluid mosaic model for the structure of cell membranes (Singer and Nicolson, 1972). In the Singer and Nicolson model, the plasma membrane is described as an amphipathic lipid bilayer, containing integral membrane proteins that span the membrane using both polar and non-polar residues. This model supported thermodynamic movement of these proteins indicating

for the first time, the potential of proteins to be freely or differentially mobile in the plasma membrane, as suggested by the earlier work by Frye and Edidin.

In 1976, Axelrod and colleagues published their initial work on mobility measurement using fluorescence photobleaching recovery kinetics (Axelrod et al., 1976). This technique took advantage of the fact that fluorophores attached to lipids or proteins would loose their fluorescence and become "bleached" when exposed to a high intensity laser. Importantly, excitation intensity and duration could be adjusted so as not to damage the conjugated target whose lateral diffusion is being monitored. When focused and intensified, a small area of sample could be bleached and then monitored as the surrounding flourophores intermixed with the now bleached area. The rate of this recovery could be quantified and related to the diffusion of the fluorophores using an equation that assumed both "pure" two-dimensional diffusion and an excitation source with a Gaussian intensity profile. Another assertion was that the bleaching occurred at a speed significantly faster than the diffusion rate for the area (> 10% of the halftime for diffusion), so as not to mask any of the initial recovery during the bleaching phase. They experimentally tested this technique and verified its validity using a fluorescent dye in a water/glycerol (1:1) mix. This technique, originally termed fluorescence photobleaching and recovery (FPR), has since been renamed fluorescence recovery after photobleaching (FRAP) and will be referred to as FRAP throughout the rest of the chapter.

The first determination of integral membrane protein lateral mobility using FRAP was performed on rhodamine conjugated rhodopsin from frog outer retinal segments in 1981 (Wey et al., 1981). Using high speed flash photometry, The same lab previously reported a diffusion rate of rhodopsin in the membrane to be $(3.5 \pm 1.5) \times 10^{-9}$ cm^2/s

(0.35μm^2/s) (Poo and Cone, 1974). The conjugation of the rhodamine moiety had no effect on rhodopsin diffusion rate, making fluoraphore conjugation a viable option for non-photoreactive integral membrane proteins. One limitation of this system was that it required conjugation of organic dyes antibodies, limiting use to reconstituted, or *ex-vivo* preparations.

The use of genetically encoded green fluorescent protein (GFP) labeled fusion proteins for FRAP was first demonstrated by Cole *et al*, examining Golgi protein retention (Cole et al., 1996). Golgi membrane proteins were fused to GFP and FRAP studies of Golgi membrane was performed in transfected HeLa cells. This study revealed that within Golgi stacks, a highly mobile pool of proteins moves laterally along this membrane, with diffusion constants ranging from 3 to $5x10^{-9}cm^2$/s (0.3 to 0.5 μm^2/s). Examination of mutant Golgi proteins that appeared visually to be retained in specific stacks within the Golgi complex maintained this 0.3 to 0.5 μm^2/s diffusion rate. Although these proteins appeared "retained" in the Golgi membrane, they were clearly free to diffuse along that membrane and were not immobilized *per se*.

Several neuronal proteins have been the subject of FRAP experiments in both cultured neurons and non-native cell lines. Angelides first described that fluorescently labeled Na^+ channels from chick embryonic myotubes displayed altered fluorescence intensity, depending on cellular localization (synaptic v. non-synaptic). In additon, they found that the synaptically localized Na^+ channels were immobilized compared to the non-synaptic channels (Angelides, 1986). Examination of rat dissociated spinal cord neurons revealed a similar distribution of Na^+ channels, with a diffuse localization along the cell body plasma membrane compared to a clustering of signal at the axon hillock and

at nerve terminals (Angelides et al., 1988). FRAP experiments revealed that these punctate fluorescent signals were immobilized in the membrane, whereas the diffusely localized channels in the cell body were freely mobile.

To date, mobility estimates for a neurotransmitter transporter have not been reported using FRAP techniques. This information is of particular interest where distinct compartments appear to contain transporter proteins and associated molecules. The creation of transgenic *C. elegans* expressing GFP:DAT-1 fusions in DA neurons provides an opportunity to examine movements of one such transporter in an intact nervous system *in vivo*. With findings of GFP:DAT-1 localization reminiscent of sodium channel distribution in rat spinal cords as described by Angelidis, we reasoned that FRAP might also reveal differential kinetics of GFP:DAT-1 mobility in different compartments of DA neurons *in vivo*.

METHODS

In Vivo FRAP

In order to explore mobility of DAT-1 in different cellular compartments using FRAP, animals were prepared as described in Chapter IV and imaged via confocal microscopy using the Alexa 488 filter set with a 40x oil objective. Both the cell body and the synapse were normalized by adjusting the detector gain in order to maximize fluorescent intensity across the region of interest (cell body or synapse) for each experiment yet remain within the linear range of the detector. Images were captured using a 6x live zoom on the compartment of interest at 3% laser power. A series of 1.2μm optical slices (95.9nM pinhole) were taken over the course of the experiment and

set with no time delay between images. Five pre-bleach baseline images were collected before a single pulse of 488 laser at maximum intensity was exposed to a 15x15 unit box, with a bleach spot radius of 1.05μm within the sample. Another 25 samples were then collected without time delay (.986s between data point collection due to scan rate) and the region of interest that correlated to the bleach region was saved for analysis.

Sample Preparation for Live Imaging

In order to mount the live nematodes for FRAP analysis, animals were prepared as described previously in Chapter IV, except a more potent anesthetic (.02% tetramisol, .2% tricane, and 1% levamisol) was added to the mounting media. Animals were then allowed to paralyze in the anesthetic for 10 minutes before being mounted on a 2% agarose pad. Cover slips were then placed onto the sample and imaged within 30 minutes of original anesthetic exposure. Each experiment lasted only a total of 1 min.

FRAP Data Analysis

Sample Imaging

Image series, which represent time points during the FRAP experiment, were loaded using the LSM510 software and the region of interest that was analyzed. Another 15x15 pixel region of interest (1.10μm^2) at an area opposite the experimental bleached area was also monitored to determine fluorescence decay from a contiguous membrane within the cell body and determine immobile fraction. A third 15x15 pixel control area that was outside the bleached cell body was monitored to adjust for any bleaching that may have occurred during sample collection over the course of the experiment. Any samples that

demonstrated appreciable (>5%) bleaching over the course of the experiment were excluded from the data set.

In synaptic areas, FRAP experiments were conducted using the same 15 x 15 unit area, which typically encompassed nearly the entire synaptic region. To determine synaptic immobile fraction, cytosolic GFP, which is assumed to be freely mobile, was set as the 100% recovery threshold, to take into account geometric constraints of the synapse. Data from each region of interest was then collected along with the time stamp from each image and exported to an Excel spreadsheet.

Data collection and Normalization

The region of interest from the first 5 images, which represented the pre-bleach samples, was averaged to obtain a pre-bleach average intensity. This pre-bleach average was then used to normalize intensity points collected during the experiment such that:

$$(\text{Norm AFU}(t) = \text{AFU}(t)/\text{AFUave}_{pre}) \quad (1)$$

These normalized AFU values (which ranged from 0 to 100) were then used to generate both FRAP and fluorescent recovery curves. The second region of interest, which represents the non-bleached region of interest, was normalized the same way as the bleach region. Normalized non-bleached data points were then used to determine the immobile fraction of the protein being analyzed. Final bleach levels were calculated using the last five normalized fluorescence intensity points collected for each experiment and then averaged for each strain.

Immobile fraction was determined by subtracting the final fluorescence levels for the non-bleached fraction ($A3_f$) from the bleach depth achieved (Bd) to achieve what should represent the maximal achievable recovery level (Max Rec):

$$(A3_f - Bd) = \text{Max Rec} \quad (2)$$

where $A3_f$ represents an average value for the last 5 data points collected once equilibrium is reached for the non-bleached area and Bd represents an average value for the bleach depth achieved for the bleached area. The final bleached recovery level ($A2_f$) was then subtraced from Bd and divided by the Max Rec to achieve the mobile fraction:

$$(A2_f - Bd)/\text{Max Rec} \times 100\% = \text{Mobile Fraction} \quad (3)$$

where, $A2_f$ represents an average value for the last 5 data points collected once equilibrium is reached for the bleached area. The immobile fraction was then determined by subtracting the mobile fraction from 100.

Curve fitting, immobile fraction, and Diffusion coefficients

Data that had been normalized was then imported into GraphPad Prism (GraphPad, San Diego, CA) for graphical and statistical analysis. Mean and standard error of the mean (S.E.M.) were calculated for each point and plotted.

Fluorescence recovery half times were obtained by setting the first data point collected after the bleach to zero and calculating K using a one-phase exponential association equation (Prism, Synergy Software):

$$F(t) = F(t_{max})(1 - e^{-Kt}) \quad (4)$$

This equation relates to the two dimensional diffusion equation described by Axelrod (Axelrod et al., 1976) in terms of fluorescence where,

$$K = \pi D/w^2 \quad (5)$$

as described by Matsumoto (equation 2, (Matsumoto et al., 2005), where D is the two dimensional diffusion coefficient and w is the half-width of the Gaussian source beam bleach radius. In our experiments, our bleach radius was 1.05μm and the radius of the

laser used was .145μm wide (personal communication, S. Goowin, Vanderbilt Cell Imaging Core). Omega, (*w)* for our experiments was therefore estimated to be 1.195μm as is consistent with evaluations of *w* by Wey and Cone (Wey et al., 1981).

RESULTS

GFP:DAT-1 is Amenable to FRAP Based Mobility Assignments in vivo

To examine the possibility of utilizing FRAP-based mobility measurements in *C. elegans* neurons *in vivo*, strains expressing a GFP:DAT-1 fusion in DA neurons produced as described in Chapter IV, were subjected to fluorescence photobleaching followed by monitoring of fluorescent recovery. Using a high intensity laser focused on a small area of the cell body (with a bleach diameter of 1.05μm), we achieved specific photobleach of the selected area and observed rapid recovery of fluorescence signal (Fig 22A).

To determine *in vivo* GFP:DAT-1 mobility and immobile fraction, three areas of interest are monitored during these FRAP experiments. A control non-bleached region that is discontiguous with the compartment undergoing photobleaching is monitored to ensure that individual fluorescent sampling of each time point does not contribute to a decrease in fluorescence over the course of the experiment (Fig 22B, area 1). In this example, our control area is a synaptic bouton that is elaborated from an adjacent cell body out of the plane of focus. The second region monitored is the region specifically bleached using a single high intensity laser pulses (412 wavelength at 100% power for 1 iteration). This bleaching intensity was selected because it effectively bleaches 85% of the synaptic area (see below). Five baseline measurements from this area are taken

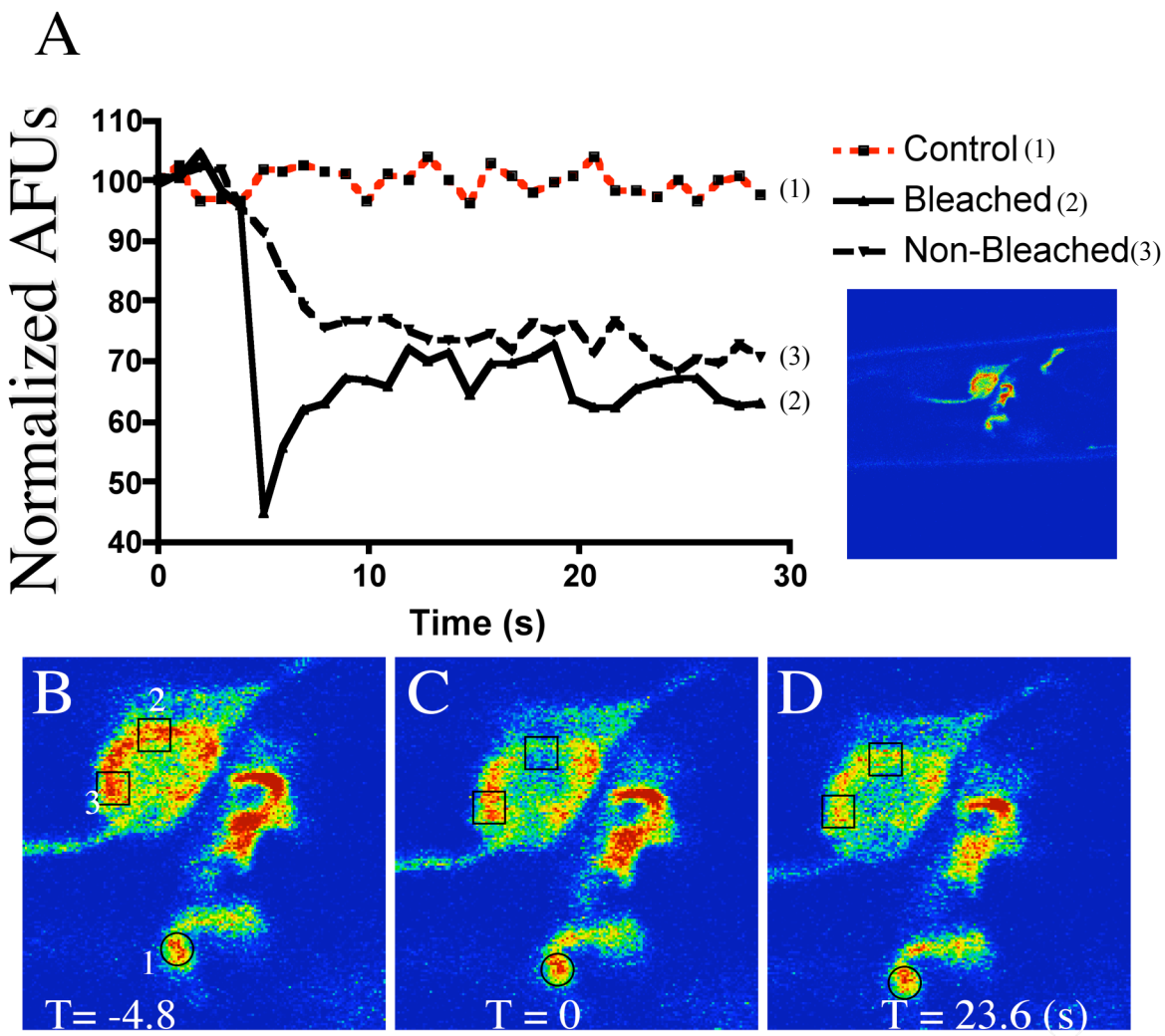

Figure 22. Example of Typical Cell Body FRAP Experiment.

A single cell body inside a living nematode (**A**, inset) is selected for FRAP experiments. An area of interest is then exposed to high intensity laser and monitored over the time course of the experiment. (**B**,**C**,**D**, area 2). A non-bleached region, which is contiguous with the experimental (bleached) region is also monitored (**B**,**C**,**D**, area 3). Data from these 2 areas are then normalized to prebleach fluorescent levels and plotted v. time (**A**). Curves from both the bleached and non-bleached regions are then used to determine both immobile fraction and diffusion rates for the fluorescent protein used in the experiment. A third region (circle in **B**, **C**, **D**, area 1) which is not part of the same neuron, is monitored to normalize for sample bleaching that may occur after continual scans.

before the high intensity bleach, followed by monitoring at .986ms intervals until recovery is achieved. Qualitatively, this area can be monitored before (Fig 22B, box 2), immediately after bleach (Fig 22C, box 2), and once a plateau of recovery has been achieved (Fig 22D, box 2). Quantitatively, pixel intensity under this area of interest is recorded by the LSM510 software and an integrated value is recorded for each image captured. The integrated intensity values are then plotted for each image and bleach and recovery curves are generated (Fig 22 A).

In order to quantify the immobile GFP:DAT1 fraction in this small compartmentalized area, we monitored a third area of interest that is contiguous with the compartment subjected to photobleaching (in this case the cell body). This compartment is monitored under the assumption that it provides a spatially contiguous source for the relocation of fluorescent DAT-1 into the bleached area. In this case, fluorescent decay after photobleaching is recorded. Once equalibrium is achieved the one half final florescence difference between these two areas (equation 2) represents the immobile fraction for either compartment.

Cell Body and Synaptic FRAP of GFP:DAT-1 Reveals Differential Kinetics and Immobile Fraction Levels

Examination of GFP:DAT-1 mobility yield distinct mobility rates in the different cellular compartments of the DA neurons. When FRAP experiment were performed on DA cell bodies, a moderate bleach level followed by rapid and robust recovery of the fluorescent signal was detected as is illustrated in the representative experiment (Fig

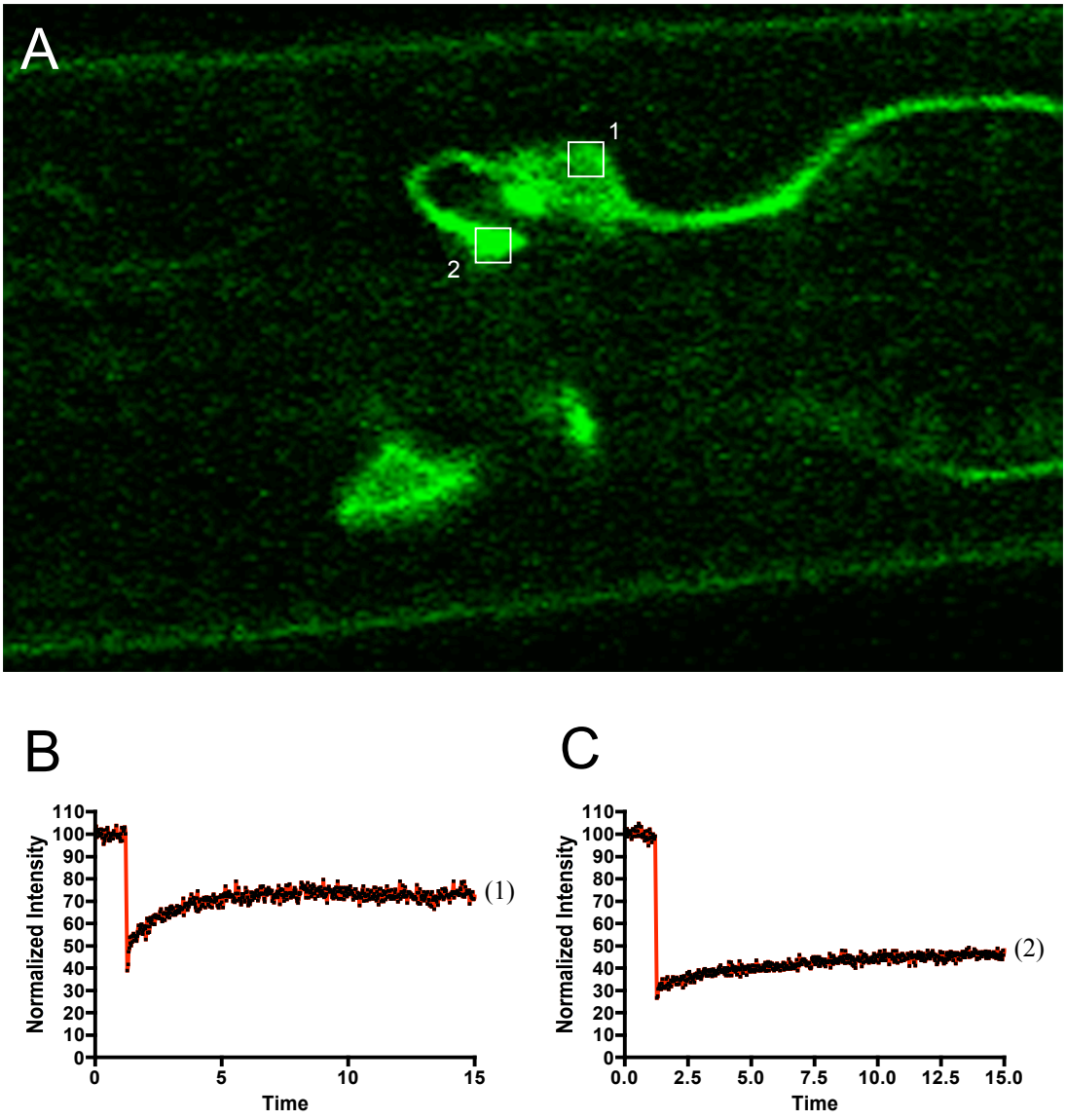

Figure 23. Differential Recovery of Fluorescence in the Synapse Compared to the Cell Body.

An example image of fluorescent bleaching area used to assess mobility in the different subcompartments of single neuron. **A.** Cell body and synaptic fluorescence in the DA neurons and specific bleach areas used to generate data in **B** and **C** are noted. Cell body fluorescence recovery curves taken from region 1(**A**) reveal rapid and robust recovery of signal to a stable plateau. This contrasts to negligible recovery seen in the synaptic area (**A**, box 2), which displays only an initial curve (0-2 sec post bleach), and then displays a more linear ascent to a stable plateau.

23B). This bleach depth and recovery trend were observed consistently in all cell body FRAP experiments across different animals with summary data shown in figure 24A.

When FRAP was monitored in synaptic areas, a deeper and more robust bleach depth was achieved, which is consistent with highly immobile proteins, and minimal recovery was noted (Fig 23C). This pattern of synaptic FRAP was also a reliable finding in synaptic areas across animals, with summary data shown in Figure 27. With initial results displaying differential mobility kinetics in the two different cell regions, further FRAP studies were performed to compare GFP:DAT-1 to cytosolic GFP as well as DAT-1 mutant strains.

GFP:DAT-1 in Cell Body Fraction Consists of Very Small Immobile Fraction

To examine differential membrane and cytosolic mobility rates and immobile fraction percentages in DA cell bodies, both the GFP:DAT-1 fusion line (BY312) and the GFP cytosolic line (BY250) were subjected to cell body FRAP experiments. As noted above, this intensity was set such that the experimental GFP:DAT-1 fluorescence was typically bleached to ~ 15% of pre-bleach levels in synaptic compartments (see below). Once set, the bleaching parameters did not change for any other strains or regions tested. This laser intensity results in a less robust bleach depth in the cell body (~65% of baseline) with recovery after 10 seconds to a plateaued level (Fig 24A). Monitoring of a non-bleached region of interest in comparison to the selected bleach region revealed consistently elevated final level for the non-bleached region. Using these two final bleach levels for each experiment revealed a 15% immobile fraction for GFP:DAT-1 in the cell body (Fig 24A, inset).

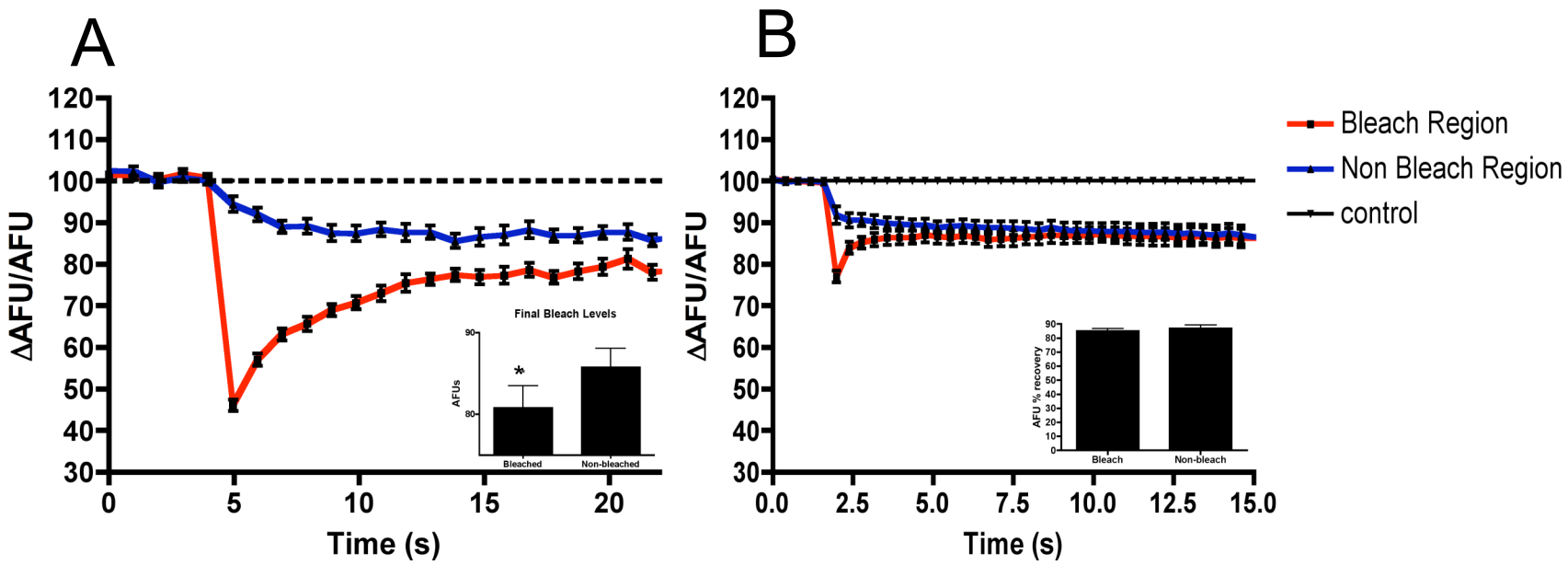

Figure 24. Cumulative FRAP Curves for GFP:DAT-1 and GFP in the Cell Body.

A. GFP:DAT-1 recovery of experimental region of interest after photobleaching achieves an equilibrium level that is distinct from the non-bleached area monitored in the contiguous membrane (red v. blue trace). This difference is statistically significant when compared using a paired Student's t-test (**A**, inset. $P < .05$), and is used to determine the immobile fraction for GFP:DAT-1 (using equation 2). **B.** Cytosolic GFP recovery of the bleached and non-bleached region after photobleaching achieve a similar equilibrium that is indistinguishable (**B**, inset) indicating no immobile fraction for this molecule

Bleaching the cell body of the cytosolic GFP line using the same bleaching parameters results in a reduced bleach depth (~33% of baseline) with rapid recovery (~3 seconds) to plateau (Fig 24B). To record more of the recovery phase when using this cytosolic GFP line, scan rate was increased to 425ms/slice. This did not effect overall bleaching of the sample but increased resolution of the recovery phase of the experiment. Again, the final five data points collected for both the mobile and immobile fraction were averaged and compared. Consistent with a freely moving fluorophore, there is no difference between the bleached and non-bleached regions at equilibrium, suggesting free exchange between these two areas and no immobile fraction (Fig 24B, inset). The immobile fraction noted for DAT-1 fusion likely reflects a pool of mature plasma membrane embedded DAT-1 in the cell body that is not free to relocalize during the time course of our experiments.

A Large Percentage of GFP:DAT-1 is Immobilized at the Synapse

Using the same FRAP parameters used for cell body measurements, both GFP and GFP:DAT-1 fusions were analyzed in regions previously defined to be synaptic (Chapter IV). Bleaching of the GFP:DAT-1 fusion in synaptic regions resulted in ~ 90% bleaching of GFP signal, with slow recovery to plateau (~14 seconds) (Fig 25). As observed with cell body FRAP studies, bleaching of cytosolic GFP in the presynaptic terminal resulted in a reduced bleach depth relative to GFP:DAT-1, with only ~45% bleaching of the baseline GFP signal and a rapid recovery (~3 seconds) to plateau (Fig 25). Again, the last 5 data points were averaged to calculate a final plateaued recovery. Statistical analysis (one-way ANOVA, $p < .05$) revealed a significant difference between

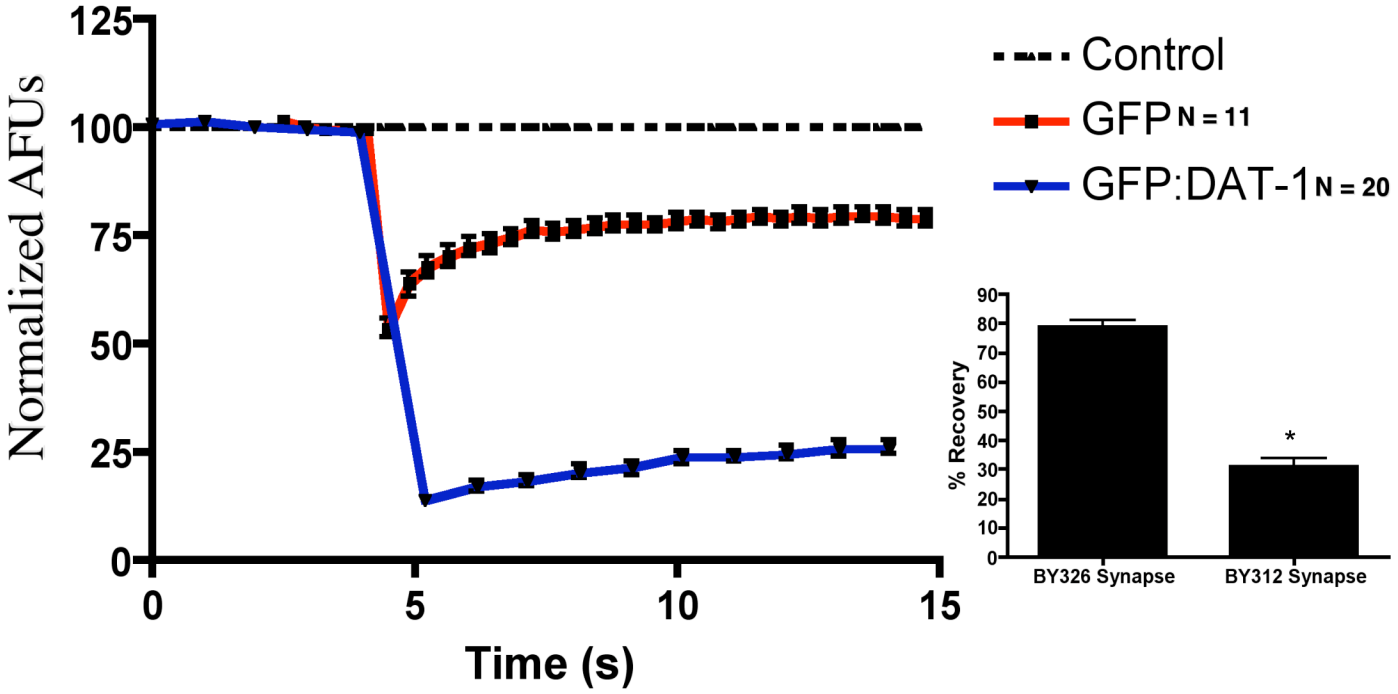

Figure 25. Comparison of GFP:DAT-1 and GFP Mobility in the Synapse.

Cumulative FRAP experiments were plotted to compare overall GFP and GFP:DAT-1 fusion protein FRAP curves in the presynaptic terminal. GFP recovery after photobleaching is substantial and rapidly equilibrates to a stable plateau (red trace). The GFP:DAT-1 fusion displays almost total bleaching, with a slow linear accumulation of fluorescence (blue trace). Examination of the recovery levels for the two fluorophores reveals a significant difference in fluorescence recovery (* $P < .05$, Student's t-test).

the amount of GFP recovery achieved in the synapse compared to the amount of GFP:DAT-1 fusion recovery seen (Fig 25, inset).

Because the synaptic region is a very small structure, it is impossible to monitor a contiguous non-bleached region. To determine the immobile fraction, GFP:DAT-1 recovery was subtracted from GFP alone recovery plateau (which should represent the highest amount of available recovery for a freely moving fluorophore given the geometric constraints of the structure) and an immobile fraction of 49% is suggested. This level of recovery indicates that there is a very large percentage of GFP:DAT-1 that is immobilized in the synapse by an as yet unknown mechanism. Comparison of total recovery for either cytosolic GFP or the GFP:DAT-1 fusion in the two compartments (cell body v. synapse) reveals that whereas cytosolic GFP recovery is not significantly different between the two compartments, there is a significant difference in the immobile fraction reported for GFP:DAT-1 in the synapse compared to the cell body (Fig 26).

GFP:DAT-1 Mobility is 100 Fold Slower Than Cytosolic GFP in the Cell Body

To determine mobility rate of both the GFP:DAT-1 and cytosolic GFP in DA cell bodies, the recovery phase of the FRAP experiment was examined and a recovery rate constant (K) was determined. Both signals were normalized from 0 (lowest bleach depth) to 100 (final recovery plateau level), which is necessary to determine K (Fig 27). Data points were then used to generate curves using a one-phase exponential association model (see methods above) and determine K. Modeling recovery using this equation, the mobility rate constant, K, equaled 0.295 for GFP:DAT-1. Converting K to diffusion using the modified Axelrod equation (methods) resulted in a diffusion constant of

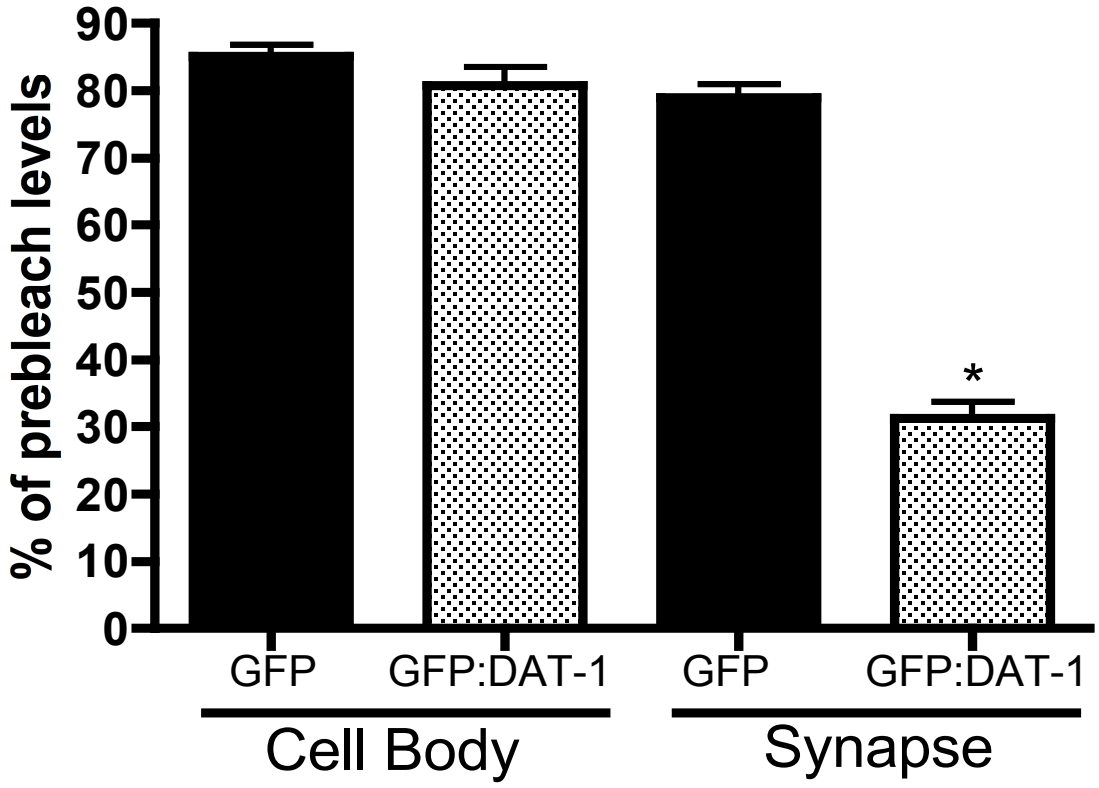

Figure 26. Comparison of Final Recovery Levels After Photobleach in Different Cellular Compartments.

Examination of recovery levels for both GFP and GFP:DAT-1 in the different compartments assayed using FRAP-based techniques reveals that although there is no difference between either GFP or GFP:DAT-1 in the cell body, there is a significant decrease in GFP:DAT-1 recovery in the synapse compared to synaptic GFP. GFP:DAT-1 recovery levels are also significantly reduced compared to GFP:DAT-1 and GFP cell body recovery (* $P < .05$, Student's two tailed t-test), indicating a relative immobilization of GFP:DAT-1 in the presynaptic terminal.

0.13μm^2/s. This diffusion rate is consistent with both integral membrane protein mobility but is considerably reduced compared to measurements of receptors from dissociated cultures (Velazquez et al., 1989). Using this equation to model cytosolic GFP mobility reveals that GFP in the cell body is 100 fold faster, with a mobility rate constant (K) of 2.896 and a diffusion rate of 1.32μm^2/s.

Both Cytosolic GFP and GFP:DAT-1 Diffusion Rate is Reduced in the Synapse

To assess GFP:DAT-1 mobility in the synapse, recovery curves for both the GFP and GFP:DAT-1 fusion were calculated as described above (Fig 28). For both cytosolic GFP and GFP:DAT-1 the mobility kinetics are reduced in the synaptic region as compared to values obtained in the cell body. Whereas the GFP rate constant was 2.896 in the cell body, K in the synapse is reduced to 0.895. This equates to a diffusion rate of 0.406μm^2/s. This reduction in diffusion rate equates to about a 9x reduction in GFP mobility in the synapse. The GFP:DAT-1 fusion rate constant is also reduced, from 0.295 in the cell body to 0.138 in the synapse. This equates to a diffusion rate of 0.063μm^2/s for this fusion in the synapse and a 4x reduction in mobility in this structure. These findings suggest a greatly reduced protein mobility in the presynaptic terminals. However, DAT-1 still appears to diffuse at rates far slower than GFP (over 40 times slower in this structure).

The GFP:DAT-1 ΔIML Mutant Resembles Wild Type GFP:DAT-1 In Vivo

PDZ domain interactions have been proposed to influence plasma membrane expression and localization of DAT (Torres et al., 2001). Thus the PDZ recognition

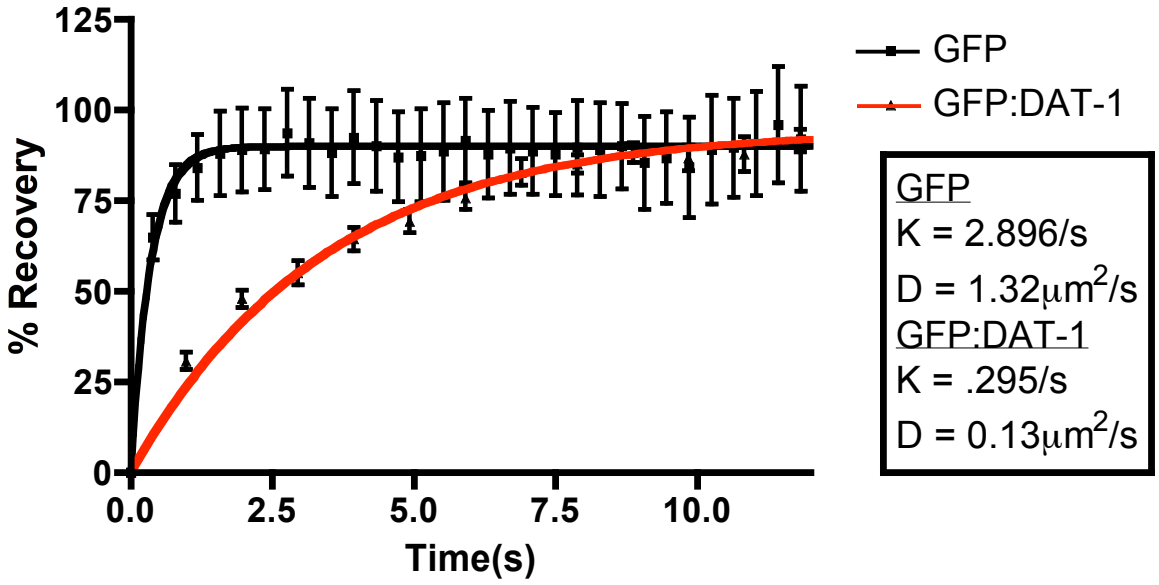

Figure 27. FRAP Recovery Curves for GFP and GFP:DAT-1 in the Cell Body.

Data generated from FRAP experiments is used to generate recovery curves in order to determine the rate constant of recovery (K). The first data point collected after bleaching is normalized to zero and the final data points are normalized to 100. Curve fitting using a single exponential association model (equation (3)) is used to generate K and best fit lines are shown above. K values are then used to determine the diffusion rate of the molecules according to a modified Axelrod equation (4). Error bars represent S.E.M. with an N = 20 for each.

sequences could support transporter mobility in both the cell body and the terminals. To test the effects of PDZ binding domain disruption on GFP:DAT-1 trafficking, lines expressing GFP:DAT-1(ΔIML) that were noted to posses an intracellular accumulation of GFP signal were examined by FRAP. Robust bleaching and recovery was noted in these strains (Fig 29A). Examination of both bleached and non-bleached areas in the cell body revealed the same difference seen with the GFP:DAT-1 fusion, which translates to a 15% immobile fraction (Fig 29 A, inset). Diffusion rates were calculated for the mutant GFP:DAT-1(ΔIML) line and compared to both the GFP and GFP:DAT-1 proteins in the DA cell bodies. The rate constant obtained for GFP:DAT-1(ΔIML) recovery was 0.348. This equates to a diffusion rate of $0.158\mu m^2/s$. This value for the GFP:DAT-1(ΔIML) lines are, for the most part, indistinguishable from the GFP:DAT-1 lines ($0.158\mu m^2/s$ v. $0.134\mu m^2/s$ respectively, $p > .05$ Student's t-test).

CONCLUSIONS

In this chapter we utilized FRAP techniques to examine the *in vivo* movement of GFP:DAT-1 fusion protein and mutants in various cellular compartments within intact DA neurons *in vivo*. FRAP experiments performed on the wild type GFP:DAT-1 fusion reveal differential kinetics and immobile fractions within different compartments of the DA neurons, reminiscent of experiments performed by Angelides on voltage gated sodium channels using cultured rat spinal cord neurons (Angelides et al., 1988).

In their study, Angelides *et al*. used a fluorescent analog of a sodium channel specific neurotoxin to label voltage-gated sodium channels on cultured mature rat cortical and spinal cord neurons. These cultures elaborated highly branched cell processes, and it

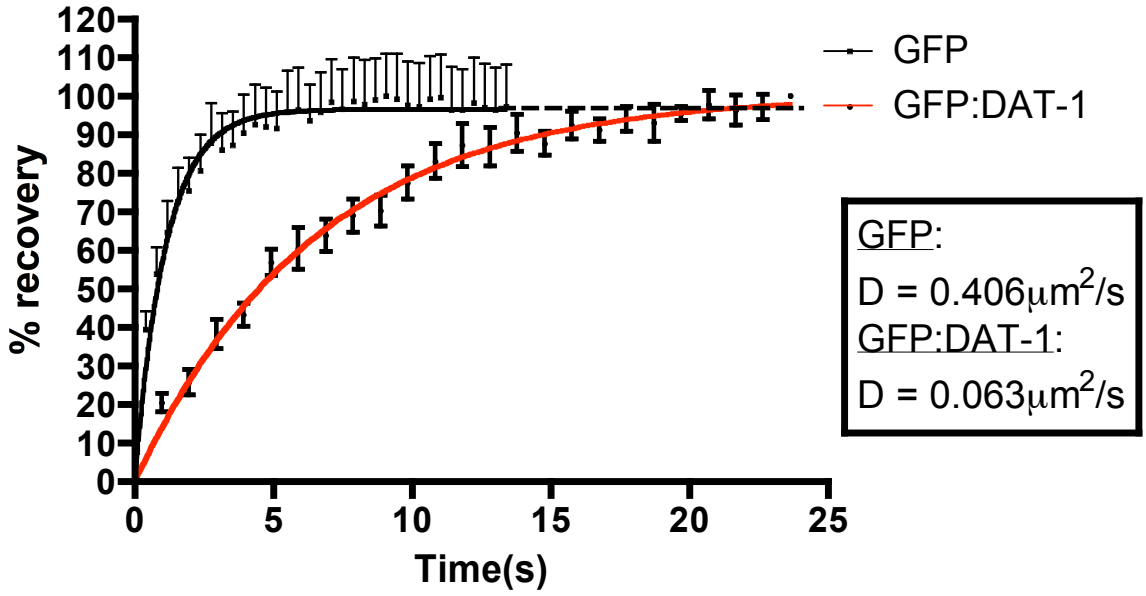

Figure 28. FRAP Recovery Curves for GFP and GFP:DAT-1 in the Synapse.

Data collected from FRAP experiments performed in the presynaptic terminal were normalized such that the first point collected was set to zero and the final 5 points were averaged and used to normalize the values to 100. A first order exponential association model (equation 3) was then used to generate a curve fit and define the rate kinetic K. Best fit curves for both GFP (black trace) and GFP:DAT-1 (red trace) are shown above. The corresponding kinetics were then used to determine diffusion rate using a modified Axelrod model (equation 4). Error bars represent S.E.M with an N = 20 for each.

was common to note swellings suggestive of varicosities and terminal boutons. Fluorescent labeling revealed diffuse cell body staining with concentrated punctate patterns at both the axon hillock and at terminals consistent with synaptic connections to cell bodies. When diffusion rates were calculated for each of these compartments, mobility of sodium channels in the cell body were over 80 times faster than rates in the axon hillock and over 600 times faster compared to rates at terminals. Although we do not see such robust changes in mobility at the synapse, analysis of the synaptic recovery curve leads us to hypothesize that the diffusion rate calculated here most likely represents potentially 3 populations of GFP:DAT-1 proteins.

The first population, represented by the rapid recovery in the lower part of the curve (Fig 23, 0-2 sec after bleach) likely represents GFP:DAT-1 proteins that are freely diffusing in the membrane and able to rapidly invade our 1.05μm bleach space. The second population of GFP:DAT-1 proteins likely represented here corresponds to fusion protein delivery into they synapse from the axon, and is graphically depicted by the more linear area of the curve (Fig 23, 2-12 sec after bleach). The final pool of GFP:DAT-1 in this synaptic population is the immobile fraction which we argue accounts for almost 50% of the GFP:DAT-1 found in the synapse. Immobile fractions of sodium channels and GABA receptors were in the range of 80 – 90% immobile in synaptic areas, however immobility was quantified differently in these studies (Angelides et al., 1988; Velazquez et al., 1989) (see below)

Consistent with the hypothesis that GFP:DAT-1 is primarily immobilized at synaptic areas, Angelides reported that Na^+ channel fluorescence concentration at terminals is dictated by synaptic connections. In experiments examining either

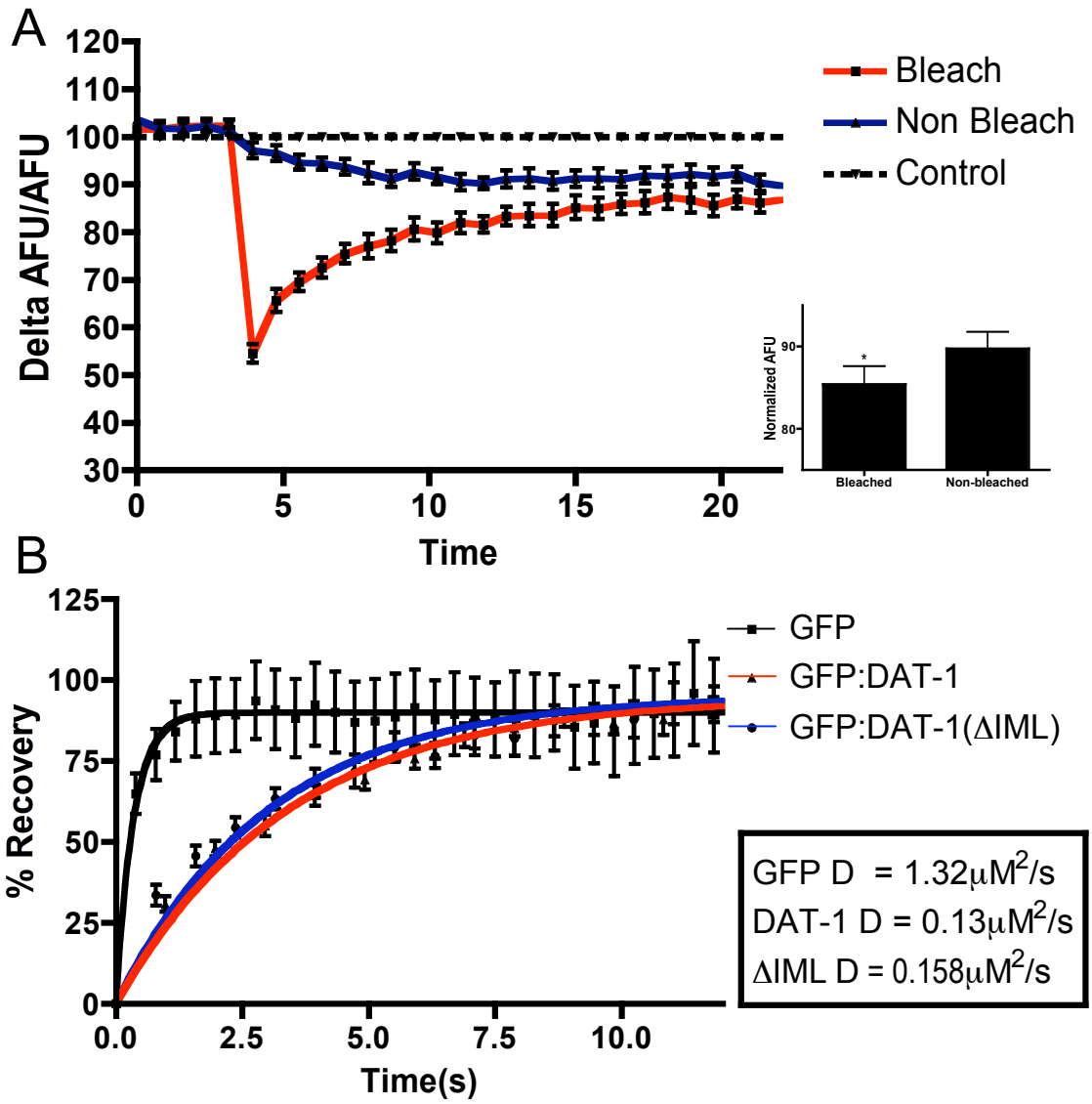

Figure 29. Comparison of GFP:DAT-1(ΔIML) and GFP:DAT-1 FRAP Curves in the Cell Body.

A. Composite FRAP experiments using the GFP:DAT-1(ΔIML) fusion protein. Recovery of both the bleached and non-bleached areas after photobleaching achieve distinguishable equilibrium levels which are used to calculate immoble fraction for this mutant. Final recovery levels for each region are significantly different (**A**, inset. $p < .05$, paired Student's t-test). **B**. FRAP recovery curves were generated using a first order exponential association model (equation 3) to determine K. K for this mutant was determined to be 0.348/s which equates to a diffusion rate of $0.158\mu M^2/s$.

denervated chick myotubes or myotubes co-cultured with spinal cord neurons, only the myotubes co-cultured with the spinal cord neurons displayed any punctate fluorescent staining (Angelides, 1986). Although we have not attempted to quantify accumulation from dissociated cultures to examine the effect of deinnervation on this signal, the fact that GFP signal accumulates at areas which co-label which fluorescently-labeled VMAT (VMAT:mRFP) suggests that there are proteins or mechanisms in place to retain or accumulate DAT-1 at sites of synaptic activity.

Initially, we had hypothesized that diffusion rates for the ΔPDZ fusion in the cell body would reveal lower mobility due to the visual intracellular accumulation noted in this line (Fig 17B). The area assessed by FRAP was sufficiently large to include both the plasma membrane and intracellular pool of the GFP:DAT-1(ΔIML) protein and previous studies of ΔPDZ DATs had shown biochemical evidence of an accumulation of immature protein (Bjerggaard et al., 2004), consistent with retarded progression through Golgi glycosylation pathways. Our study however, indicates that the inclusion of this intracellular, presumably Golgi-retained, protein has no effect on GFP:DAT-1(ΔIML) diffusion rates compared to wild type GFP:DAT-1 rates. This is consistent with lateral mobility of Golgi proteins reported by Cole *et al.* in their examination of apparently "retained" Golgi mutant proteins (Cole et al., 1996).

Our assessment of synaptic immobility for the GFP:DAT-1 fusion differs from traditional definitions utilized in FRAP analysis. Typically, mobile fraction is defined as the difference in fluorescence after bleach at time infinity subtracted from bleach depth achieved and divided by 100 minus the bleach depth to obtain a percent mobile fraction.

$$[(AFU(f_\infty) - Bd)/(100 - Bd)] \times 100 \quad (6)$$

The immobile fraction is then determined by subtracting the mobile fraction from 100. In our experiments, this would give an immobile fraction for GFP of 45.29% and of 79.57% for GFP:DAT-1, which would be more consistent with the immobile fractions of both sodium and GABA channels reported previously (Angelides et al., 1988; Velazquez et al., 1989). Because almost the entirety of the synaptic region is being bleached, and this area represents a closed structure, we decided instead to normalize to soluble GFP, which is expected to have no true immobile fraction in this structure. Our estimate of 49% immobile fraction is therefore a conservative estimate, adjusted for the fact that the geometric constraints of the synapse clearly over estimate immobility (as is evident from immobile fraction reported for the soluble GFP). Further studies with additional fluorescent membrane proteins expressed in DA neurons should be useful in further estimating DAT immobilization. Of particular utility would be membrane proteins that display a uniform density across cellular compartments.

CHAPTER VI

CONCLUSIONS AND FUTURE DIRECTIONS

In this section I will briefly review the findings reported in the thesis and speculate more generally on some of the results, with an emphasis on hypotheses needing future evaluation. Sections below are divided into specific overall themes that can direct future work related to DAT-1 localization.

OVERALL REVIEW

Antibodies directed against the intracellular COOH-terminus of *C. elegans* DAT-1 specifically identified DAT-1 in the DA head neurons, including both the CEP and ADE cell groups. Although the specifics of their cellular architecture differ, DAT-1 was consistently found at varying levels in the major compartments of these neurons, with synaptic, cell body, and dendritic localization evident. DAT-1 signal was absent in *dat-1* KO alleles (*dat-1(ok157)*) and displayed enrichment in presynaptic terminals compared to cell bodies. It should be noted that, even in older animals, specific staining was difficult to detect in PDE cell bodies and processes.

A presynaptic enrichment of DAT-1 is consistent with previous studies performed by several labs examining the localization of DAT in both rat and human brain tissue (Hersch et al., 1997; Nirenberg et al., 1997; Ciliax et al., 1999). Without the ultrastructure provided by high resolution EM, we were fortunate to evaluate this localization to published synaptic wiring for expectations regarding “synaptic” areas

elaborated by the DA head neurons (White et al., 1986). We observed DAT-1 specific reactivity at low levels in dendrites with an enrichment of DAT-1 staining in cell bodies and areas consistent with presynaptic terminals of both the CEP and ADE neurons in the esophageal nerve ring. Although antibody staining of wild type animals provided validation of GFP:DAT-1 cellular localization, relative quantification of immunofluorescence signal would have been confounding, due to the variability of relative staining caused by the permeabilization steps needed for antibody immunoreactivity.

Expression of a GFP:DAT-1 fusion in DA neurons recapitulated native immunostaining localization in wild type DAT-1 animals. This construct rescued 6-OHDA toxicity in the *dat-1(ok157)* background, indicating that our fusion was functional *in vivo*. *In vitro* culture experiments using this GFP:DAT-1 fusion line confirmed GFP:DAT-1 protein is capable of [^{3}H]DA uptake. Additionally, we found that GFP:DAT-1 maintained channel like states, with similar current amplitudes recorded in wild type strains (Carvelli et al., 2004). Interestingly, this fusion produces an increase in channel activity in the form of increased mean open time for DA gated ion permeation, indicating that interactions of proteins that mediate this activity may have been disrupted using the NH_2-terminal tag (Carvelli et al., 2004).

Relative quantification of GFP:DAT-1 fluorescence revealed a specific accumulation of GFP:DAT-1 signal in synaptic regions (consistent with VMAT:mRFP localization) when compared to the cell body from which the axon was derived, consistent with qualitative findings from antibody studies. This analysis revealed a preferential distribution of GFP:DAT-1 fluorescence with highest density in the synapse,

followed by the cell body, and finally in the dendrites. This distribution was specific for GFP:DAT-1 fusions as both a nuclear localized GFP and cytosolic fluorophore (pTimer) displayed highest density in the cell body.

Establishment of wild type GFP:DAT-1 localization allowed for comparisons to localization patterns in mutant lines including 1) analysis of an *unc-104* mutant, 2) mutants identified in a forward genetic screen for 6-OHDA toxicity suppression, 3) a truncated GFP:DAT-1(ΔIML) protein bearing loss of a putative PDZ recognition sequence. Examination of GFP:DAT-1 in the *unc-104(e1265)* mutant background revealed a reduction in synaptic density for DAT-1, with preservation of relative GFP:DAT-1 synaptic enrichment. Reasons for this decreased synaptic density are currently unclear, but hypotheses are discussed below.

DAT-1 mutants recovered from a forward genetic screen for 6-OHDA toxicity suppression displayed altered GFP:DAT-1 localization or expression when the mutations were placed into the GFP:DAT-1 fusion and expressed in DA neurons. These studies support the validity of the model for evaluating mutant DAT-1 alleles, as our *in vivo* expression largely matches expectations inferred from *in vitro* biochemical experiments.

Finally we tested the specific hypothesis that a conserved type II PDZ binding motif in DAT-1 (IML) would participate in synaptic accumulation. Previous studies using rDAT and hDAT proteins suggested that the PDZ binding domain at the distal COOH-terminus of DAT-1 may be required for DAT stability, plasma membrane insertion, and potentially synaptic elaboration (Torres et al., 2000; Bjerggaard et al., 2004). To test this hypothesis *in vivo* using *C. elegans*, the PDZ binding domain found in DAT-1 (IML) was both truncated, creating a disruptive HSD* COOH-terminal tail, or

masked using addition of GFP sequence to the COOH-terminus. Both mutations resulted in intracellular accumulation of GFP:DAT-1 signal at high expression levels. When the GFP:DAT-1(ΔIML) transgene was integrated, expression of the fusion protein was decreased and this intracellular accumulation was lost, resulting in a mostly wild type localization. When quantified, both mutants displayed synaptic accumulation that was indistinguishable from wild type GFP:DAT-1. Both molecules were also capable of restoring 6-OHDA sensitivity to the *dat-1(ok157)* KO strain, indicating *in vivo* plasma membrane expression and localization.

This mutant PDZ expressing strain was also tested in FRAP studies, examining DAT mobility in *C. elegans* DA neurons *in vivo*. Initial FRAP studies performed on GFP:DAT-1 lines revealed a diffusion consistent with previously studies membrane proteins. Synaptic GFP:DAT-1 diffusion rates were not altered per se, but immobile fraction was increased from 2.5% (in the cell body) to between 50 and 80% in the synapse (depending on immobile fraction measurements used). Although cytosolic GFP also displayed an apparent immobile fraction in the synapse, this difference was not significantly different from cell body immobile fraction for GFP in the cell body. The GFP:DAT-1(ΔIML) mobility rate was similar to the wild type GFP:DAT-1 fusion protein mobility rate, indicating that the PDZ binding domain of DAT-1 does not effect cell body mobility. This PDZ mutant line has not been evaluated for synaptic immobility or diffusion and should be pursued further.

DAT CELLULAR EXPRESSION AND AGING

Examination of our lowest expressing GFP:DAT-1 fusion line in mixed staged animals revealed that GFP:DAT-1 expression was highest in young L2/L3 animals. This observation led us to investigate the role of the 700bp promoter region of DAT-1 used in our studies, which we hypothesized might direct this differential expression of our transgene. Using the DAT-1 promoter to drive expression of a molecular fluorophore that changes its fluorescent property over time (pTIMER), revealed that this promoter region was most active in young L2/L3 animals (consistent with our GFP data), and that transcription/translation was being halted at young adult (Fig 30). Interestingly, expression of the mFRP tagged VMAT using the same DAT-1 promoter fragment displayed robust expression in the adult, indicating DAT-1 protein in these neurons may be relatively unstable. Permeabilization of synchronized and staged animals confirmed a loss of native DAT-1 in aged worms, with less than 20% of animals over the age of L4 displaying any appreciable DAT-1 specific staining (data not shown).

While our aging data is preliminary, the findings are consistent with studies in human brain samples (Bannon et al., 1992). A forward genetic screen could be implemented looking for regulators of both DAT-1 degradation and transcription factors that effect this regulation using either the GFP:DAT-1 fusion line or the pTimer lines. In the first case, worms could be mutagenized and retention of GFP:DAT-1 signal in the adult could be used to identify genes effecting this degradation (and potentially transcriptional regulators). In the second case, the pTimer line could be mutagenized and animals could be sorted using a "worm sorter" to identify strains that retain dual labeling

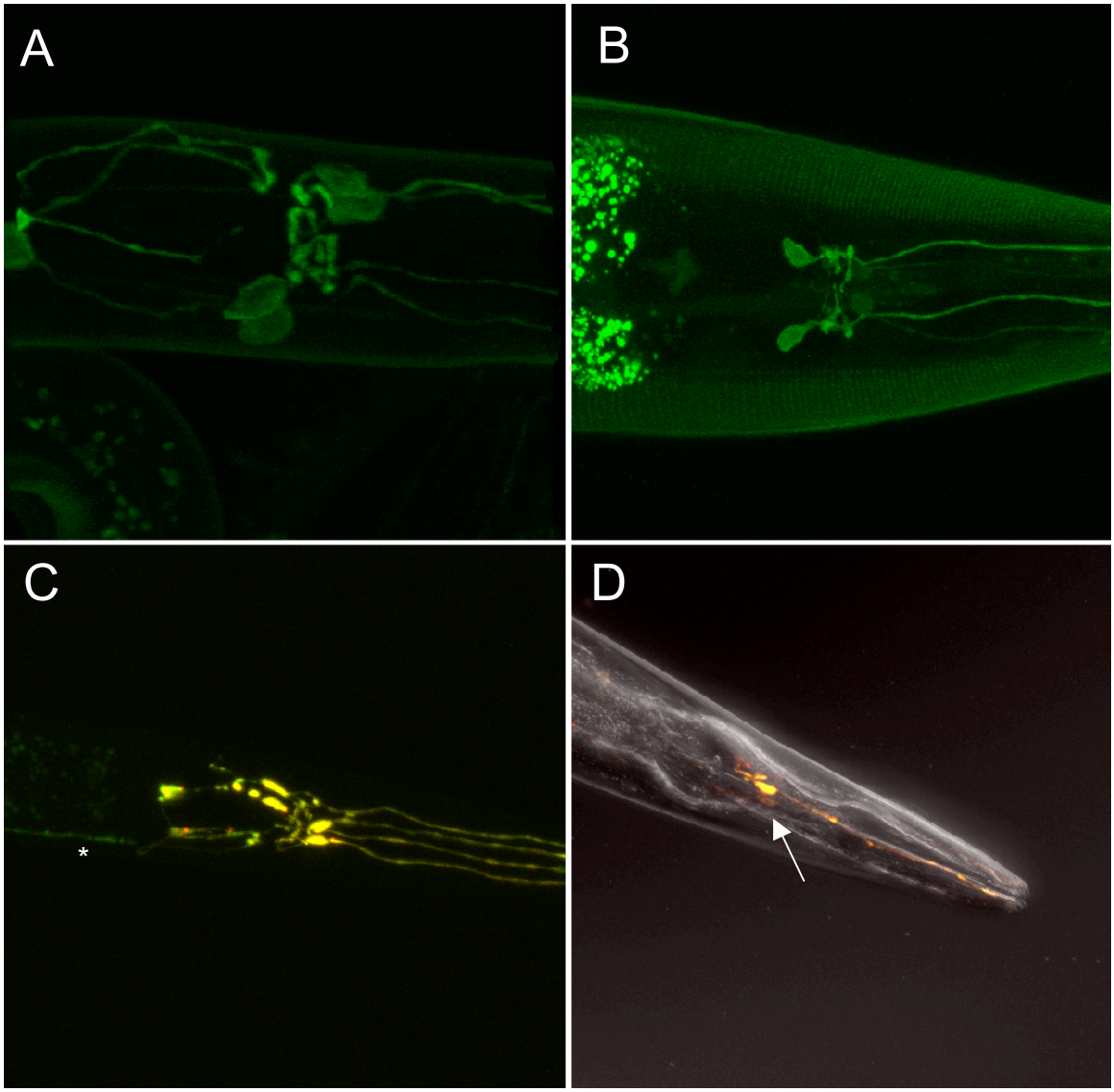

Figure 30. Loss of Expression of Both GFP:DAT-1 and pTimer Fluorescence in Older Animals.

A. Complete expression of GFP:DAT-1 in all head neurons of an L3 animal. **B**. GFP:DAT-1 expression is lost in the adult with only two of the CEP neurons expressing GFP:DAT-1 in this representative animal. **C**. Examination of DAT-1 promoter efficiency in young v. old animals. L3 animal expressing pTimer fluorophore in all DA neurons of the worm. PDE expression has just begun in this animal (green fluorescence in PDE projection (asterisk) with extensive two color labeling in the head neurons. **D**. Young adult animals have already lost expression of both colors in most neurons with only one CEP neuron remaining transcriptionally/translationally active. Note only red fluorescence in CEP neuron just behind the two color neuron (arrow)

(both green and red fluorescence). Either of these screens would be fairly straightforward with the latter requiring minimal effort to initially identify candidate genes. Finally, the transcriptional regulator Nurr-1 has been implicated in DAT regulation (Bannon et al., 2002), and homologues to this protein exist in *C. elegans* (wormbase, www.wormbase.org) .

SYNAPTIC DENSITY OF DAT-1

Data from our GFP:DAT-1 fusion lines in the *unc-104(e1265)* background showed a reduced synaptic density for DAT-1 accumulation. While synaptic enrichment of DAT-1 was evident, focal accumulation levels at the synapse were reduced, indicating that either proteins that depend on UNC-104 for synaptic localization or DA signaling affects DAT-1 synaptic density. To test the first possible scenario, UNC-104 dependent proteins with known mutant alleles should be investigated. A recent paper published by Sieburth *et al*. used the a more severe allele of UNC-104 *(unc-104(KIF1A)* to examine synaptic mutant proteins identified using a large aldecarb resistance based RNAi screen (Sieburth et al., 2005). Of the original 185 synaptic proteins identified, 16 were found to be UNC-104 dependent. Of the proteins listed, M04D8.2, an insulin/IGF receptor (*ins-22*) is perhaps the most intriguing. Insulin has been found to increase DAT surface density in mammalian cells, potentially by inhibition of PP2A via AKT (Azoui et al., 1996; Begum and Ragolia, 1996) . Additionally, given the effects of insulin on AMPH induced rDAT and hDAT internalization (Galici et al., 2003; Garcia et al., 2005; Owens et al., 2005), signaling though this pathway should be explored.

The second possibility presented by these data is that reduced DA signaling in the UNC-104 mutant might contribute to a decrease in synaptic density. To test this, synaptic density measures can be acquired in known DA synthesis mutants (*bas-1* and *cat-1*) as well as in mutants lacking the presynaptic DA D2-like receptor, dop-2. The synthesis mutants are particularly attractive, as any density reduction seen in the *cat-1* (TH homologue) mutant should be reversed with the exogenous addition of L-DOPA, whereas L-DOPA in the *bas-1* (AADC) line should have no effect.

Alternative means of DAT-1 localization that does not utilize UNC-104 should also be examined. Recent work on the GABA transporter indicates that GAT-1 buds from the Golgi complex and is inserted into membranes using components of the Exocyst complex, specifically the exo-70 protein (Farhan et al., 2004). Another Exocyst protein, Sec-5, was reported to disrupt integral membrane trafficking important for synaptic elaboration in drosophila, without effecting neurotransmitter release, indicating that this protein localizes a sub-set of proteins outside of those targeted by UNC-104 (Murthy et al., 2003). Because mutations in the exocyst proteins often lead to lethality, as in the Murphy study mentioned above, cultured DAT-1 neurons expressing GFP (from the BY250 strain) could be FACS sorted and exposed to double stranded RNA (dsRNA) for targeted disruption of Exocyst homologues. This dsRNA should result in RNAi of the targeted proteins and each condition can be screened for loss of [^{3}H] DA uptake in these sorted cultures. These experiments are also relatively straight forward, requiring minimal generation of novel tools (mainly the dsRNA constructs).

FUTURE FRAP EXPERIMENTS

Initial FRAP studies on GFP:DAT-1 lines display a large immobile fraction of DAT-1 protein in synaptic areas. Because we are the first group to explore FRAP of a presynaptic membrane protein using traditional FRAP methods, it is difficult to compare our results to any known protein mobility rates. As such, it would be important to express a transmembrane domain spanning protein fused to GFP to determine lateral mobility of this protein in both the presynaptic terminal and cell body. This would help better define the immobile fraction noted for DAT-1 in these studies as this may be a physical constraint of membrane protein diffusion in small close compartments such as the synapse.

APPENDIX A

TANDEM AFFINITY PURIFICATION OF DAT-1 INTERACTING PROTEINS.

INTRODUCTION

The rate of DA clearance from synaptic terminals depends upon the number of plasma membrane associated and active DA transporters (DATs). Plasma membrane insertion and retention of the hDAT is influenced by several signaling pathways and by direct protein-protein interactions (Copeland et al., 1996; Bauman et al., 2000; Torres et al., 2001; Carneiro et al., 2002). As such, identifying novel proteins that interact with DATs is important for understanding modulation of these transporters and establishing a functional effecting on DA clearance. In this Appendix, I describe my attempts at isolating *C. elegans* DA transporter (DAT-1) associated proteins using a tandem affinity purification (TAP) tagged DAT-1 transporter expressed *in vivo*, and discuss limitations and future directions of such experiments.

Post-translational DAT modulation is well established in the literature. In many cell hosts, pharmacological manipulation using phorbol esters including phorbol 12-myristlate 13-acetate (PMA) reduce transport capacity (V_{max}) by reducing the number of transporters on the plasma membrane (Kitayama et al., 1994; Copeland et al., 1996; Huff et al., 1997). This reduction in transport capacity has been linked to PKC or PKC inhibition using bisindolylmaleimide or staurosporine to suppress phorbol ester-induced decrease in V_{max} (Zhang et al., 1997; Zhu et al., 1997). Consistent with the activity of a kinase, activation of PKC using PMA or by inhibiting protein phosphatases using

okadaic acid or calyculin, yields a significant increase in basal phosporylation state of rDAT in synaptosomes (Vaughan et al., 1997). DAT also associates with protein phosphatase 2A, suggesting the possibility that DAT phosphorylation is tightly controlled through protein-protein associations (Bauman et al., 2000).

Since this initial finding, several interacting proteins have been reported to associate with DAT including some linked to PKC activation pathways. Studies by Torres *et al*. first demonstrated that PICK1, directly interacts with the C-terminus of hDAT via a type II PDZ binding motif (see Chapter IV). Truncation of this binding motif resulted in loss of PICK1-DAT interaction and intracellular accumulation of hDAT protein in transfected midbrain cultures (Torres et al., 2001). Co-expression of PICK1 with hDAT resulted in an increased V_{max} with increased surface clustering of DAT, indicating that PICK1 might stabilize DAT on the plasma membrane. In chapter IV, I show that this interaction may contribute more to transporter biosyntheis and stability rather than synaptic localization. Another PKC interacting protein, the receptor for activated C-kinase (RACK1) has also been reported to interact with the N-terminus of hDAT (Lee et al., 2004), which puts RACK1 close to N-terminal PKC consensus sequences important for DAT modulation.

Non-PKC interacting proteins have also been found to physically associate with DATs *in vitro*. The SNARE protein syntaxin has been reported to interact with the N-terminus of several monoamine transporters and has recently been demonstrated to interact with DAT (Lee et al., 2004). The synaptic protein α-synuclein, which is implicated in the DA neurodegenerative disease, Parkinson's disease, has also been found to associate with DAT and results in a decrease in V_{max} with no change in DA affinity or

K_m *in vitro* (Wersinger and Sidhu, 2003). *In vivo* expression of both mutant and normal human α-synuclein in *C. elegans* DA neurons resulted in an increased susceptibility to the neurotoxin 6-OHDA, a process that is known to be DAT-1 dependent (Lakso et al., 2003; Kuwahara et al., 2006).

Another presynaptic adaptor protein was recently demonstrated to interact with the N-terminus of DATs, providing a link to intracellular signaling pathways known to signal via tyrosine kinases. Yeast two hybrid experiments using the n-terminus of DAT revealed an interaction with the LIM domain containing protein Hic-5 (Carneiro et al., 2002). DAT interaction with Hic-5 resulted in reduced DA uptake due to a loss of plasma membrane associated transporters. The DAT/Hic-5 interaction was dependent upon the Hic-5 LIM domain *in vitro*, and evidence of *in vivo* interaction was reported using coimmunoprecipitation (Carneiro et al., 2002) from striatal brain extracts .

Investigation into the human movement disorder, early onset torsin dystonia, which results from mutant torsinA protein accumulation in DA neurons, revealed an *in vivo* interaction of torsin with DAT (Cao et al., 2005). Expression of wild type torsinA in *C. elegans* DA neurons revealed that torsin expression reduced 6-OHDA induced DA toxicity and sequestered GFP:DAT-1 fusion proteins in cell bodies within the DA neurons (Cao et al., 2005). Mutant torsins reduced this protective effect in these neurons. Although direct interaction was not tested, GFP:DAT-1 sequestration in cell bodies indicates that torsin may forms a complex with DAT-1 *in vivo*, a hypothesis that should be investigated further.

Several techniques for identifying putative protein interactions have been established and used for identifying DAT interacting proteins. The most successful to

date has been the use of yeast-two-hybrid system, which takes advantage of yeast selection (both positive and negative) to identify putative interacting fragments (Fields and Song, 1989). This system takes advantage of transcription factors, which, in the absence of protein-protein interactions, are inactive. To take advantage of this system, selective fragments of your protein of interest are fused to one of these binding factors and used as "bait" (historically, Torres *et al.* used the hDAT COOH-terminus (Torres et al., 2001)) to probe a random cDNA fragment library fused to the "prey" protein. If the bait fragment and prey fragment interact, yeast transcription is activated, affecting either color-based selection or survival on minimal media.

Yeast-two-hybrid system was used in the Caron laboratory to discover both PICK1 and HIC-5 interactions with the COOH-terminal domain of hDAT (Torres et al., 2001; Carneiro et al., 2002), and while this system has proven successful in the past, there are many disadvantages to yeast-two-hybrid based screens. The first of these has to do with the physical requirements of the screen itself. Because the screen depends on transcriptional regulation of two nuclear proteins fused to peptide fragments to create a positive result, the native accessability of these protein domains is impossible to assay. In other words, just because the peptide fragments interact in the nucleus of yeast does not mean that full length translated and properly folded proteins will interact *in vivo*. This leads to a large number of "false positive" interactions (Fields, 2005).

The second of the limitations of yeast-two-hybrid has been alluded to in the first, and that is, only a fragment of the full-length peptide is used as the bait protein. In the case of earlier studies, only the intracellular COOH-terminus was used, limiting the number of potential interacting proteins returned by the system. This can be overcome

by sub-cloning other fragments into the bait vectors, however this increases the work substantially.

Another method employed by biochemists in a search for protein-protein interactions is co-immunoprecipitation (co-IP) with a target protein followed by protein analysis by 2-D gel or mass spectrometry. In this system, full-length protein of interest is detected by specific antibodies and isolated under mild conditions. Proteins that interact with your protein of interest co-IP as a result. Immunoisolated complexes are then resolved on a 2-D polyarylamide gel, typically using both pH and isoelectric point or mobility to discriminate individual proteins. These proteins are then visualized using protein dyes (Commassie or silver). Novel proteins are then removed from the gel and trypsin digested for analysis by mass spectrometry. While this system appears relatively straightforward, there are a few caveats that should be considered. Firstly, generation or use of a highly specific and efficient antibody suitable for IP procedures is required. If no specific antibody is available, generation of a good IP antibody can take months to years (if you ever get one). Once a suitable antibody has been obtained, different solubilization conditions effect co-IP quality. Different detergent and ionic concentrations effect protein-protein interactions and can alter the success of the co-IP procedure. Also, specificity of your antibody for your protein of interest is paramount in returning a limited number of false positives. This issue can be diminished by pre-absorbing the antibody against non-transfected cells but can be problematic if attempting to IP proteins out of native tissue (unless knock out animals have been generated).

The final limitation to this technique comes in novel protein selection and identification by mass. Once IP experiments have been performed, novel proteins are

identified by visualization using either commercial dyes or silver staining. These procedures are effective only within certain concentration ranges (from μg to mg, depending on the techinique). Low affinity or abundant interactions will therefore be lost using this technique. Proteins that are isolated are then trypsin digested and subject to mass separation and spectral identification using a mass spectrometer, which can yield a prediction of the protein sequence.

Recent development of a tandem affinity purification (TAP) system in yeast had yielded novel proteins important in mRNA splicing, which had not previously been identified using genetic screening techniques (Rigaut et al., 1999). This TAP technique takes advantage of a dual affinity purification tag fused to the protein of interest. This dual tag allows for two sequential rounds of affinity column purification, which reduces non-specific binding of background proteins. Another advantage of this dual tag is that it takes advantage of well characterized, commercially available, high affinity reagents for the IP reactions, overcoming problems discussed above. Bound protein complexes are then eluted and either isolated by gel electrophoresis or entire protein complexes are precipitated and digested for analysis by mass spectrometry.

Another recent advancement in protein identification using tandem mass spectrometry provides a unique opportunity for identification of large protein complexes that have been immunopurified from organisms with published genomic sequence. This technique for direct analysis of large protein complexes using mass spectrometry, termed DALPC, couples mulitdimentional liquid chromatography (LC) and tandem mass spectrometry (MS/MS) to separate and fragment peptides (Link et al., 1999). Mass spectra from peptide sequences are then compared to theoretical spectra from translated

protein sequences inferred from the published genome using the SEQUEST algorithm. Combination of both the TAP and the LCS/MS/MS techniques allows for the rapid identification of protein targets and potential protein-protein interactions that can then be then tested and verified using biochemistry and molecular biology techniques.

With the recent publication of the *C. elegans* genome sequencing project, we reasoned that large scale IP of DAT-1 using TAP tag technology coupled with DALPC, would yield novel and conserved DAT-1 interacting proteins. Mammalian homologs of these proteins can then be identified and tested for interaction and functional significance in higher organisms.

MATERIALS AND METHODS

C. elegans Strains

All strains were derived from the wild-type N2 Bristol isolate and maintained at 14 to 25°C using standard methods (Brenner, 1974). The *dat-1(ok157)* strain was a gift of J. Duerr and J. Rand (Oklahoma Medical Research Foundation, Oklahoma City). The BY250 strain was a gift from G Wong.

TAP Vectors

In order to generate an NH_2-terminal DAT-1 fusion protein, both *in vitro* and *in vivo* vectors were produced. The original pFA6 vector containing an N-terminal tandem affinity purification (TAP) construct has been described previously and was a gift from K. Gould, Vanderbilt University. The DAT-1 promoter region (P_{dat-1}) and the dat-1 cDNA amplification has been described previously (Nass et al., 2002). For studies using

TAP vectors, three separate constructs were made, one for *in vitro* and another two for *in vivo* expression. The *in vitro* construct utilized an hCMV promoter amplified from pcDNA3.1 using sense oligo RB1244 (5' – CGC GGA TCC ATA TAC GCG TTG ACA TTG ATT ATT GAC – 3') and antisense oligo RB1245 (5' – CGC CTT AAT TAA CAG AGA GCT CTG CTT ATA TAG – 3'). This amplified hCMV was then inserted 5' of the TAP tag using BamHI and PacI sites added during PCR amplification (underlined in oligos). Dat-1 cDNA was inserted in frame 3' of the TAP construct using AscI and BglII sites to create the final hCMV::TAP:DAT-1 expression vector (pBY537, see Table 6). To create the *in vivo* TAP:DAT-1 expression vector and the TAP alone control vector, amplified $P_{dat\text{-}1}$ was inserted into the pBY537 vector using BamHI and PacI sites replacing hCMV, creating pBY533. To create the TAP alone control vector, the DAT-1 promoter region was removed from pBY533 using BamHI and PacI enzymes. This promoter was then placed into the original pFA6 TAP vector using these same sites creating pBY578.

Construction of Transgenics and Stable Integrants

In order to create lines expressing the TAP:DAT-1 fusion in DA neurons, stable transformants were created by co-injection of plasmid constructs with a marker plasmid using standard methods (Mello et al., 1991). Transgenic animals containing the TAP:DAT-1 translational fusion (pBY533) were obtained after co-injection of a final concentration of 15ng/µl of pBY533, 60ng/µl of pRF4[*rol-6(su1006)*], and 50ng/ul of carrier DNA (pBluescript) in PBS directly into the *dat-1* strain. Transgenic animals

Table 6. Plasmid Constructs Used for TAP Experiments

DNA Plasmid Constructs		
pFA6	Expression	Yeast
	Vector inserts	TAP
pRB533	Expression	*C. elegans*
	Vector inserts	P_{dat-1}::TAP:DAT-1
	Translated Protein	TAP:DAT-1
pRB537	Expression	Mamalian Cell Culture
	Vector inserts	hCMV::TAP:DAT-1
	Translated Protein	TAP:DAT-1
pRB578	Expression	*C. elegans*
	Vector inserts	P_{dat-1}::TAP
	Translated Protein	Cytosolic TAP

containing the TAP alone control vector (pBY578) were obtained using the same conditions. L4 animals from lines containing extrachromasomal arrays that conveyed low penetrance for the *rol-6* phenotype were exposed to 50ug/ml trimethyl Psoralen for array integration as previously reported (Clark and Chiu, 2003). All integrated lines were then outcrossed 4 times to *dat-1* animals.

C. elegans dat-1 Genotyping

This technique was described previously in Chapter IV.

P_{dat-1}:TAP:DAT-1 Genotyping

In order to verify that strains had been integrated with the TAP:DAT-1 construct and not just the *rol-6* plasmid, genomic DNA was obtained from P_{dat-1}::TAP:DAT-1 integrated lines (BY327 and BY328) as described above. A sense oligonucleotide that was initially used to amplify the DAT-1 promoter region (RB 1239 5' – CGG CGG ATTC CAA GCT TCC ATG AAA TGG AAC TTG AAT CC – 3') and an oligo directed against an 18 base sequence of the protein A domain of TAP (RB 1226 5' – CGG TGC TTG AGA TTC ATT – 3') were used to amplify a 1.1 Kb cDNA fragment. Animals lacking the integrated pBY533 vector should yield no appreciable cDNA after amplification. DNA from genomic preps was used at a concentration of 1ng/μl. PCR based analysis was done using Advantage 2 PCR kit from BD Biosciences with 1ng of DNA, 100pM of RB 1239 and 1pM of RB 1226 in a total reaction volume of 25μl. PCR was performed in a Peltier thermal cycler PTC-200 from MJ Research using an initial "hot start" of 94°C for 2

minutes then followed by 30 cycles of 94°C melting for 15 seconds, 60°C annealing for 30 seconds, and 68°C extension for 2 minutes.

Cell Culture and Transformation

To initially test function of the tagged TAP:DAT-1 protein, COS-7 cells were plated at 50,000 cells per well in 24 well tissue culture treated plates (Perkin Elmer) with 500µL of DMEM (InVitrogen) complete medium (10% FBS (Hyclone), 100units/mL Penicillin, 100ug/mL Streptomycin, and 2mM L-Glutamine). The cells were transfected with 200ng of either DAT-1 cDNA (pRB235, (Jayanthi et al., 1998)), the TAP alone control vector (pFA6), or the TAP:DAT-1 fusion vector (pRB537) using 0.6µL of FuGENE 6 Transfection reagent per well (Roche Diagnostics). Cells were allowed to incubate further with transfection reagent plus DNA for 48hr before either western or uptake experiments were performed.

Western Blot Procedures

In order to verify immunoreactivity of the TAP tag, membranes from transfected COS-7 cells were collected by addition of 100µl of membrane prep solution (0.1µl sigma protease inhibitor, 100mM NaCl, 50mM TRIS) followed by scraping on ice. Dissociated cells were then collected in a 1.5ml microcentrifuge tubes and membranes were pelleted by centrifugation in a Sorval microcentrofuge for at 16,000 x g (13,000 RPM) for 15min at 4°C. The supernatant was then discarded and the resultant pellet was re-suspended in 300µl of RIPA buffer with protease inhibitor. Protein was then loaded onto a 10% polyacrylamide gel and run for 3 hours. Proteins were then transferred to a nitrocellulose

membrane overnight in Towbin transfer buffer (25mM Tris, 192mM glycine, and 20% methanol). After transfer, the membrane was stripped in western blot stripping solution (60mM Tris pH 6.8, .2% SDS and 10mM β-ME). The membrane was then blocked for 2 hours using 5% milk solution in PBS/T. TAP:DAT-1 was detected using either our DAT-1 COOH-terminal antibody (Rb1565) or mouse purified IgG at 1:5000 (1 hour), followed by either goat anti mouse or goat anti-rabbit horseradish peroxidase-conjugated secondary at 1:10,000 (1 hr).

[^{3}H] Dopamine Uptake Procedures

COS-7 cells transfected as described above were washed once with 37^{0}C KRH buffer including 10mM D-glucose, 100μM ascorbic acid, 100μM paragyline, and 1mM tropolone. Cells were pre-incubated at 37^{0}C in the same buffer for 10 min. Some wells contained the DAT-1 antagonist imipramine (1μM final) to assess nonspecific uptake. All cells were incubated for 10 min at 37^{0}C with 50nM of [^{3}H]DA (dihydroxyphenylethylamine 3,4, -[$^{7\text{-}3}$H], Perkin Elmer) prior to washing 3X with ice-cold KRH buffer. Counts accumulated were solubilized using Microscint 20 (Perkin-Elmer) scintillation fluid with gentle rocking for 1 hr before quantitation using a Top Count scintillation counter (Packard).

Whole Worm Protein Extraction

Lines were initially plated on large 100mm OP50/NA22 plates and allowed to starve to force dauer formation. Each line was then washed off the plates using sterile H2O and pelleted. 100μl of concentrated worm slurry was then added to a total of 8 100mm 8P

plates. Once animals were gravid, animals were then synchronized per protocol (Carvelli et al., 2004) and plated again on 32 8P plates per line. Animals were grown for 24 hr at 20°C and then washed off the 8P plates with M9 solution. These L2/L3 lines were then washed 3x in M9 in large 50ml conical tubes (falcon) and then rewashed another 2x in isotonic sucrose. Lines were then pelleted in isotonic sucrose and quick frozen in liquid nitrogen. Lines were allowed to thaw on ice and subjected to French press at 500psi, on high. Each line was put through the French press twice to ensure disruption. The extracts were then either subjected to differential centrifugation or used directly for TAP purification. For lysates subjected to differential centrifugation, an initial P1 pellet was collected by centrifugation at 2,000 rpm for 10 minutes. The supernatant from this was collected in a high-speed centrifuge tube and subjected to 20,000x*g* for 1.5 hr. The supernatant from this spin was then decanted and collected as an S2 fraction and the precipitate from this spin was collected and kept as a P2 fractions. Fractions were then analyzed by western blot.

TAP Purification and Protein Preparation

Protein lysates collected as described above were subjected to TAP purification as described (Rigaut et al., 1999). Once the final eluate was collected, proteins were precipitated using 2% trichloroacetic acid (TCA). Precipitated pellets was were washed using 100% acetone. After precipitation, the protein precipitate was resuspended and trypsin digested as previously described (Link et al., 1999). A portion of the eluate was analyzed on a gradient (4-20%) polyacrylamide gel and visualized by silver staining using Bio-Rad Silver Stain Plus reagent (Bio-Rad, Hercules, CA).

RESULTS

TAP:DAT-1 Construct Design

To avoid disruption of known COOH-terminal protein interactions, we used the NH_2-terminal TAP tag which results in initial translation of the IgG binding domain (Protein A) followed by a tobacco etch virus (TEV) cleavage sequence, and finally the calmodulin binding protein (CBP) (Fig 31A). This NH_2-terminal tag allows for initial purification using IgG Sepharose beads followed by TEV protease cleavage and subsequent calmodulin resin purification. This NH_2-terminal tag, fused to DAT-1, results in a free COOH-terminus and only hinders N-terminal interactions at the very proximal NH_2-terminus (Fig 31B).

TAP:DAT-1 Fusion Protein Supports Dopamine Uptake in vitro

To determine if fusion of the TAP tag to the NH_2-terminus of the *C. elegans* DAT (DAT-1) would affect transporter function, we expressed full length fusion protein (TAP:DAT-1) in COS-7 cells and monitored DA uptake. An equivalent amount DA of control empty vector (pFA6), non-tagged DAT-1 expression vector (pRB235), and our experimental TAP:DAT-1 construct (pRB537) was transfected and resulted in equivalent uptake amounts for both the tagged and non-tagged version of DAT-1. This uptake was blocked in both cases by the DAT-1 antagonist imipramine at 1μm (Fig. 31C), revealing it to be specific for DAT-1. No specific uptake was noted in our control vector expressing cells.

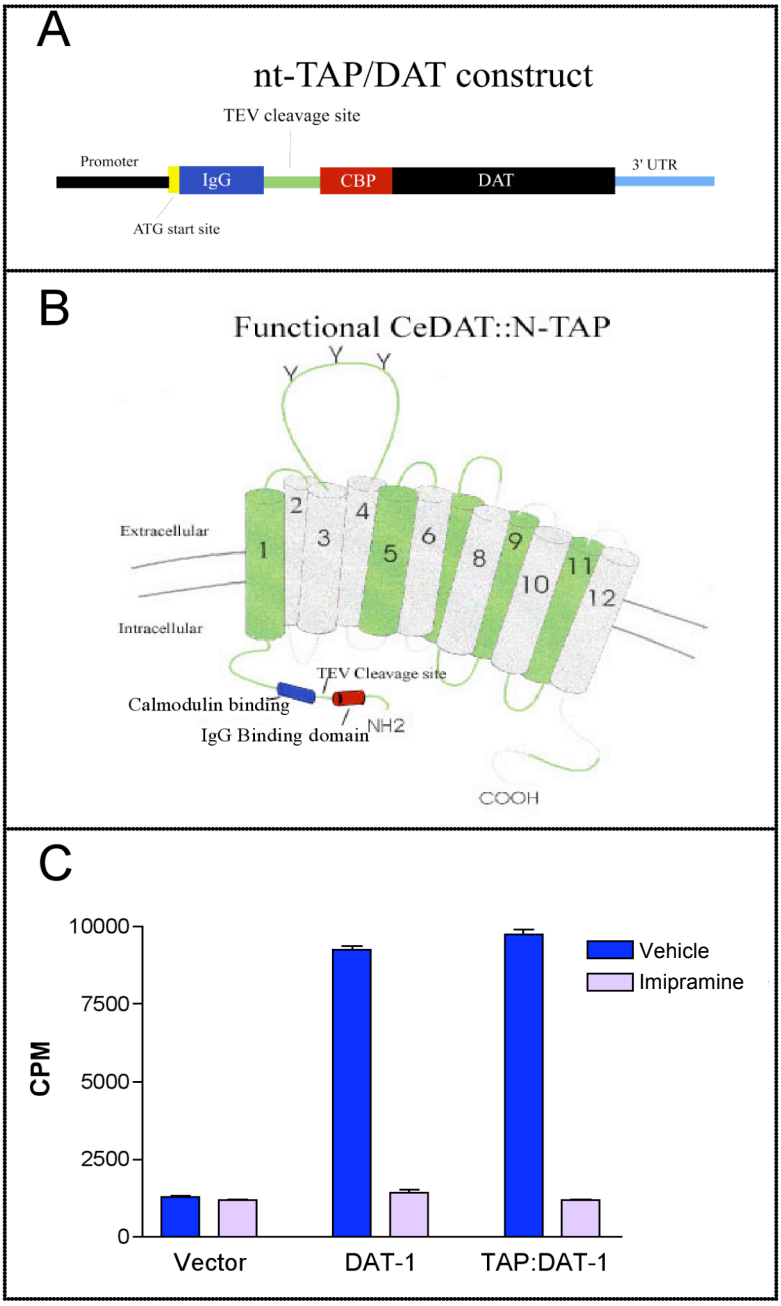

Figure 31. TAP:DAT-1 Construct and DA Uptake Results.

A. Schematic representation of the N-terminal TAP tag with initial translation of the protein A domain followed by the TEV cleavage site and CBP domain. **B**. Illustration of translated TAP:DAT-1 fusion displaying N-terminal TAP tag and free C-terminal DAT-1 domain. **C**. Uptake results for different DAT-1 constructs in transfected COS-7 cells. Both the non-tagged DAT-1 and the TAP tagged DAT-1 show robust specific uptake of [^{3}H]-DA. Uptake through both constructs is also blocked using the known DAT-1 antagonist imipramine.

Western Blot of COS-7 Cell Extracts

COS-7 cells transfected with either pFA6 (control vector), pBY235 (DAT-1), or pBY537 (TAP:DAT-1 fusion) were harvested and tested for immunoreactivity using previously described antibody DAT-1 RB1566. This antibody was originally raised against the intracellular COOH-terminus of DAT-1 but failed to recognize endogenous DAT-1 protein by western blot. To test whether this antibody would interact with the Protein A binding domain of the TAP:DAT-1 fusion, both DAT-1 and TAP:DAT-1 was extracted from COS-7 and analyzed by western blot. RB1566 identified both purified GST (Fig 32, lane 1) and the protein A domain of TAP:DAT-1 (Fig 32, lane 4) binds the IgG region of this antibody. This antibody however failed to recognize DAT-1 (lane 3), as discussed in Chapter III. Purified rabbit IgG and mouse IgG also bind to the protein A domain of both TAP and TAP:DAT-1 fusion by western (data not shown).

TAP:DAT-1 Expression in vivo

Animals expressing either the TAP:DAT-1 fusion protein (BY324) or the control TAP alone protein (BY325) were initially subjected to both *dat-1* and TAP genotyping to verify integration of the TAP construct and absence of wild type *dat-1* allele. The full length *dat-1* gene yields a 3.8kb fragment where as the *dat-1* knockout (*ok157*) generates only a 1.8Kb PCR product. As a control for heterogygous genotype, 0.5ng of both the wild type (N2) genome and the knockout (*dat-1*) genome were mixed and yielded both the 3.8 and 1.8 Kb bands, eliminating a false *dat-1* designation that could result from the smaller amplicon masking the presence of the larger. The BY324 and BY325 lines were then probed for the presence of the TAP construct, using pRB534 as a control. Both the

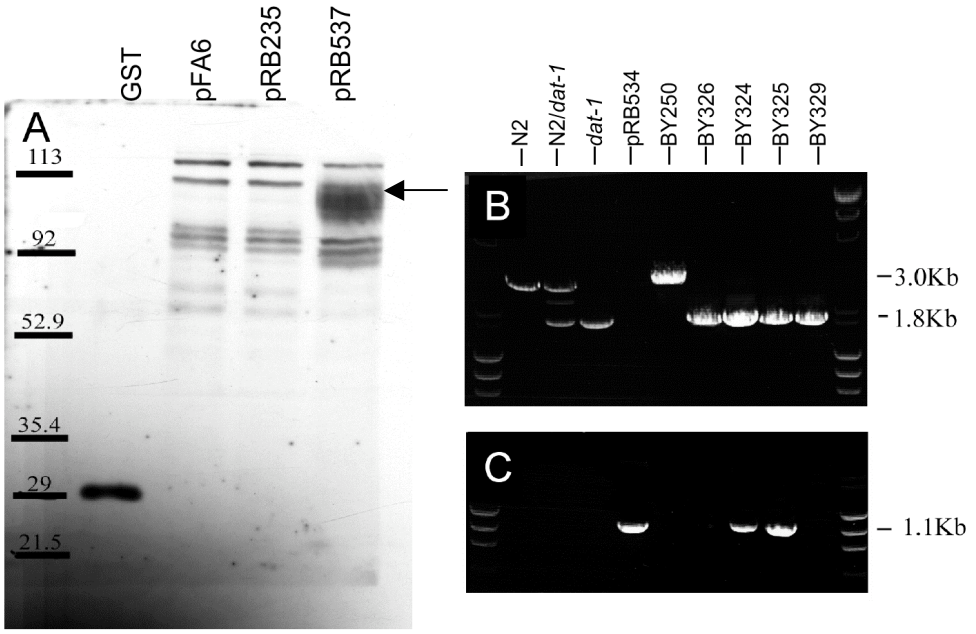

Figure 32. Western Blot and Genotyping Data of TAP Cells and Strains.

A. Proteins purified from COS-7 cells using antibody RB1566 displays specific immunoreactivity for both GST (positive control) and TAP:DAT-1 (arrow). While this antibody was originally designed to recognize the DAT-1 COOH-terminus, DAT-1 is not detected under these conditions (pRB235, lane 3). Background bands from the pFA6 parental vector are seen in lane 2. **B**. Genotyping of all strains for either the wild type *dat-1* allele or the *dat-1(ok157)* allele reveals that all TAP expression strains (BY324 and BY325) are in the *dat-1(ok157)* knockout background as expected. Control lines BY250 and BY326 used in 6-OHDA experiments are also shown. **C**. Genotyping for the integrated TAP construct reveals that both TAP expression strains contain the TAP construct. The injected vector (pRB534) yields the expected 1.1Kb band while a negative control line (GFP:DAT-1 fusion, BY329) does not produce an amplicon.

control TAP DNA (from BY325, see Table 7) and the TAP:DAT-1 fusion DNA (from BY324) yielded the expected 1.1Kb fragment, consistent with the control. Satisfied that both lines contained copies of the TAP construct, we proceeded to examine protein expression in whole worm extracts from both lines.

Western Blot of Purified Worm Extracts Containing TAP and TAP:DAT-1 fusions

Worms identified as containing integrated TAP and TAP:DAT-1 fusion vectors by PCR were then allowed to clone and extracts were generated for western blot analysis of TAP:DAT-1 collected proteins. Whole worm lysis was originally separated by differential centrifugation to generate 3 separate lysate fractions as described in the methods. Western blotting using purified mouse IgG identified TAP:DAT-1 full length protein in the control lane (lane 1, pRB537) and in the S2 and P2 fractions (Fig. 33A, lanes 3 and 4). These bands were absent in the TAP alone expression worms but a band consistent with the mobility of full length TAP was detected in both the P1 and S2 pellets (~40Kd, lanes 5 and 6).

TAP Purification of Whole Worm Extracts and DALPC Analysis

With evidence of full length TAP-DAT-1 fusion of protein expression via western blot analysis, we proceeded with TAP purification and DALPC analysis of DAT associated proteins. Total worm lysate from both the BY324 and BY325 lines were subjected to dual column affinity purification. Fractions from each step of the purification were saved for gel analysis and the final eluate was divided in two. Half was precipitated using TCA and the other half was and run with the saved fractions from each

Table 7. *C. elegans* Strains Used to Test TAP:DAT-1 Function in *vivo*..

C. elegans Strains Created or Used		
BY250 (vtIs7)	Genotype	N2 Background P_{dat-1}::GFP integrated
	Protein Expression	GFP in all DA Neurons
BY324(vtIs14)	Genotype	*dat-1(ok157)* pRB533 integrated pRF4 integrated
	Protein expression	TAP:DAT-1 in DA neurons
	Phenotype	*Rol-6(su1006)* in cuticle roller
BY325(vtIs15)	Genotype	*dat-1(ok157)* pRB578 integrated pRF4 integrated
	Protein expression	TAP in DA neurons
	Phenotype	*Rol-6(su1006)* in cuticle roller
BY326	Genotype	vtIs7 *dat-1(ok157)*
	Protein Expression	GFP in All DA neurons
BY327	Genotype	vtIs7 vtIs14 *dat-1(ok157)*
	Protein expression	TAP:DAT-1 in DA neurons GFP in all DA neurons
	Phenotype	*Rol-6(su1006)* in cuticle roller
BY328	Genotype	vtIs7 vtIs15 *dat-1(ok157)*
	Protein expression	TAP in DA neurons GFP in all DA neurons
	Phenotype	*Rol-6(su1006)* in cuticle roller

of the purification steps on a 4 – 20% gradient gel for analysis by silver staining. Protein purification using the TAP method reveals specific purification of several distinct protein bands not seen in the control purified eluate (Fig 33C, asterisks). With confidence of specific purification, we proceeded with LCS/MS/MS and peptide identification.

Peptides generated from the final eluate, which become candidate interacting proteins, were identified by the SEQUEST algorithm. Consistent with functional TAP tag, a calmodulin (cmd-1) homologue was isolated from the control animals. Peptide fragments were considered specific by subtracting protein fragments identified in our experimental TAP:DAT-1 expressing line (BY324) against those identified using the TAP alone control line (BY325).

Analysis of SEQUEST generated data did not yield DAT-1 specific peptides, nor did we recover any potential PICK1 homologues identified in worm base as might be expected (www.wormbase.org). We did recover specific peptides that corresponded to both identified and novel proteins in *C. elegans*. Proteins were distributed primarily as proteins with unknown function in *C. elegans* (40%), protein processing factors (20%), structural proteins (15%), signaling proteins (15%), and membrane proteins (10%) (Table 8).

6-OHDA Analysis of both TAP and TAP:DAT-1 Expressing Lines

To test the function of our TAP:DAT-1 fusion protein *in vivo*, animals integrated with either the TAP or TAP:DAT-1 fusion construct were crossed to BY326 (*dat-1* null with cytosolic GFP in all DA neurons). Lines that were both pure for GFP expression and conveyed a 100% *rol* phenotype, were subjected to 50mM 6-OHDA. This

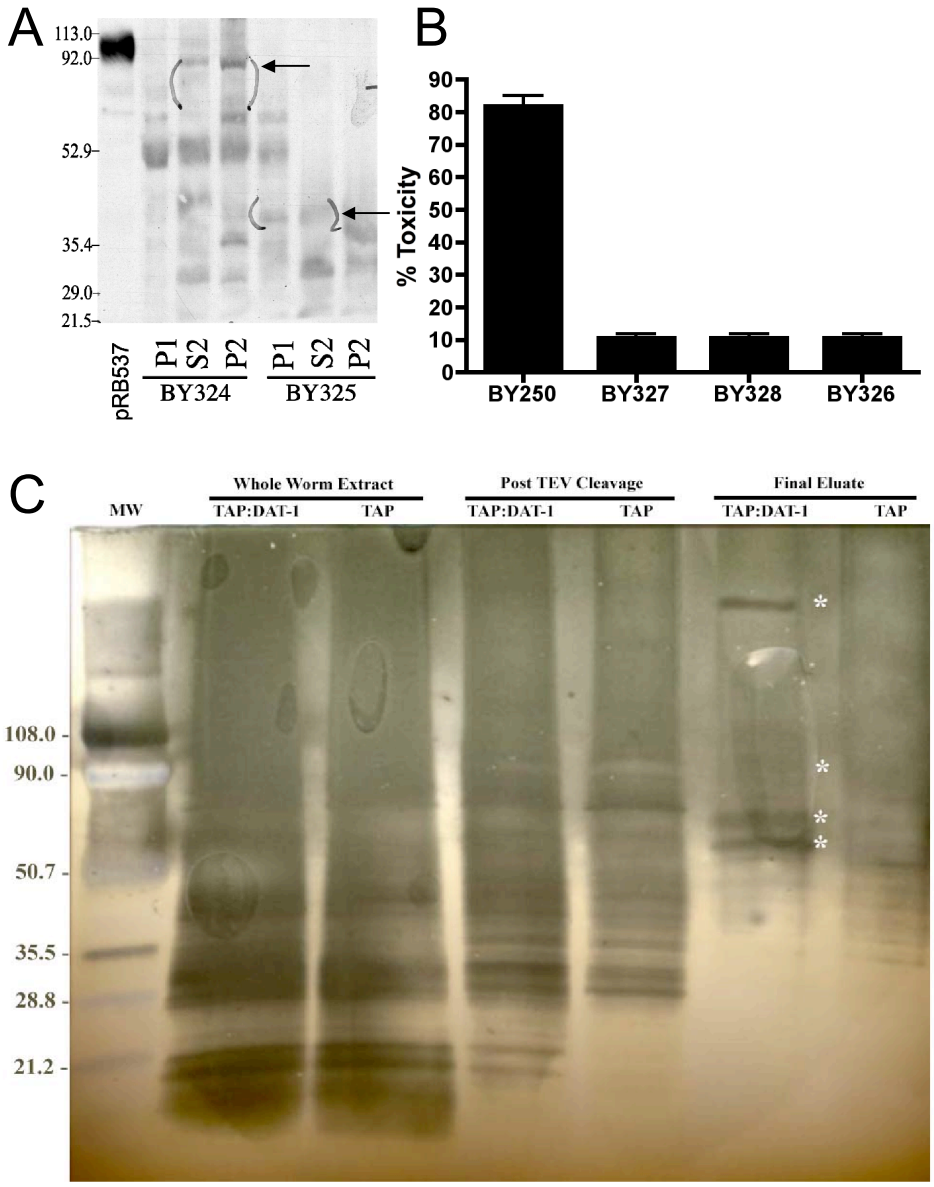

Figure 32. Biochemistry and Uptake Experiments from TAP Expression Worm Lines.

A. Lysate from TAP strains were subjected to differential centrifugation and the different fractions were tested for TAP immunoreactivity. Control protein from COS-7 cells expressing the TAP:DAT-1 fusion (lane 1) is recognized by purified mouse IgG. Similar bands are noted in the S2 and P2 pellets for the TAP:DAT-1 expressing line (BY324, lane 3 and 4 arrows) but not in the TAP alone expressing line (BY325). A band that is consistent with TAP alone mobility is noted in BY325 lines (lane 5 and 6, arrows). **B**. 6-OHDA induced toxicity in TAP expressing lines reveals that the TAP:DAT-1 fusion does not restore DA neuron susceptibility to 6-OHDA. Wild type stains (BY250) loose over 80% of their neurons whereas TAP:DAT-1 (BY327), TAP alone (BY328), and the *dat-1* KO line (BY326) do not restore sensitivity. **C**. Lysates from whole worm extracts after TAP purification show specific purification of protein bands in the TAP:DAT-1 expressing line (lane 6, asterisks).

concentration of 6-OHDA has previously been shown to cause significant DA neuron toxicity in *dat-1* wild type animals (Nass et al., 2002).

Neither the TAP control nor the TAP:DAT-1 fusion line rescued the *dat-1* knockout phenotype, failing to convey DA neuronal susceptibility to 6-OHDA (Fig 33B). The TAP:DAT-1 expressing line displayed almost complete resistance to 6-OHDA, which was indistinguishable from *dat-1* knockout animals. Animals expressing the wild type *dat-1* allele (BY250) convey greater than 80% toxicity to these neurons and a similarly tagged GFP:DAT-1 fusion is able to restore almost WT levels of 6-OHDA induced toxicity (Chapter IV).

CONCLUSIONS

While it is disappointing that the TAP:DAT-1 fusion protein did not restore 6-OHDA sensitivity, significant progress was made toward use of multi-tagged transporter for immunoisolation in *C. elegans*. It should be noted that this system was recently used to identify nicotinic receptor (UNC-29) associated proteins in *C. elegans*, identifying several novel protein-protein interactions important for nicotinic sensitivity (Gottschalk et al., 2005). Total recovery of nicotine paralysis was seen with the COOH-terminal UNC-29:TAP fusion, indicating successful plasma membrane elaboration of the receptor. The expressed version of the TAP tag used by Gottschalk *et al*. differed slightly in the Protein A domain (direct communication, A. Gottschalk) which may account for loss of rescue with our NH_2-terminal tagged version.

The original TAP tag had to be modified in plants due to the presence of a nuclear localization signal in the calmodulin binding domain. When fused to GFP, the originally

published TAP protein resided primarily in the nucleus with very little cytoplasmic elaboration of the GFP signal (Rohila et al., 2004). This may not have been an issue in the original system as proteins tagged for immunoisolation by Rigaut *et al*. were splicing factors which normally reside in the nucleus (Rigaut et al., 1999).

A significant amount of TAP:DAT-1 protein was produced and differential isolation of the TAP control and TAP:DAT-1 fusion yielded novel and potential DAT-1 interacting proteins. While TAP:DAT-1 failed to rescue 6-OHDA sensitivity *in vivo*, several potential DAT-1 interacting proteins were identified which may be important for early DAT-1 synthesis and potentially DAT-1 trafficking during biogenesis. It is unlikely however that any of the proteins identified will be important for plasma membrane retention/insertion or for synaptic localization. In fact, proteins expected to be found at the plasma membrane or synapse (PICK1 and syntaxin) were not recovered by this technique. Interestingly, one of our hits was recently reported to be a DAT-interacting protein in both cell culture and from rat synaptosomes taken from midbrain cultures (a homolog of RACK1 (K04D7.1, Table 8).

FUTURE DIRECTIONS

Significant changes to the tandem affinity purification tag should be made before attempting immunoisolation of DAT-1 (or other *C. elegans* transporters). While the use of this tag originally appeared promising, lack of verifiable expression level in individual neurons is problematic. *In vitro* expression showed no significant impairment of TAP:DAT-1 fusion uptake capacity, and both PCR and western blot based analysis from

Table 8. DAT-1 Interacting Proteins Identified by Mass Spectrometry

Cytoskeletal/Structural Proteins

Actin Interacting Protein
Actin
Tubulin β Chain

Plasma Membrane Associated Proteins

SER-3
- Metabotropic Serotonin Receptor
- 48% identity with Human Alpha 1C Aderenergic Receptor 2

NCA-1
- Voltage Gated Ca^{++} Channel
- 87.4% identity with Human VGCNL1 (voltage gated channel like 1)
- Expressed in Head Neurons in *C. elegans* (Hamming and Snutch, 2003 Int Worm Meeting)

Cell Signaling Proteins

SRC-1
- 96.8% identity with Human protein tyrosin kinase Fyn A
- Serine /Threonine Kinase Activity
- Expressed in Neurons in C. elegans

TAX-6
- 85.3% identity with Human Calcineurin Subunit Aα
- Serine/Threonine Phosphatase activity
- Expressed in sensory neurons

GTP Binding Protein
- 52.3% identity with Rat RagA

Protein Processing Accessory Proteins

HSP-1
- Heatshock protein 1

EFT-3
- Elongation factor 1α

RSP-1
- 40s Ribosome

60s Ribosome

Proteins of Unknown Function

K04D7.1
- 97.5% homologous to rat RACK1
- Egl phenotype (consistent with DA dysfunction)
- putative nucleotide binding protein
- putative PKC binding protein

T28D6.4
- 54.5% homologous to mouse ankyrin 1
- Protein contains 8 Ank repeats

F49B2.4
- F box domain containing protein
- In yeast, homologue binds Skp-1p and is important in recyling

C31E10.8
- In yeast, homolog is a GTPase activating protein
- Activates Sec4p to regulate exocytosis

Y73F8A.2
- PP2A β subunit homolog

ZC132.4
- 35.4% homology to human synaptonemal complex 1 protein

F44E5.1
- No known or putative function

M05D6.6
- No known or putative function

integrated strains displayed both an integrated construct and protein expression. It is likely therefore that the construct was integrated at low levels into the genome and that low level expression was achieved. Without direct visualization of the tagged protein however, it is impossible to know if the fusion protein was being trafficked as expected for non-tagged DAT-1 protein. 6-OHDA studies would suggest that at least plasma membrane insertion and retention was not achieved.

In the future, a directly identifiable tandem affinity tag should be tested for use in *C. elegans*. One of the advantages of the *C. elegans* system is direct visualization of cells and neurons *in vivo*. Substitution of the protein A domain of the TAP tag with a Fire vector GFP would be recommended. This construct contains artificial introns within the GFP sequence that increases mRNA stability and protein expression i*n vivo*. An NH_2-terminal GFP would allow for direct visualization and commercial antibodies could be used in the first immuo-isolation step.

Addition of the GFP would ensure appropriate expression of the tagged protein and cellular and subcellular localization could be determined. Of course, as is true with any GFP fusion, *in vivo* function in the form of knockout rescue should be tested. In the case of DAT-1, GFP:DAT-1 fusion has already been shown to confer *dat-1* dependent 6-OHDA toxicity to the DA neurons and cellular localization matches that of native protein probed with DAT-1 directed antibodies.

Retention of the TEV clevage sequence or a similar non-worm protease sequence would be recommended in order to free the complex from high affinity antibody interactions between the GFP and anti-GFP antibodies. Alternatively, purified GFP

could be used to compete off the GFP tagged protein from the primary immuno-isolation complex.

Because there is some concern with a nuclear localization sequence within the calmodulin binding domain of the TAP tag, either a modified CBP domain should be used or an alternate tag should be employed. A hemaglutanin A (HA) tag might be advisable as HA resin is commercially available and the HA tag and anti-HA resin has been directly tested for immunoprecipitation of DAT-1 protein (Nass et al., 2005). After washing, the HA resin could be analyzed directly via polyacrylamide gel for band isolation or purified hemagglutanin could be used to compete the protein complex off the HA resin. This new method of isolation would provide several improvements over the current system including i*n vivo* visualization of tagged protein localization. Use of this novel TAP (GFP:TEV:HA) tag would retain the dual purification steps and greatly improve current TAP technology and should be investigated.

Any identified proteins could be easily assayed for both *in vitro* function and co-IP. With the release of the *C. elegans* ORFeome (Reboul et al., 2003; Lamesch et al., 2004), over 13,000 *C. elegans* cDNAs are now commercially available in Gateway™ vectors (Open Biosystems, Huntsville, Al). Hits available from this library can be rapidly moved from Gateway™ entry vectors to destination vectors for mammalian expression. These destination vectors have specific tags (GFP, HA, 6-his, etc.) which can be used for biochemistry to map a direct interaction. At the same time, DA uptake experiments with co-expression of DAT-1 can be used to assay function. The potential for identification of native DAT-1 interacting proteins using this technology is significant and should be investigated in the future using improved tags.

REFERENCES

Angelides KJ (1986) Fluorescently labelled Na+ channels are localized and immobilized to synapses of innervated muscle fibres. Nature 321:63-66.

Angelides KJ, Elmer LW, Loftus D, Elson E (1988) Distribution and lateral mobility of voltage-dependent sodium channels in neurons. J Cell Biol 106:1911-1925.

Axelrod D, Koppel DE, Schlessinger J, Elson E, Webb WW (1976) Mobility measurement by analysis of fluorescence photobleaching recovery kinetics. Biophys J 16:1055-1069.

Azoui R, Cuche J, Renaud J, Safar M, Dagher G (1996) A dopamine transporter in human erythrocytes: modulation by insulin. Experimental Physiology 81:421-434.

Bannon MJ, Poosch MS, Xia Y, Goebel DJ, Cassin B, Kapatos G (1992) Dopamine transporter mRNA content in human substantia nigra decreases precipitously with age. ProcNatlAcadSci 89:7095-7099.

Bannon MJ, Pruetz B, Manning-Bog AB, Whitty CJ, Michelhaugh SK, Sacchetti P, Granneman JG, Mash DC, Schmidt CJ (2002) Decreased expression of the transcription factor NURR1 in dopamine neurons of cocaine abusers. ProcNatlAcadSci 99:6382-6385.

Bauman AL, Apparsundaram S, Ramamoorthy S, Wadzinski BE, Vaughan RA, Blakely RD (2000) Cocaine and antidepressant-sensitive biogenic amine transporters exist in regulated complexes with protein phosphatase 2A. J Neurosci 20:7571-7578.

Beaulieu JM, Sotnikova TD, Marion S, Lefkowitz RJ, Gainetdinov RR, Caron MG (2005) An Akt/beta-arrestin 2/PP2A signaling complex mediates dopaminergic neurotransmission and behavior. Cell 122:261-273.

Begum N, Ragolia L (1996) cAMP counter-regulates insulin-mediated protein phosphatase-2A inactivation in rat skeletal muscle cells. JBC 271:31166-31171.

Bell WJ (1991) Searching behaviour : the behavioural ecology of finding resources, 1st Edition. London ; New York: Chapman and Hall.

Benoit-Marand M, Jaber M, Gonon F (2000) Release and elimination of dopamine in vivo in mice lacking the dopamine transporter: functional consequences. Eur J Neurosci 12:2985-2992.

Bertler A, Rosengren E (1959) Occurrence and distribution of dopamine in brain and other tissues. Experientia 15:10-11.

Birkmayer W, Hornykiewicz O (1961) [The L-3,4-dioxyphenylalanine (DOPA)-effect in Parkinson-akinesia.]. Wien Klin Wochenschr 73:787-788.

Bjerggaard C, Fog JU, Hastrup H, Madsen K, Loland CJ, Javitch JA, Gether U (2004) Surface targeting of the dopamine transporter involves discrete epitopes in the distal C terminus but does not require canonical PDZ domain interactions. J Neurosci 24:7024-7036.

Blakely RD, Berson HE, Fremeau RT, Jr., Caron MG, Peek MM, Prince HK, Bradley CC (1991) Cloning and expression of a functional serotonin transporter from rat brain. Nature 354:66-70.

Brenner S (1974) The genetics of *Caenorhabditis elegans*. Genetics 77:71-94.

Burns RS, LeWitt PA, Ebert MH, Pakkenberg H, Kopin IJ (1985) The clinical syndrome of striatal dopamine deficiency. Parkinsonism induced by 1-methyl-4-phenyl-1,2,3,6-tetrahydropyridine (MPTP). NEJM 312:1418-1421.

Campbell RE, Tour O, Palmer AE, Steinbach PA, Baird GS, Zacharias DA, Tsien RY (2002) A monomeric red fluorescent protein. ProcNatlAcadSci 99:7877-7882.

Cao S, Gelwix CC, Caldwell KA, Caldwell GA (2005) Torsin-mediated protection from cellular stress in the dopaminergic neurons of Caenorhabditis elegans. J Neurosci 25:3801-3812.

Carlsson A (2001) A half-century of neurotransmitter research: impact on neurology and psychiatry. Nobel lecture. Biosci Rep 21:691-710.

Carlsson A, Waldeck B (1958) A fluorimetric method for the determination of dopamine (3-hydroxytyramine). Acta Physiol Scand 44:293-298.

Carlsson A, Lindqvist M, Magnusson T (1957) 3,4-Dihydroxyphenylalanine and 5-hydroxytryptophan as reserpine antagonists. Nature 180:1200.

Carneiro AM, Ingram SL, Beaulieu JM, Sweeney A, Amara SG, Thomas SM, Caron MG, Torres GE (2002) The multiple LIM domain-containing adaptor protein Hic-5 synaptically colocalizes and interacts with the dopamine transporter. J Neurosci 22:7045-7054.

Carvelli L, McDonald PW, Blakely RD, Defelice LJ (2004) Dopamine transporters depolarize neurons by a channel mechanism. ProcNatlAcadSci 101:16046-16051.

Carvelli L, Moron JA, Kahlig KM, Ferrer JV, Sen N, Lechleiter JD, Leeb-Lundberg LM, Merrill G, Lafer EM, Ballou LM, Shippenberg TS, Javitch JA, Lin RZ, Galli A (2002) PI 3-kinase regulation of dopamine uptake. J Neurochem 81:859-869.

Chalfie M, Sulston JE, White JG, Southgate E, Thomson JN, Brenner S (1985) The neural circuit for touch sensitivity in Caenorhabditis elegans. J Neurosci 5:956-964.

Chang M, Lee S-H, Kim J-H, Lee K-H, Kim Y-S, Son H, Lee Y-S (2001) Protein kinase C-mediated functional regulation of dopamine transporter is not achieved by direct phosphorylatin of the dopamine transporter protein. J of Neurochem 77:754-761.

Chase DL, Pepper JS, Koelle MR (2004) Mechanism of extrasynaptic dopamine signaling in Caenorhabditis elegans. Nat Neurosci 7:1096-1103.

Ciliax BJ, Heilman C, Demchyshyn LL, Pristupa ZB, Ince E, Hersch SM, Niznik HB, Levey AI (1995) The dopamine transporter: immunochemical characterization and localization in brain. J Neurosci 15:1714-1723.

Ciliax BJ, Drash GW, Staley JK, Haber S, Mobley CJ, Miller GW, Mufson EJ, Mash DC, Levey AI (1999) Immunocytochemical localization of the dopamine transporter in human brain. J Comp Neurol 409:38-56.

Clark SG, Chiu C (2003) C. elegans ZAG-1, a Zn-finger-homeodomain protein, regulates axonal development and neuronal differentiation. Dev 130:3781-3794.

Cole NB, Smith CL, Sciaky N, Terasaki M, Edidin M, Lippincott-Schwartz J (1996) Diffusional mobility of Golgi proteins in membranes of living cells. Science 273:797-801.

Compton MT, Miller AH (2002) Antipsychotic-induced hyperprolactinemia and sexual dysfunction. Psychopharmacol Bull 36:143-164.

consortium *Ce*s (1998) Genome sequence of the nematode C. elegans: a platform for investigating biology. Science 282:2012-2018.

Copeland BJ, Vogelsberg V, Neff NH, Hadjiconstantinou M (1996) Protein kinase C activators decrease dopamine uptake into striatal synaptosomes. JPET 277:1527-1532.

Cowell RM, Kantor L, Hewlett GH, Frey KA, Gnegy ME (2000) Dopamine transporter antagonists block phorbol ester-induced dopamine release and dopamine transporter phosphorylation in striatal synaptosomes. Eur J Pharmacol 389:59-65.

Coyle JT, Snyder SH (1969) Catecholamine uptake by synaptosomes in homogenates of rat brain: stereospecificity in different areas. The Journal of Pharmacology and Experimental Therapeutics 170:221-231.

Crow TJ (1971) The relation between electrical self-stimulation sites and catecholamine-containing neurons in the rat mesencephalon. Experientia 27:662.

Dahlstrom A, Fuxe K (1964) Localization of monoamines in the lower brain stem. Experientia 20:398-399.

Dal Toso R, Sommer B, Ewert M, Herb A, Pritchett DB, Bach A, Shivers BD, Seeburg PH (1989) The dopamine D2 receptor: two molecular forms generated by alternative splicing. Embo J 8:4025-4034.

Daniels GM, Amara SG (1999) Regulated trafficking of the human dopamine transporter. Clathrin-mediated internalization and lysosomal degradation in response to phorbol esters. JBC 274:35794-35801.

Deken SL, Beckman ML, Boos L, Quick MW (2000) Transport rates of GABA transporters: regulation by the N-terminal domain and syntaxin 1A. Nature Neurosci 3:998-1003.

Desai C, Horvitz HR (1989) Caenorhabditis elegans mutants defective in the functioning of the motor neurons responsible for egg laying. Genetics 121:703-721.

Di Chiara G, Imperato A (1988) Drugs abused by humans preferentially increase synaptic dopamine concentrations in the mesolimbic system of freely moving rats. ProcNatlAcadSci 85:5274-5278.

Dong Y, Nasif FJ, Tsui JJ, Ju WY, Cooper DC, Hu XT, Malenka RC, White FJ (2005) Cocaine-induced plasticity of intrinsic membrane properties in prefrontal cortex pyramidal neurons: adaptations in potassium currents. J Neurosci 25:936-940.

Duerr JS, Frisby DL, Gaskin J, Duke A, Asermely K, Huddleston D, Eiden LE, Rand JB (1999) The *cat-1* gene of Caenorhabditis elegans encodes a vesicular monoamine transporter required for specific monoamine-dependent behaviors. J Neurosci 19:72-84.

Ehringer H, Hornykiewicz O (1960) [Distribution of noradrenaline and dopamine (3-hydroxytyramine) in the human brain and their behavior in diseases of the extrapyramidal system.]. Klin Wochenschr 38:1236-1239.

Estevez M, Estevez AO, Cowie RH, Gardner KL (2004) The voltage-gated calcium channel UNC-2 is involved in stress-mediated regulation of tryptophan hydroxylase. J Neurochem 88:102-113.

Falck B, Hillarp NA, Thieme G, Torp A (1962) Fluorescence of catechol amines and related compounds condensed with formaldehyde. J Histochem Cytochem 10:348-354.

Falck B, Hillarp NA, Thieme G, Torp A (1982) Fluorescence of catechol amines and related compounds condensed with formaldehyde. Brain Res Bull 9:xi-xv.

Fallon JH (1988) Topographic organization of ascending dopaminergic projections. Ann N Y Acad Sci 537:1-9.

Farhan H, Korkhov VM, Paulitschke V, Dorostkar MM, Scholze P, Kudlacek O, Freissmuth M, Sitte HH (2004) Two discontinuous segments in the carboxyl terminus are required for membrane targeting of the rat gamma-aminobutyric acid transporter-1 (GAT1). JBC 279:28553-28563.

Ferguson SM, Savchenko V, Apparsundaram S, Zwick M, Wright J, Heilman CJ, Yi H, Levey AI, Blakely RD (2003) Vesicular localization and activity-dependent trafficking of presynaptic choline transporters. J Neurosci 23:9697-9709.

Fields S (2005) High-throughput two-hybrid analysis. The promise and the peril. Febs J 272:5391-5399.

Fields S, Song S (1989) A novel genetic system to detect protein-protein interactions. Nature 340:245-247.

Finney M, Ruvkun G (1990) The unc-86 gene product couples cell lineage and cell identity in *C. elegans*. Cell 63:895-905.

Fischman AJ, Babich JW, Elmaleh DR, Barrow SA, Meltzer P, Hanson RN, Madras BK (1997) SPECT imaging of dopamine transporter sites in normal and MPTP-Treated rhesus monkeys. J Nucl Med 38:144-150.

Frye LD, Edidin M (1970) The rapid intermixing of cell surface antigens after formation of mouse-human heterokaryons. J Cell Sci 7:319-335.

Fuxe K (1965) Evidence for the existence of monoamine neurons in the central nervous system. IV. Distribution of monoamine nerve terminals in the central nervous system. . Acta physiologica scandinavica 64(suppl. 247):37-120.

Gainetdinov RR, Sotnikova TD, Caron MG (2002) Monoamine transporter pharmacology and mutant mice. Trends Pharmacol Sci 23:367-373.

Gainetdinov RR, Jones SR, Fumagalli F, Wightman RM, Caron MG (1998) Re-evaluation of the role of the dopamine transporter in dopamine system homeostasis. Brain Res Brain Res Rev 26:148-153.

Galici R, Galli A, Jones DJ, Sanchez TA, Saunders C, Frazer A, Gould GG, Lin RZ, France CP (2003) Selective decreases in amphetamine self-administration and regulation of dopamine transporter function in diabetic rats. Neuroendocrinol 77:132-140.

Garcia BG, Wei Y, Moron JA, Lin RZ, Javitch JA, Galli A (2005) Akt is essential for insulin modulation of amphetamine-induced human dopamine transporter cell-surface redistribution. Mol Pharmacol 68:102-109.

Gerdeman GL, Partridge JG, Lupica CR, Lovinger DM (2003) It could be habit forming: drugs of abuse and striatal synaptic plasticity. Trends Neurosci 26:184-192.

Giros B, Mestikawy SE, Bertrand L, Caron MG (1991) Cloning and functional characterization of a cocaine-sensitive dopamine transporter. FEBS Lett 295:149-154.

Giros B, Jaber M, Jones SR, Wightman RM, Caron MG (1996) Hyperlocomotion and indifference to cocaine and amphetamine in mice lacking the dopamine transporter. Nature 379:606-612.

Giros B, Sokoloff P, Martres MP, Riou JF, Emorine LJ, Schwartz JC (1989) Alternative splicing directs the expression of two D2 dopamine receptor isoforms. Nature 342:923-926.

Giros B, El Mestikawy S, Godinot N, Zheng K, Han H, Yang-Feng T, Caron MG (1992) Cloning, pharmacological characterization, and chromosome assignment of the human dopamine transporter. Mol Pharmacol 42:383-390.

Glowinski J, Axelrod J (1964) Inhibition of Uptake of Tritiated-Noradrenaline in the Intact Rat Brain by Imipramine and Structurally Related Compounds. Nature 204:1318-1319.

Gottschalk A, Almedom RB, Schedletzky T, Anderson SD, Yates JR, 3rd, Schafer WR (2005) Identification and characterization of novel nicotinic receptor-associated proteins in Caenorhabditis elegans. Embo J 24:2566-2578.

Granas C, Ferrer J, Loland CJ, Javitch JA, Gether U (2003) N-terminal truncation of the dopamine transporter abolishes phorbol ester- and substance P receptor-stimulated phosphorylation without impairing transporter internalization. JBC 278:4990-5000.

Gray JM, Hill JJ, Bargmann CI (2005) A circuit for navigation in Caenorhabditis elegans. Proc Natl Acad Sci U S A 102:3184-3191.

Graybiel AM, Hirsch EC, Agid Y (1990) The nigrostriatal system in Parkinson's disease. Adv Neurol 53:17-29.

Guastella J, Nelson N, Nelson H, Czyzyk L, Keynan S, Miedel MC, Davidson N, Lester HA, Kanner BI (1990) Cloning and expression of a rat brain GABA transporter. Science 249:1303-1306.

Gudelsky GA (1981) Tuberoinfundibular dopamine neurons and the regulation of prolactin secretion. Psychoneuroendocrinology 6:3-16.

Haase J, Killian AM, Magnani F, Williams C (2001) Regulation of the serotonin transporter by interacting proteins. Biochem Soc Trans 29:722-728.

Hajdu-Cronin YM, Chen WJ, Patikoglou G, Koelle MR, Sternberg PW (1999) Antagonism between G(o)alpha and G(q)alpha in Caenorhabditis elegans: the RGS protein EAT-16 is necessary for G(o)alpha signaling and regulates G(q)alpha activity. Genes Dev 13:1780-1793.

Hall DH, Hedgecock EM (1991) Kinesin-related gene *unc-104* is required for axonal transport of synaptic vesicles in *C. elegans*. Cell 65:837-847.

Hall DH, Russell RL (1991) The posterior nervous system of the nematode Caenorhabditis elegans: serial reconstruction of identified neurons and complete pattern of synaptic interactions. J Neurosci 11:1-22.

Hansra N, Arya S, Quick MW (2004) Intracellular domains of a rat brain GABA transporter that govern transport. J Neurosci 24:4082-4087.

Hare EE, Loer CM (2004) Function and evolution of the serotonin-synthetic bas-1 gene and other aromatic amino acid decarboxylase genes in Caenorhabditis. BMC Evol Biol 4:24.

Hayashi Y, Shi SH, Esteban JA, Piccini A, Poncer JC, Malinow R (2000) Driving AMPA receptors into synapses by LTP and CaMKII: requirement for GluR1 and PDZ domain interaction. Science 287:2262-2267.

Hersch SM, Yi H, Heilman CJ, Edwards RH, Levey AI (1997) Subcellular localization and molecular topology of the dopamine transporter in the striatum and substantia nigra. J Comp Neurol 388:211-227.

Hertting G, Axelrod J (1961) Fate of tritiated noradrenaline at the sympathetic nerve-endings. Nature 192:172-173.

Hillarp NA, Fuxe K, Dahlstrom A (1966) Demonstration and mapping of central neurons containing dopamine, noradrenaline, and 5-hydroxytryptamine and their reactions to psychopharmaca. Pharmacol Rev 18:727-741.

Hills T, Brockie PJ, Maricq AV (2004) Dopamine and glutamate control area-restricted search behavior in Caenorhabditis elegans. J Neurosci 24:1217-1225.

Hodgkin J (1995) Genetic nomenclature guide. Caenorhabditis elegans. Trends Genet:24-25.

Hoffman BJ, Mezey E, Brownstein MJ (1991) Cloning of a serotonin transporter affected by antidepressants. Science 254:579-580.

Hoffman BJ, Hansson SR, Mezey E, Palkovits M (1998) Localization and dynamic regulation of biogenic amine transporters in the mammalian central nervous system. Front Neuroendocrinol 19:187-231.

Holton KL, Loder MK, Melikian HE (2005) Nonclassical, distinct endocytic signals dictate constitutive and PKC-regulated neurotransmitter transporter internalization. Nature Neurosci 8:881-888.

Horvitz HR, Brenner S, Hodgkin J, Herman RK (1979) A uniform genetic nomenclature for the nematode Caenorhabditis elegans. Mol Gen Genet 175:129-133.

Horvitz HR, Chalfie M, Trent C, Sulston JE, Evans PD (1982) Serotonin and octopamine in the nematode Caenorhabditis elegans. Science 216:1012-1014.

Huang SP, Tattar TA, Rohde RA, Zuckerman BM (1982) Caenorhabditis elegans: Effects of 5-hydroxytryptophan and dopamine on behavior and development. Experimental Parasitology 54(1):72-79.

Huff RA, Vaughan RA, Kuhar MJ, Uhl GR (1997) Phorbol esters increase dopamine transporter phosphorylation and decrease transport Vmax. J Neurochem 68:225-232.

Ingram SL, Prasad BM, Amara SG (2002) Dopamine transporter-mediated conductances increase excitability of midbrain dopamine neurons. Nature Neurosci 5:971-978.

Isakov N, Bleackley RC, Shaw J, Altman A (1985) Teleocidin and phorbol ester tumor promoters exert similar mitogenic effects on human lymphocytes. BBRC 130:724-731.

Jayanthi LD, Apparsundaram S, Malone MD, Ward E, Miller DM, Eppler M, Blakely RD (1998) The Caenorhabditis elegans gene T23G5.5 encodes an antidepressant- and cocaine-sensitive dopamine transporter. Mol Pharmacol 54:601-609.

Jorgensen EM (2004) Dopamine: should I stay or should I go now? Nat Neurosci 7:1019-1021.

Kahlig KM, Javitch JA, Galli A (2004) Amphetamine regulation of dopamine transport. Combined measurements of transporter currents and transporter imaging support the endocytosis of an active carrier. JBC 279:8966-8975.

Kandel ER, Schwartz JH (1982) Molecular biology of learning: modulation of transmitter release. Science 218:433-443.

Kapatos G, Hirayama K, Shimoji M, Milstien S (1999) GTP cyclohydrolase I feedback regulatory protein is expressed in serotonin neurons and regulates tetrahydrobiopterin biosynthesis. J Neurochem 72:669-675.

Kennedy LT, Hanbauer I (1983) Sodium-sensitive cocaine binding to rat striatal membrane: possible relationship to dopamine uptake sites. J Neurochem 41:172-178.

Khoshbouei H, Wang H, Lechleiter JD, Javitch JA, Galli A (2003) Amphetamine-induced dopamine efflux. A voltage-sensitive and intracellular Na+-dependent mechanism. JBC 278:12070-12077.

Khoshbouei H, Sen N, Guptaroy B, Johnson L, Lund D, Gnegy ME, Galli A, Javitch JA (2004) N-terminal phosphorylation of the dopamine transporter is required for amphetamine-induced efflux. PLoS Biol 2:E78.

Kilty JE, Lorang D, Amara SG (1991) Cloning and expression of a cocaine-sensitive rat dopamine transporter. Science 254:578-580.

Kim CH, Takamiya K, Petralia RS, Sattler R, Yu S, Zhou W, Kalb R, Wenthold R, Huganir R (2005) Persistent hippocampal CA1 LTP in mice lacking the C-terminal PDZ ligand of GluR1. Nature Neurosci 8:985-987.

Kitayama S, Dohi T, Uhl GR (1994) Phorbol esters alter functions of the expressed dopamine transporter. Eur J Pharmacol 268:115-119.

Koushika SP, Nonet ML (2000) Sorting and transport in C. elegans: aA model system with a sequenced genome. Curr Opin Cell Biol 12:517-523.

Kuwahara T, Koyama A, Gengyo-Ando K, Masuda M, Kowa H, Tsunoda M, Mitani S, Iwatsubo T (2006) Familial Parkinson mutant alpha-synuclein causes dopamine neuron dysfunction in transgenic Caenorhabditis elegans. JBC 281:334-340.

Lakso M, Vartiainen S, Moilanen AM, Sirvio J, Thomas JH, Nass R, Blakely RD, Wong G (2003) Dopaminergic neuronal loss and motor deficits in Caenorhabditis elegans overexpressing human alpha-synuclein. J Neurochem 86:165-172.

Lamesch P, Milstein S, Hao T, Rosenberg J, Li N, Sequerra R, Bosak S, Doucette-Stamm L, Vandenhaute J, Hill DE, Vidal M (2004) C. elegans ORFeome version 3.1:

increasing the coverage of ORFeome resources with improved gene predictions. Genome Res 14:2064-2069.

Lee FJ, Liu F, Pristupa ZB, Niznik HB (2001) Direct binding and functional coupling of alpha-synuclein to the dopamine transporters accelerate dopamine-induced apoptosis. Faseb J 15:916-926.

Lee KH, Kim MY, Kim DH, Lee YS (2004) Syntaxin 1A and receptor for activated C kinase interact with the N-terminal region of human dopamine transporter. Neurochem Res 29:1405-1409.

Lin Z, Zhang PW, Zhu X, Melgari JM, Huff R, Spieldoch RL, Uhl GR (2003) Phosphatidylinositol 3-kinase, protein kinase C, and MEK1/2 kinase regulation of dopamine transporters (DAT) require N-terminal DAT phosphoacceptor sites. JBC 278:20162-20170.

Link AJ, Eng J, Schieltz DM, Carmack E, Mize GJ, Morris DR, Garvik BM, Yates JR, 3rd (1999) Direct analysis of protein complexes using mass spectrometry. Nat Biotechnol 17:676-682.

Lints R, Emmons SW (1999) Patterning of dopaminergic neurotransmitter identity among Caenorhabditis elegans ray sensory neurons by a TGFbeta family signaling pathway and a Hox gene. Development 126:5819-5831.

Liu KS, Sternberg PW (1995) Sensory regulation of male mating behavior in Caenorhabditis elegans. Neuron 14:79-89.

Loder MK, Melikian HE (2003) The Dopamine Transporter Constitutively Internalizes and Recycles in a Protein Kinase C-regulated Manner in Stably Transfected PC12 Cell Lines. JBC 278:22168-22174.

Loer CM, Kenyon CJ (1993) Serotonin-deficient mutants and male mating behavior in the nematode Caenorhabditis elegans. J Neurosci 13:5407-5417.

Luttrell LM, Ostrowski J, Cotecchia S, Kendall H, Lefkowitz RJ (1993) Antagonism of catecholamine receptor signaling by expression of cytoplasmic domains of the receptors. Science 259:1453-1457.

Madsen KL, Beuming T, Niv MY, Chang CW, Dev KK, Weinstein H, Gether U (2005) Molecular determinants for the complex binding specificity of the PDZ domain in PICK1. JBC 280:20539-20548.

Mathews EA, Garcia E, Santi CM, Mullen GP, Thacker C, Moerman DG, Snutch TP (2003) Critical residues of the Caenorhabditis elegans unc-2 voltage-gated calcium channel that affect behavioral and physiological properties. J Neurosci 23:6537-6545.

Matsumoto G, Stojanovic A, Holmberg CI, Kim S, Morimoto RI (2005) Structural properties and neuronal toxicity of amyotrophic lateral sclerosis-associated Cu/Zn superoxide dismutase 1 aggregates. J Cell Biol 171:75-85.

McIntire SL, Jorgensen E, Kaplan J, Horvitz HR (1993) The GABAergic nervous system of Caenorhabditis elegans. Nature 364:337-341.

Melikian HE, Buckley KM (1999) Membrane trafficking regulates the activity of the human dopamine transporter. J Neurosci 19:7699-7710.

Mello CC, Kramer JM, Stinchcomb D, Ambros V (1991) Efficient gene transfer in C.elegans: extrachromosomal maintenance and integration of transforming sequences. Embo J 10:3959-3970.

Miller DM, 3rd, Niemeyer CJ (1995) Expression of the unc-4 homeoprotein in Caenorhabditis elegans motor neurons specifies presynaptic input. Dev 121:2877-2886.

Miller KG, Emerson MD, Rand JB (1999) Goalpha and diacylglycerol kinase negatively regulate the Gqalpha pathway in C. elegans. Neuron 24:323-333.

Missale C, Nash SR, Robinson SW, Jaber M, Caron MG (1998) Dopamine receptors: from structure to function. Physiol Rev 78:189-225.

Mogenson GJ, Takigawa M, Robertson A, Wu M (1979) Self-stimulation of the nucleus accumbens and ventral tegmental area of Tsai attenuated by microinjections of spiroperidol into the nucleus accumbens. Brain Res 171:247-259.

Monsma FJ, Jr., McVittie LD, Gerfen CR, Mahan LC, Sibley DR (1989) Multiple D2 dopamine receptors produced by alternative RNA splicing. Nature 342:926-929.

Moron JA, Zakharova I, Ferrer JV, Merrill GA, Hope B, Lafer EM, Lin ZC, Wang JB, Javitch JA, Galli A, Shippenberg TS (2003) Mitogen-activated protein kinase regulates dopamine transporter surface expression and dopamine transport capacity. J Neurosci 23:8480-8488.

Mortensen OV, Amara SG (2003) Dynamic regulation of the dopamine transporter. Eur J Pharmacol 479:159-170.

Murthy M, Garza D, Scheller RH, Schwarz TL (2003) Mutations in the exocyst component Sec5 disrupt neuronal membrane traffic, but neurotransmitter release persists. Neuron 37:433-447.

Nass R, Blakely RD (2003) The Caenorhabditis elegans dopaminergic system: opportunities for insights into dopamine transport and neurodegeneration. Annu Rev Pharmacol Toxicol 43:521-544.

Nass R, Miller DM, III, Blakely RD (2001) *C. elegans*: A novel pharmacogenetic model to study parkinson's disease. Parkinsonism and Related Disorders 7:185-191.

Nass R, Hall DH, Miller DM, 3rd, Blakely RD (2002) Neurotoxin-induced degeneration of dopamine neurons in Caenorhabditis elegans. ProcNatlAcadSci 99:3264-3269.

Nass R, Hahn MK, Jessen T, McDonald PW, Carvelli L, Blakely RD (2005) A genetic screen in Caenorhabditis elegans for dopamine neuron insensitivity to 6-hydroxydopamine identifies dopamine transporter mutants impacting transporter biosynthesis and trafficking. J Neurochem 94:774-785.

Neve KA, Seamans JK, Trantham-Davidson H (2004) Dopamine receptor signaling. J Recept Signal Transduct Res 24:165-205.

Nirenberg MJ, Vaughan RA, Uhl GR, Kuhar MJ, Pickel VM (1996) The dopamine transporter is localized to dendritic and axonal plasma membranes of nigrostriatal dopaminergic neurons. The Journal of Neuroscience 16:436-447.

Nirenberg MJ, Chan J, Pohorille A, Vaughan RA, Uhl GR, Kuhar MJ, Pickel VM (1997) The dopamine transporter: comparative ultrastructure of dopaminergic axons in limbic and motor compartments of the nucleus accumbens. J Neurosci 17:6899-6907.

Nonet ML (1999) Visualization of synaptic specializations in live C. elegans with synaptic vesicle protein-GFP fusions. J Neurosci Methods 89:33-40.

Nonet ML, Grundahl K, Meyer BJ, Rand JB (1993) Synaptic function is impaired but not eliminated in C. elegans mutants lacking synaptotagmin. Cell 73:1291-1305.

Nonet ML, Saifee O, Zhao H, Rand JB, Wei L (1998) Synaptic transmission deficits in Caenorhabditis elegans synaptobrevin mutants. J Neurosci 18:70-80.

Olds J, Milner P (1954) Positive reinforcement produced by electrical stimulation of septal area and other regions of rat brain. J Comp Physiol Psychol 47:419-427.

Olson PA, Tkatch T, Hernandez-Lopez S, Ulrich S, Ilijic E, Mugnaini E, Zhang H, Bezprozvanny I, Surmeier DJ (2005) G-protein-coupled receptor modulation of striatal CaV1.3 L-type Ca2+ channels is dependent on a Shank-binding domain. J Neurosci 25:1050-1062.

Owens WA, Sevak RJ, Galici R, Chang X, Javors MA, Galli A, France CP, Daws LC (2005) Deficits in dopamine clearance and locomotion in hypoinsulinemic rats

unmask novel modulation of dopamine transporters by amphetamine. J Neurochem 94:1402-1410.

Pacholczyk T, Blakely RD, Amara SG (1991) Expression cloning of a cocaine- and antidepressant-sensitive human noradrenaline transporter. Nature 350:350-354.

Pletscher A, Shore PA, Brodie BB (1955) Serotonin release as a possible mechanism of reserpine action. Science 122:374-375.

Poo M, Cone RA (1974) Lateral diffusion of rhodopsin in the photoreceptor membrane. Nature 247:438-441.

Prasher DC, Eckenrode VK, Ward WW, Prendergast FG, Cormier MJ (1992) Primary structure of the Aequorea victoria green-fluorescent protein. Gene 111:229-233.

Pristupa ZB, McConkey F, Liu F, Man HY, Lee FJ, Wang YT, Niznik HB (1998) Protein kinase-mediated bidirectional trafficking and functional regulation of the human dopamine transporter. Synapse 30:79-87.

Quick MW (2003) Regulating the conducting states of a mammalian serotonin transporter. Neuron 40:537-549.

Rand JB, Duerr JS, Frisby DL (1998) Using Caenorhabditis elegans to study vesicular transport. Methods Enzymol 296:529-547.

Rankin CH (1991) Interactions between two antagonistic reflexes in the nematode Caenorhabditis elegans. J Comp Physiol [A] 169:59-67.

Rankin CH, Broster BS (1992) Factors affecting habituation and recovery from habituation in the nematode Caenorhabditis elegans. Behav Neurosci 106:239-249.

Reboul J, Vaglio P, Rual JF, Lamesch P, Martinez M, Armstrong CM, Li S, Jacotot L, Bertin N, Janky R, Moore T, Hudson JR, Jr., Hartley JL, Brasch MA, Vandenhaute J, Boulton S, Endress GA, Jenna S, Chevet E, Papasotiropoulos V, Tolias PP, Ptacek J, Snyder M, Huang R, Chance MR, Lee H, Doucette-Stamm L, Hill DE, Vidal M (2003) C. elegans ORFeome version 1.1: experimental verification of the genome annotation and resource for proteome-scale protein expression. Nat Genet 34:35-41.

Rice ME (2000) Distinct regional differences in dopamine-mediated volume transmission. Prog Brain Res 125:277-290.

Riddle DL (1997) C. elegans II. Plainview, N.Y.: Cold Spring Harbor Laboratory Press.

Rigaut G, Shevchenko A, Rutz B, Wilm M, Mann M, Seraphin B (1999) A generic protein purification method for protein complex characterization and proteome exploration. Nat Biotechnol 17:1030-1032.

Ritz MC, Lamb RJ, Goldberg SR, Kuhar MJ (1987) Cocaine receptors on dopamine transporters are related to self-administration of cocaine. Science 237:1219-1223.

Rodriguez Diaz M, Abdala P, Barroso-Chinea P, Obeso J, Gonzalez-Hernandez T (2001) Motor behavioural changes after intracerebroventricular injection of 6-hydroxydopamine in the rat: an animal model of Parkinson's disease. Behav Brain Res 122:79-92.

Rohila JS, Chen M, Cerny R, Fromm ME (2004) Improved tandem affinity purification tag and methods for isolation of protein heterocomplexes from plants. Plant J 38:172-181.

Rose JK, Rankin CH (2001) Analyses of habituation in Caenorhabditis elegans. Learn Mem 8:63-69.

Ross SB, Renyi AL (1967) Inhibition of the uptake of tritiated catecholamines by antidepressant and related agents. Eur J Pharmacol 2:181-186.

Sanyal S, Wintle RF, Kindt KS, Nuttley WM, Arvan R, Fitzmaurice P, Bigras E, Merz DC, Hebert TE, van der Kooy D, Schafer WR, Culotti JG, Van Tol HH (2004) Dopamine modulates the plasticity of mechanosensory responses in Caenorhabditis elegans. Embo J 23:473-482.

Sawin ER, Ranganathan R, Horvitz HR (2000) C. elegans locomotory rate is modulated by the environment through a dopaminergic pathway and by experience through a serotonergic pathway. Neuron 26:619-631.

Schafer WR, Kenyon CJ (1995) A calcium-channel homologue required for adaptation to dopamine and serotonin in *Caenorhabditis elegans*. Nature 375:73-78.

Sherer TB, Kim JH, Betarbet R, Greenamyre JT (2003) Subcutaneous rotenone exposure causes highly selective dopaminergic degeneration and alpha-synuclein aggregation. Exp Neurol 179:9-16.

Shimada S, Kitayama S, Lin C, Patel A, Nanthakumar E, Gregor P, Kuhar M, Uhl G (1991) Cloning and expression of a cocaine-sensitive dopamine transporter complementary DNA. Science 254:576-577.

Sieburth D, Ch'ng Q, Dybbs M, Tavazoie M, Kennedy S, Wang D, Dupuy D, Rual JF, Hill DE, Vidal M, Ruvkun G, Kaplan JM (2005) Systematic analysis of genes required for synapse structure and function. Nature 436:510-517.

Singer SJ, Nicolson GL (1972) The fluid mosaic model of the structure of cell membranes. Science 175:720-731.

Sorkina T, Doolen S, Galperin E, Zahniser NR, Sorkin A (2003) Oligomerization of dopamine transporters visualized in living cells by fluorescence resonance energy transfer microscopy. JBC 278:28274-28283.

Spano PF, Govoni S, Trabucchi M (1978) Studies on the pharmacological properties of dopamine receptors in various areas of the central nervous system. Adv Biochem Psychopharmacol 19:155-165.

Staudinger J, Lu J, Olson EN (1997) Specific interaction of the PDZ domain protein PICK1 with the COOH terminus of protein kinase C-alpha. JBC 272:32019-32024.

Staudinger J, Zhou J, Burgess R, Elledge SJ, Olson EN (1995) PICK1: a perinuclear binding protein and substrate for protein kinase C isolated by the yeast two-hybrid system. J Cell Biol 128:263-271.

Sugiura M, Fuke S, Suo S, Sasagawa N, Van Tol HH, Ishiura S (2005) Characterization of a novel D2-like dopamine receptor with a truncated splice variant and a D1-like dopamine receptor unique to invertebrates from Caenorhabditis elegans. J Neurochem 94:1146-1157.

Sulston J, Dew M, Brenner S (1975) Dopaminergic neurons in the nematode caenorhabditis elegans. Journal of CompNeur 163:215-226.

Sung U, Apparsundaram S, Blakely RD (2000) Intracellular calcium regulates associations between norepinephrine transporter and syntaxin 1A. In: Society for Neuroscience. New Orleans, LA.

Sung U, Apparsundaram S, Galli A, Kahlig KM, Savchenko V, Schroeter S, Quick MW, Blakely RD (2003) A regulated interaction of syntaxin 1A with the antidepressant-sensitive norepinephrine transporter establishes catecholamine clearance capacity. J Neurosci 23:1697-1709.

Suo S, Sasagawa N, Ishiura S (2002) Identification of a dopamine receptor from Caenorhabditis elegans. Neurosci Lett 319:13-16.

Suo S, Sasagawa N, Ishiura S (2003) Cloning and characterization of a Caenorhabditis elegans D2-like dopamine receptor. J Neurochem 86:869-878.

Suo S, Ishiura S, Van Tol HH (2004) Dopamine receptors in C. elegans. Eur J Pharmacol 500:159-166.

TerBush DR, Maurice T, Roth D, Novick P (1996) The Exocyst is a multiprotein complex required for exocytosis in Saccharomyces cerevisiae. Embo J 15:6483-6494.

Torres GE, Yao WD, Mohn AR, Quan H, Caron MG (2000) Specific interaction between the dopamine transporter and the PDZ domain-containg protein pick1. In: Society for Neurocience, p 17.13. New Orleans, LA.

Torres GE, Yao WD, Mohn RR, Quan H, Kim K, Levey AI, Staudinger J, Caron MG (2001) Functional interaction between monoamine plasma membrane transporters and the synaptic PDZ domain-containing protein PICK1. Neuron 30:121-134.

Trent C, Tsuing N, Horvitz HR (1983) Egg-laying defective mutants of the nematode Caenorhabditis elegans. Genetics 104:619-647.

Usdin TB, Mezey E, Chen C, Brownstein MJ, Hoffman BJ (1991) Cloning of the cocaine-sensitive bovine dopamine transporter. Proceedings in the National Academy of Sciences in the USA 88:11168-11171.

Vandenbergh DJ, Persico AM, Uhl GR (1992) A human dopamine transporter cDNA predicts reduced glycosylation, displays a novel repetitive element and provides racially-dimorphic *Taq* I RFLPs. Mol Brain Res 15:161-166.

Vaughan RA, Huff RA, Uhl GR, Kuhar MJ (1997) Protein kinase C-mediated phosphorylation and functional regulation of dopamine transporters in striatal synaptosomes. JBC 272:15541-15546.

Velazquez JL, Thompson CL, Barnes EM, Jr., Angelides KJ (1989) Distribution and lateral mobility of GABA/benzodiazepine receptors on nerve cells. J Neurosci 9:2163-2169.

Ward S, Thomson N, White JG, Brenner S (1975) Electron microscopical reconstruction of the anterior sensory anatomy of the nematode Caenorhabditis elegans. J Comp Neurol 160:313-337.

Wei AD, Butler A, Salkoff L (2005) KCNQ-like potassium channels in Caenorhabditis elegans. Conserved properties and modulation. J Biol Chem 280:21337-21345.

Weinshenker D, Garriga G, Thomas JH (1995) Genetic and pharmacological analysis of neurotransmitters controlling egg laying in C. elegans. J Neurosci 15:6975-6985.

Weinshenker D, Wei A, Salkoff L, Thomas JH (1999) Block of an ether-a-go-go-like K(+) channel by imipramine rescues egl-2 excitation defects in Caenorhabditis elegans. J Neurosci 19:9831-9840.

Wersinger C, Sidhu A (2003) Attenuation of dopamine transporter activity by alpha-synuclein. Neurosci Lett 340:189-192.

Wey CL, Cone RA, Edidin MA (1981) Lateral diffusion of rhodopsin in photoreceptor cells measured by fluorescence photobleaching and recovery. Biophys J 33:225-232.

White JG, Southgate E, Thompson JN, Brenner S (1986) The structure of the nervous system of the nematode *Caenorhabditis elegans*. Philos Trans R Soc Lond B Biol Sci 314:1-340.

Wicks SR, Rankin CH (1995) Integration of mechanosensory stimuli in Caenorhabditis elegans. J Neurosci 15:2434-2444.

Wintle RF, Van Tol HH (2001) Dopamine signaling in Caenorhabditis elegans-potential for parkinsonism research. Parkinsonism Relat Disord 7:177-183.

Yamashita A, Singh SK, Kawate T, Jin Y, Gouaux E (2005) Crystal structure of a bacterial homologue of Na+/Cl--dependent neurotransmitter transporters. Nature 437:215-223.

Zhang L, Coffey LL, Reith ME (1997) Regulation of the functional activity of the human dopamine transporter by protein kinase C. Biochem Pharmacol 53:677-688.

Zhou HM, Brust-Mascher I, Scholey JM (2001) Direct visualization of the movement of the monomeric axonal transport motor UNC-104 along neuronal processes in living Caenorhabditis elegans. J Neurosci 21:3749-3755.

Zhu CB, Carneiro AM, Dostmann WR, Hewlett WA, Blakely RD (2005) p38 MAPK activation elevates serotonin transport activity via a trafficking-independent, protein phosphatase 2A-dependent process. JBC 280:15649-15658.

Zhu SJ, Kavanaugh MP, Sonders MS, Amara SG, Zahniser NR (1997) Activation of protein kinase C inhibits uptake, currents and binding associated with the human dopamine transporter expressed in Xenopus oocytes. JPET 282:1358-1365.